

PLOS Pathogens

Divergent metabolism between *Trypanosoma congolense* and *Trypanosoma brucei* results in differential drug sensitivity

--Manuscript Draft--

Manuscript Number:	PPATHOGENS-D-21-00223
Full Title:	Divergent metabolism between <i>Trypanosoma congolense</i> and <i>Trypanosoma brucei</i> results in differential drug sensitivity
Short Title:	Divergent metabolism between <i>Trypanosoma congolense</i> and <i>Trypanosoma brucei</i>
Article Type:	Research Article
Section/Category:	Parasitology
Keywords:	<i>Trypanosoma congolense</i> ; <i>Trypanosoma brucei</i> ; Animal African Trypanosomiasis; metabolism; drug target identification
Abstract:	<p>Animal African Trypanosomiasis (AAT) is a debilitating livestock disease prevalent across sub-Saharan Africa, a main cause of which is the protozoan parasite <i>Trypanosoma congolense</i>. In comparison to the well-studied <i>T. brucei</i>, there is a major paucity of knowledge regarding the biology of <i>T. congolense</i>. Here, we use a combination of omics technologies and novel genetic tools to characterise core metabolism in <i>T. congolense</i> mammalian-infective bloodstream-form parasites, and test whether metabolic differences compared to <i>T. brucei</i> impact upon drug sensitivity. Like <i>T. brucei</i>, glycolysis plays a major part in <i>T. congolense</i> energy metabolism. However, the rate of glucose uptake is significantly reduced in <i>T. congolense</i>, with cells remaining viable when cultured in concentrations as low as 2 mM. Instead of pyruvate, the primary glycolytic endpoints are succinate, malate and acetate. Comparative transcriptomics analysis showed higher levels of activity associated with the mitochondrial pyruvate dehydrogenase complex and acetate generation, and the glycosomal succinate shunt in <i>T. congolense</i>. However, based on omics analysis and chemical inhibition, there does not appear to be significant levels of oxidative phosphorylation. Stable-isotope labelling of glucose enabled the comparison of carbon usage between <i>T. brucei</i> and <i>T. congolense</i>, highlighting differences in nucleotide and fatty acid metabolism. To validate the metabolic similarities and differences, both species were treated with pharmacological inhibitors, confirming a lack of essential electron transport chain activity in <i>T. congolense</i>, but increased sensitivity to inhibition of mitochondrial pyruvate import. Strikingly, <i>T. congolense</i> exhibited significant resistance to inhibitors of fatty acid synthesis, including a 780-fold greater EC₅₀ against the lipase and fatty acid synthase inhibitor Orlistat, compared to <i>T. brucei</i>. These data highlight that bloodstream form <i>T. congolense</i> diverges from <i>T. brucei</i> in key areas of metabolism, with several features that are intermediate between bloodstream- and insect-stage <i>T. brucei</i>. These results have implications for drug development, mechanisms of drug resistance and host-pathogen interactions.</p>
Additional Information:	
Question	Response
<p>Financial Disclosure</p> <p>Enter a financial disclosure statement that describes the sources of funding for the work included in this submission. Review the submission guidelines for detailed requirements. View published research articles from PLOS Pathogens for specific examples.</p> <p>This statement is required for submission</p>	<p>LM, PS, EP, HdK and MPB were funded by BBSRC grant BB/N007492/1, and LM, PS, EP, RR and MPB by BB/S00243X/1. CG and BW were funded by University of Nottingham Strategic Support Funds (Wellcome Trust), and GAM by Sir Halley Stewart Medical Research Grant (R410). MPB is funded by a Wellcome Trust core grant to the Wellcome Centre for Integrative Parasitology (grant 104111/Z/14/Z). This article is based on research funded in part by the Bill & Melinda Gates Foundation (Investment ID OPP1176784) and with UK aid from the UK Government (Project 300504) through GALVmed. The findings and conclusions contained within are those of the authors and do not necessarily reflect positions or policies of the Bill & Melinda Gates Foundation or the UK Government. The Roslin Institute is core funded by the BBSRC (BS/E/D/20002173). The funders had no role in study design, data collection and</p>

and **will appear in the published article** if the submission is accepted. Please make sure it is accurate.

Unfunded studies

Enter: *The author(s) received no specific funding for this work.*

Funded studies

Enter a statement with the following details:

- Initials of the authors who received each award
- Grant numbers awarded to each author
- The full name of each funder
- URL of each funder website
- Did the sponsors or funders play any role in the study design, data collection and analysis, decision to publish, or preparation of the manuscript?
- **NO** - Include this sentence at the end of your statement: *The funders had no role in study design, data collection and analysis, decision to publish, or preparation of the manuscript.*
- **YES** - Specify the role(s) played.

* typeset

analysis, decision to publish, or preparation of the manuscript.

Competing Interests

Use the instructions below to enter a competing interest statement for this submission. On behalf of all authors, disclose any [competing interests](#) that could be perceived to bias this work—acknowledging all financial support and any other relevant financial or non-financial competing interests.

This statement **will appear in the published article** if the submission is accepted. Please make sure it is accurate. View published research articles from [PLOS Pathogens](#) for specific examples.

The authors have declared that no competing interests exist.

NO authors have competing interests

Enter: *The authors have declared that no competing interests exist.*

Authors with competing interests

Enter competing interest details beginning with this statement:

I have read the journal's policy and the authors of this manuscript have the following competing interests: [insert competing interests here]

* typeset

This statement is **required** for submission and **will appear in the published article** if the submission is accepted. Please make sure it is accurate and that any funding sources listed in your Funding Information later in the submission form are also declared in your Financial Disclosure statement.

Data Availability

Authors are required to make all data underlying the findings described fully available, without restriction, and from the time of publication. PLOS allows rare exceptions to address legal and ethical concerns. See the [PLOS Data Policy](#) and [FAQ](#) for detailed information.

A Data Availability Statement describing where the data can be found is required at submission. Your answers to this question constitute the Data Availability Statement and **will be published in the article**, if accepted.

Important: Stating 'data available on request from the author' is not sufficient. If your data are only available upon request, select 'No' for the first question and explain your exceptional situation in the text box.

Yes - all data are fully available without restriction

<p>Do the authors confirm that all data underlying the findings described in their manuscript are fully available without restriction?</p>	
<p>Describe where the data may be found in full sentences. If you are copying our sample text, replace any instances of XXX with the appropriate details.</p> <ul style="list-style-type: none"> • If the data are held or will be held in a public repository, include URLs, accession numbers or DOIs. If this information will only be available after acceptance, indicate this by ticking the box below. For example: <i>All XXX files are available from the XXX database (accession number(s) XXX, XXX).</i> • If the data are all contained within the manuscript and/or Supporting Information files, enter the following: <i>All relevant data are within the manuscript and its Supporting Information files.</i> • If neither of these applies but you are able to provide details of access elsewhere, with or without limitations, please do so. For example: <i>Data cannot be shared publicly because of [XXX]. Data are available from the XXX Institutional Data Access / Ethics Committee (contact via XXX) for researchers who meet the criteria for access to confidential data.</i> <i>The data underlying the results presented in the study are available from (include the name of the third party and contact information or URL).</i> • This text is appropriate if the data are owned by a third party and authors do not have permission to share the data. <p>* typeset</p>	<p>RNA-seq data is deposited at GEO (accession number: GSE165290; URL: https://www.ncbi.nlm.nih.gov/geo/query/acc.cgi?acc=GSE165290). Metabolomics data is deposited at MetaboLights (accession number: MTBLS2372; URL: www.ebi.ac.uk/metabolights/MTBLS2372). All other relevant data are within the manuscript and its Supporting Information files.</p>
<p>Additional data availability information:</p>	

1 **Divergent metabolism between *Trypanosoma***
2 ***congolense* and *Trypanosoma brucei* results in**
3 **differential drug sensitivity**
4

5 P. C. Steketee^{1*}, E. A. Dickie², J. Iremonger¹, K. Crouch², E. Paxton¹, S. Jayaraman¹, O. A.
6 Alfituri¹, G. Awuah-Mensah³, R. Ritchie², A. Schnauffer⁴, H. P. de Koning⁵, C. Gadelha³, B.
7 Wickstead³, M. P. Barrett^{2,6} and L. J. Morrison¹

8 ¹The Roslin Institute, Royal (Dick) School of Veterinary Studies, University of Edinburgh,
9 Edinburgh, UK

10 ²Wellcome Centre for Integrative Parasitology, Institute of Infection, Immunity and
11 Inflammation, University of Glasgow, Glasgow, UK

12 ³School of Life Sciences, University of Nottingham, Nottingham, UK

13 ⁴Institute of Immunology and Infection Research, University of Edinburgh, Edinburgh, UK

14 ⁵Institute of Infection, Immunity and Inflammation, University of Glasgow, Glasgow, UK

15 ⁶Glasgow Polyomics, University of Glasgow, UK

16 *Corresponding author: Pieter.Steketee@ed.ac.uk

17

18

19 **Abstract**

20 Animal African Trypanosomiasis (AAT) is a debilitating livestock disease prevalent across sub-
21 Saharan Africa, a main cause of which is the protozoan parasite *Trypanosoma congolense*.
22 In comparison to the well-studied *T. brucei*, there is a major paucity of knowledge regarding
23 the biology of *T. congolense*. Here, we use a combination of omics technologies and novel
24 genetic tools to characterise core metabolism in *T. congolense* mammalian-infective
25 bloodstream-form parasites, and test whether metabolic differences compared to *T. brucei*
26 impact upon drug sensitivity. Like *T. brucei*, glycolysis plays a major part in *T. congolense*
27 energy metabolism. However, the rate of glucose uptake is significantly reduced in *T.*
28 *congolense*, with cells remaining viable when cultured in concentrations as low as 2 mM.
29 Instead of pyruvate, the primary glycolytic endpoints are succinate, malate and acetate.
30 Comparative transcriptomics analysis showed higher levels of activity associated with the
31 mitochondrial pyruvate dehydrogenase complex and acetate generation, and the glycosomal
32 succinate shunt in *T. congolense*. However, based on omics analysis and chemical inhibition,
33 there does not appear to be significant levels of oxidative phosphorylation. Stable-isotope
34 labelling of glucose enabled the comparison of carbon usage between *T. brucei* and *T.*
35 *congolense*, highlighting differences in nucleotide and fatty acid metabolism. To validate the
36 metabolic similarities and differences, both species were treated with pharmacological
37 inhibitors, confirming a lack of essential electron transport chain activity in *T. congolense*, but
38 increased sensitivity to inhibition of mitochondrial pyruvate import. Strikingly, *T. congolense*
39 exhibited significant resistance to inhibitors of fatty acid synthesis, including a 780-fold greater
40 EC_{50} against the lipase and fatty acid synthase inhibitor Orlistat, compared to *T. brucei*. These
41 data highlight that bloodstream form *T. congolense* diverges from *T. brucei* in key areas of
42 metabolism, with several features that are intermediate between bloodstream- and insect-
43 stage *T. brucei*. These results have implications for drug development, mechanisms of drug
44 resistance and host-pathogen interactions.

45 **Author summary**

46 Animal African Trypanosomiasis (AAT), also known as Nagana, is a devastating disease
47 affecting livestock across sub-Saharan Africa. AAT is primarily caused by the parasite
48 *Trypanosoma congolense*, yet our biological knowledge about this pathogen is poor,
49 especially compared to the related species *T. brucei*. Understanding core metabolism of *T.*
50 *congolense* is crucial in order to identify new drug targets, and develop novel
51 chemotherapeutics. In this work, we addressed the lack of knowledge concerning *T.*
52 *congolense* by carrying out a comprehensive analysis of core metabolism, and comparing the
53 data to *T. brucei*. We then used the findings of metabolic differences to predict differential drug
54 sensitivity. We show that unlike *T. brucei*, where glucose metabolism leads to high levels of
55 pyruvate excretion, *T. congolense* metabolises glucose to other end-products, namely
56 succinate, malate and acetate. Moreover, there are pronounced differences in the way *T.*
57 *congolense* uses glucose to feed into other areas of metabolism. Further analysis also
58 suggests that *T. congolense* prefers to scavenge lipids and fatty acids, rather than de novo
59 biosynthesis of these essential factors. To validate these findings, we show that *T. congolense*
60 is differentially susceptible to drugs compared to *T. brucei*, and in particular *T. congolense* is
61 significantly less sensitive to inhibitors of fatty acid synthesis. Our study provides a foundation
62 of functional metabolic knowledge on *T. congolense*, with key insights into how this parasite
63 differs from *T. brucei*, and highlights potential **📄** **📄** that are exploitable for pharmacological
64 intervention.

65 **Introduction**

66 The hemoflagellate protozoan parasite *Trypanosoma congolense* is a primary causative agent
67 of animal African trypanosomiasis (AAT), which can also be caused by *T. vivax* and *T. brucei*
68 [1]. AAT **📄** accounts for livestock deaths in excess of 3 million annually with up to 120 million
69 cattle at risk [2-4], making AAT one of the most important livestock diseases across sub-
70 Saharan Africa. Current methods of AAT control centre around chemotherapy and prophylaxis
71 (reviewed in [3]), but the very few available veterinary trypanocidal drugs have been used

72 extensively for decades, resulting in resistance and inadequate protection against AAT [5-7].
73 As such, there is a dire need for the development of new and improved chemotherapeutics to
74 manage AAT [3, 8].

75 Most of our biological understanding of African trypanosomes derives from studies on *T.*
76 *brucei*, subspecies of which, *T. b. gambiense* and *T. b. rhodesiense*, cause Human African
77 Trypanosomiasis (HAT) [9]. The ability to culture both procyclic (PCF; tsetse fly) and
78 bloodstream (BSF; mammalian) forms of *T. brucei in vitro*, combined with its tractability with
79 respect to genetic manipulation, have enabled extensive study of this species at molecular
80 level [10, 11]. In stark contrast, very few *T. congolense* strains are amenable to continuous
81 bloodstream form (BSF) culture, with a single strain (IL3000) used in most studies [12]. Whilst
82 genetic modification is possible in *T. congolense* PCF stage, routine BSF transfection has only
83 recently become possible [13-15]. Additionally, although *T. congolense* exhibits a superficially
84 similar morphology and life cycle to *T. brucei* [16, 17], emerging evidence increasingly
85 suggests that *T. brucei*, *T. congolense* and *T. vivax* exhibit some profound differences at the
86 genomic level [18-22], including in genes and phenotypes of direct relevance to infection
87 biology and disease epidemiology. However, there is a lack of understanding to what extent
88 these genetic differences translate into biological differences, including with respect to
89 metabolism.

90 Understanding metabolism is critical to identifying how pathogens survive and thrive in the
91 varying host environments they encounter, as well as being a means of elucidating drug
92 targets, modes of drug action and mechanisms of drug resistance [23-25]. *T. brucei*
93 metabolism has been extensively studied, aided by the application of technologies such as
94 liquid chromatography-mass spectrometry (LC-MS) and nuclear magnetic resonance (NMR)
95 spectroscopy (reviewed in detail by [26, 27]), which enable global profiling of the cellular
96 metabolome.

97 The BSF stage of *T. brucei* utilizes the high levels of glucose available in the mammalian
98 bloodstream, and depends almost exclusively on the glycolytic pathway to generate ATP [28].

99 The first seven steps of glycolysis are encompassed by a specialized organelle, the
100 glycosome, which maintains its own ATP/ADP and NAD/NADH balance, allowing glycolysis
101 to proceed at an extraordinarily high rate in comparison to most other eukaryotic cells [29].
102 The endpoint of glycolysis, pyruvate, is a waste product of *T. brucei*, and the majority is
103 excreted from the cell in large quantities. However, small amounts of pyruvate are further
104 metabolized in the mitochondrion to acetate by pyruvate dehydrogenase (PDH) and
105 acetate:succinate CoA transferase (ASCT), a secondary, yet essential pathway [30]. The
106 acetate generated from this pathway is utilized, at least partially, for the *de novo* synthesis of
107 fatty acids [31]. Indeed, both BSF and PCF *T. brucei* are highly sensitive to the lipase and fatty
108 acid synthase inhibitor Orlistat [32].

109 Conversely, in the absence of blood meals, glucose is scarce in the tsetse fly midgut [33], and
110 the main energy source of PCF *T. brucei* is L-proline, the catabolism of which leads to
111 production of acetate, succinate and L-alanine through a more developed and active
112 mitochondrion (including an active respiratory chain capable of generating ATP, which is
113 inactive in BSF *T. brucei* [34]). Until recently, it was thought that PCF *T. brucei* did not exhibit
114 active TCA metabolism, although recent data have shown that TCA intermediates such as
115 succinate and 2-oxoglutarate can stimulate PCF *T. brucei* growth [35-37].

116 Among the glycolytic enzymes, *T. brucei* expresses three isoforms of phosphoglycerate
117 kinase (PGK), which catalyze the conversion of 1,3-bisphosphoglycerate to 3-
118 phosphoglycerate [38]. These are developmentally regulated, with the major isoform in BSF
119 parasites present in the glycosome (PGK-C), whilst the primary PCF isoform is found in the
120 cytosol (PGK-B) [39]. The localization of PGK-B in the PCF cytosol is thought to result in an
121 ATP/ADP imbalance in the glycosome, which is rectified by upregulating the glycosomal
122 “succinate shunt”, a pathway that includes the ATP-generating phosphoenolpyruvate
123 carboxykinase (PEPCK)- and pyruvate phosphate dikinase (PPDK)-mediated conversion of
124 phosphoenolpyruvate (PEP) to oxaloacetate and pyruvate respectively [39, 40]. The succinate

125 shunt, combined with amino acid metabolism, results in the excretion of high levels of
126 succinate in PCF *T. brucei* [41].

127 Stable isotope labelling data has revealed that BSF *T. brucei* utilize D-glucose to a greater
128 extent than first realized, with heavy carbons disseminating into amino acid, lipid and
129 nucleotide metabolism [42]. This study also showed that some of the succinate and malate
130 excreted from BSF parasites originates from glycolysis and, unexpectedly, inhibition of
131 PEPCCK is lethal at this life-cycle stage [42]. It has also been shown that acetate production is
132 essential to BSF *T. brucei*, in particular for the synthesis of fatty acids (FAs) [30]. However,
133 acetate excretion, as well as that of succinate and malate, is negligible in BSF *T. brucei*
134 compared to that of pyruvate and L-alanine.

135 In contrast to *T. brucei*, the literature on metabolism in *T. congolense* is scarce. More than half
136 a century ago it was suggested that BSF *T. congolense* has a significantly lower rate of
137 glucose consumption compared to BSF *T. brucei* [43]. Furthermore, pyruvate is not the main
138 glycolytic end product and instead, acetate and succinate are excreted at high levels,
139 indicative of metabolism more akin to PCF *T. brucei* [43]. Further work has revealed additional
140 differences that support this hypothesis [44-46]. For example, BSF *T. congolense* primarily
141 expresses cytosolic PGK-C, rather than glycosomal PGK-B [46]. Microscopy has also
142 revealed a more developed mitochondrion in BSF *T. congolense*, with visible cristae,
143 suggesting that mitochondrial energy metabolism could play a more prominent role in BSF *T.*
144 *congolense* [47]. The high levels of acetate excretion first shown by Agosin & Von Brand [43]
145 are consistent with this hypothesis. However, other studies have shown that BSF *T.*
146 *congolense* is sensitive to inhibitors of Trypanosome Alternative Oxidase (TAO), including
147 salicylhydroxamide (SHAM); and is insensitive to cyanide, suggesting that, as for BSF *T.*
148 *brucei*, TAO (Gene ID: TcIL3000.A.H_000015900) is the sole terminal oxidase, responsible
149 for reoxidising glycerol 3-phosphate, in BSF *T. congolense* [48-51]. Notably, nitroblue
150 tetrazolium staining indicates the presence of NADH dehydrogenase (complex I) activity in

151 BSF *T. congolense* [48]. However, to date, no studies have assessed BSF *T. congolense*
152 sensitivity to chemical inhibition of the electron transport chain, or the F₁F₀-ATPase.

153 Post-genomic technologies allow for the generation of large datasets that enable analysis of
154 cellular processes on a systems scale, including metabolomics and transcriptomics.
155 Integration of these data can provide a detailed snapshot of cell metabolism at the transcript
156 and metabolite levels and help to dissect differences between species or conditions in
157 unprecedented detail [52]. Furthermore, this knowledge can aid in predication and
158 understanding of drug efficacy and mode of action.

159 This study aimed to generate the first comprehensive overview of the metabolome of BSF *T.*
160 *congolense* IL3000 parasites, allowing a global metabolic comparison of differences between
161 *T. congolense* and *T. brucei*. Glycolytic metabolism in BSF *T. congolense* appears to be
162 similar to PCF *T. brucei*, particularly in terms of metabolic outputs and gene expression.
163 However, there are pronounced differences in parasite reliance on exogenous amino acids as
164 well as carbon dissemination into pathways involved in nucleotide and lipid metabolism, as
165 shown by stable isotope-labelled metabolomics. Using these data, we further validated these
166 metabolic differences in *T. congolense* by pharmacological inhibition, which highlighted
167 increased sensitivity to inhibition of mitochondrial pyruvate uptake, as well as significant
168 resistance to inhibition of fatty acid synthesis, tested using inhibitors of fatty acid synthase and
169 acetyl-coA synthetase. Taken together, these results suggest that *T. congolense* and *T. brucei*
170 differ in some fundamental aspects of their core metabolism, which has important implications
171 in terms drug sensitivity, and therefore, development of novel chemotherapeutics.

172 **Results**

173 **Comparative RNA-sequencing of *T. congolense* and *T. brucei***

174 To permit direct comparison of BSF *T. congolense* and *T. brucei* at the transcriptome level,
175 RNAseq analysis was carried out on parasites cultured *in vitro* and trypanosome samples
176 isolated from infected mice at first peak parasitaemia (*ex vivo*) (Fig 1). Samples were prepared

177 using *T. congolense* (strain IL3000, *in vitro* and *ex vivo*) and pleomorphic *T. brucei* (strain
178 STIB 247; *in vitro* and *ex vivo*), to assess similarities and differences between trypanosomes
179 grown in culture and those from an infection (Fig 1A and 1B), and to compare and contrast
180 the transcriptome across the species (Fig 1C and 1D). Sequencing data were aligned to the
181 respective genome sequence with a mean overall alignment rate of $88.0 \pm 2.3\%$ and $94.1 \pm$
182 0.7% for *T. brucei* and *T. congolense* reads, respectively. Resultant files were sorted and
183 filtered for quality, and to minimize artefacts from multigene families, only uniquely aligned
184 reads were used for downstream analyses. Read counts were normalised using transcripts
185 per million (TPM) [53]. Orthologues were inferred between the species using Orthofinder [54],
186 in order to directly compare TPM values for 1-to-1 orthologues, as well as sum-of-TPM values
187 for groups containing families of paralogues (e.g. hexose transporters). These normalised
188 read counts are henceforth referred to as orthoTPM values (S1 Table). The Orthofinder
189 dataset (S2 Table) consisted of 6,677 orthogroups (denoted with the prefix “TbTc”), of which
190 5,398 (80.84%) were 1-to-1 orthologues. The Orthofinder tool was also used to predict genes
191 only present in one of the two species (S2 Table). There are several metabolic genes that are
192 not present in the *T. congolense* genome, including putative delta-4 and delta-6 desaturases
193 (Tb927.10.7100 & Tb11.v5.0580), a succinate dehydrogenase subunit (SDH11;
194 Tb927.8.6890) and guanine deaminase (Tb927.5.4560, Tb05.5K5.200 & Tb11.v5.0409), in
195 addition to mitochondrial pyruvate carrier 1 (MPC1; Tb927.9.3780) (S2 Table).

196 Differences between four sample groups were assessed based on orthoTPM values (Fig 1;
197 full dataset in S1 Table). There was a strong intra-species correlation between the *in vitro* and
198 *ex vivo* conditions at the transcriptome level (Pearson correlation coefficient, *T. congolense*
199 (ρ) = 0.765, Fig 1A; *T. brucei* ρ = 0.803, Fig 1B), showing that *in vitro*-derived BSF *T.*
200 *congolense* and *T. brucei* closely resemble parasites isolated from infections at the
201 transcriptome level. However, correlations between species even in the same condition were
202 lower, implying transcriptional differences between the species (*ex vivo*: ρ = 0.651, Fig 1C; *in*
203 *vitro*: ρ = 0.687, Fig 1D).

204 To compare data from this study to BSF *T. congolense* transcriptomics data generated by
205 Silvester *et al.* (generated at ascending and peak parasitaemia [55]), TPM values for each
206 annotated *T. congolense* gene were compared directly (S1 Fig, S3 Table). There was good
207 correlation between both *in vitro* and *ex vivo* *T. congolense* BSF datasets and the data from
208 Silvester *et al.* ($\rho > 0.8$, S1 Fig), with the highest correlation being between the *ex vivo* and
209 ascending data as expected ($\rho = 0.897$, S1 Fig), albeit the correlation between the ‘ascending’
210 and ‘peak parasitaemia’ in Silvester *et al.* was higher ($\rho = 0.979$, S1 Fig).



211 ***T. congolense* metabolite consumption and output**

212 Global metabolite (metabolomics) analysis of *in vitro* culture supernatant samples provides a
213 detailed insight into the metabolic inputs and outputs of cultured cells [56]. However, high
214 levels of medium components can often mask subtle but significant changes in culture medium
215 composition over time. To counteract this, a modified culture medium was designed for *T.*
216 *congolense* strain IL3000, based on previous published medium formulations (Steketee’s
217 *congolense* medium, SCM-3; for details see Materials and Methods) [14, 15].

218 A time course was initiated in SCM-3. BSF *T. congolense* IL3000 cells during exponential
219 growth phase were inoculated into fresh medium (0 h time point). Culture supernatant samples
220 were collected at 0, 8, 24, 32, 48 and 56 hours ($n = 4$ at each time point) and metabolites
221 extracted for LC-MS analysis.

222 A total of 290 putative metabolites were detected across all samples (207 after removing
223 putative metabolites that did not map to metabolic pathways, e.g. peptides and medium
224 components), of which 37 were matched to an authentic standard to confidently predict their
225 identity (S4 Table).

226 80 of the 207 putative metabolites were significantly altered across the dataset (false discovery
227 rate-adjusted $P < 0.05$; one-way repeated measures ANOVA; Fig 2A and S4 Table). To
228 analyse metabolites undergoing similar changes, K-means clustering with Pearson correlation
229 coefficient as the similarity metric was used, highlighting seven clusters with two clusters of

230 particular interest: one containing metabolites that accumulated over time, and the other
231 containing metabolites depleted over time (Fig. 2A). Log₂ fold change (Log₂ FC) between the
232 first and final time points (0 and 56 h, respectively) was also calculated for each metabolite
233 (S4 Table).

234 Glucose, the primary energy source for *T. brucei*, whilst clearly consumed, was not fully
235 depleted after 56 hours in *T. congolense* culture (Log₂ FC: -0.76; Fig 2A and 3A), in contrast
236 to *T. brucei*, where 10 mM glucose is consumed by the same time-point [56]. Ribose,
237 glucosamine, inosine and threonine were similarly depleted in *T. congolense* culture (Log₂ FC:
238 -0.78, -0.97, -2.82 and -0.89, respectively).

239 In contrast, a number of metabolites accumulated in the medium (Fig 2A). The most significant
240 of these were guanine (Log₂ FC: 6.34; Fig 2A and 5A), succinate (Log₂ FC: 5.60; Fig 2A & 3B)
241 and (S)-malate (malate, Log₂ FC: 1.37; Fig 2A and 3B). Interestingly, pyruvate (Log₂ FC: 0.24;
242 Fig 3B) was not excreted at the high levels relative to starting concentration, in contrast to BSF
243 *T. brucei* culture, where pyruvate secretion is consistently observed in both HMI-11 and in
244 Creek's Minimal medium (CMM) [56]. Instead, succinate and malate appear to be the primary
245 glycolytic outputs from BSF *T. congolense*, which is similar to PCF *T. brucei*. Elevated levels
246 of 2-oxoglutarate and a metabolite putatively identified as 2-oxoglutaramate were observed,
247 which potentially originate from alanine aminotransferase activity using L-glutamate and L-
248 glutamine, respectively, as substrates [42, 57]. Moreover, a significant build-up of N6-Acetyl-
249 L-lysine (Log₂ FC: 6.30) was observed (Fig 2B). Whilst the low molecular weight of acetate
250 means it could not be detected by the LC-MS platform used here, concentrations of this
251 molecule were measured directly using an acetate assay in samples taken at the same time
252 points from four independent cultures, which confirmed high levels of acetate excretion by
253 BSF *T. congolense* (Fig 3F).


254 Other notable observations included the depletion of several putative lysophosphatidylcholine
255 species at 56 hours (Fig 2A; S4 Table), as seen in *T. brucei* [56], coincident with increased
256 medium levels of *sn*-glycero-3-phosphocholine, choline and choline phosphate, indicating

257 lyso-phospholipase activity where the charged headgroup moiety of a lyso-species is cleaved
258 from its bound fatty acid [58]. In addition, tryptophan (Log_2 FC: -0.74; Fig 6B; S4 Table) was
259 significantly consumed ($P = 0.042$), in contrast with cysteine (Log_2 FC: -0.07; $P > 0.05$), despite
260 the latter being essential to *T. brucei* [59] (S4 Table).

261 The Log_2 metabolite fold changes after 56 hours of culture of *T. congolense* were compared
262 to those of *T. brucei* grown in HMI-11 (Fig 2B) [56]. A total of 90 metabolites were identified in
263 both datasets, with some showing divergence between the two species (Fig 2B). Several
264 metabolites only accumulated in *T. brucei* supernatant, in particular pyruvate, D-glycerate, 2-
265 oxoglutarate and 12-hydroxydodecanoic acid (Fig 2B). Conversely, succinate, *N*6-acetyl-L-
266 lysine, 4-hydroxy-4-methylglutamate, *N*6,*N*6,*N*6-trimethyl-L-lysine and choline only
267 accumulated in *T. congolense* supernatant (Fig 2B). Whilst cystine (Fig 2B; 12) was depleted
268 in *T. brucei* samples, this metabolite remained unchanged in those from *T. congolense*.


269 In summary, whilst core elements of metabolism have been conserved between BSF *T.*
270 *congolense* and *T. brucei*, several pronounced differences in *T. congolense* metabolism were
271 identified based solely on metabolic input and output in *in vitro* culture. An integrated analysis
272 of the metabolomic and transcriptomic datasets was then undertaken in order to further define
273 the metabolic differences between the two species.


274 **Energy metabolism**

275 As described above, RNA sequencing  and culture supernatant metabolomics provided initial
276 indications that *T. congolense* energy metabolism, specifically with respect to glucose usage,
277 diverges substantially from that characterized in *T. brucei* BSFs (simplified map of glycolysis
278 depicted in Fig 3G).


279 To dissect metabolic differences at the transcriptome level, pathway analysis was carried out
280 using the TrypanoCyc database [60], which contains 186 manually curated pathways covering
281 422 genes or groups of multi-copy genes (S5 Table). These analyses showed broadly similar
282 levels of gene expression of glycolytic components between BSF *T. brucei* and *T. congolense*

283 (Fig 3G and 3I). However, the *T. brucei ex vivo* samples displayed a more distinct expression
284 profile, with low transcript abundances for most glycolytic components compared to all sample
285 groups. This is most likely the result of cells being sampled near peak parasitaemia, and as
286 the pleomorphic strain STIB 247 was used, having a higher proportion of tsetse-transmissible,
287 quiescent short stumpy forms – consistent with this there was elevated expression of stumpy
288 markers such as the PAD array (TbTc_0074), PIP39 (TbTc_0700) and reduced expression of
289 RBP10 (TbTc_0619) (S1 Table) [61-63].

290 Transcripts associated with gluconeogenesis, the succinate shunt, and the acetate generation
291 pathway were upregulated in BSF *T. congolense* under both *in vitro* and *ex vivo* conditions
292 compared to BSF *T. brucei*. Key examples of this are pyruvate phosphate dikinase (PPDK),
293 phosphoenolpyruvate carboxykinase (PEPCK), glycosomal malate dehydrogenase (gMDH)
294 and two subunits of pyruvate dehydrogenase (PDH) (Fig 3I). PPDK was previously reported
295 to be expressed in BSF *T. congolense*, but  BSF *T. brucei* [44], and it may be assumed
296 that the enzyme serves a similar function in BSF *T. congolense* as it does in PCF *T. brucei*; in
297 a mainly glycolytic role to maintain ATP/ADP balance in the glycosome. The high levels of
298 glycosomal MDH expression in BSF *T. congolense* contrasts with BSF *T. brucei*, where gMDH
299 expression is reported to be mostly absent, and cytosolic MDH (cMDH) is the major isoform
300 [64]. The RNAseq analysis also supports a previous study showing high levels of glycerol
301 kinase expression in BSF *T. congolense* [45]. The most recent PacBio assembly of the *T.*
302 *congolense* reference genome indicates that the parasite encodes five copies of PEPCK in
303 tandem array (TcIL3000.A.H_000300300, TcIL3000.A.H_000300400,
304 TcIL3000.A.H_000300500, TcIL3000.A.H_000300600 & TcIL3000.A.H_000300700;
305 compared to one copy in *T. brucei* – Tb927.2.4210; [65]), whilst there are only three copies of
306 glycerol kinase in *T. congolense* (compared to five in *T. brucei* TREU 927).

307 To confirm that the elevated levels of succinate and malate seen in *T. congolense* spent
308 medium samples originated from glucose, LC-MS analysis using ¹³C-U-D-glucose was carried
309 out on intracellular metabolites from cell pellets  extracts. Stable isotope analysis has provided

310 valuable insights into *T. brucei* central carbon metabolism [42], and generating *T. congolense*
311 datasets enabled comparative analysis of glucose catabolism (albeit with an unavoidable
312 difference in medium supplementation of goat serum for *T. congolense*, rather than foetal
313 bovine serum for *T. brucei*).

314 BSF *T. congolense* was grown for 48 hours in a custom medium (SCM-6; S6 Table),
315 containing a total D-glucose concentration of 10 mM in a 1:1 ratio of D-glucose:¹³C-U-D-
316 glucose. Following metabolite extraction, LC-MS analysis was undertaken and the majority of
317 glycolytic intermediates were detected, including ¹³C-labels (Fig 3H). Moreover, labelling ratios
318 of downstream metabolites were largely similar to that of intracellular glucose, and the number
319 of carbons found to be labelled in each metabolite matched t which would be expected in
320 the BSF *T. brucei* glycolytic pathway (i.e. three ¹³C atoms in all metabolites downstream of
321 glyceraldehyde 3-phosphate and glycerol-3-phosphate). Similar to *T. brucei*, a high
322 percentage of 3-carbon labelled fructose-1,6-bisphosphate (FBP) (34.8%) was observed in *T.*
323 *congolense* (Fig 3H), probably a result of the “reverse” aldolase reaction occurring in the
324 glycosome [42]. Importantly, two-carbon labelling was observed in several acetylated
325 compounds (N-acetyloronithine & N-acetyl-L-lysine; Fig 3H), confirming that acetyl groups used
326 to generate these metabolites originate from D-glucose. Although acetyl-CoA, the product of
327 pyruvate oxidation, was not detected for technical reasons, labelling of acetylated metabolites
328 indicate that glucose-derived pyruvate is used to generate acetyl-CoA and subsequently
329 acetate in the mitochondrion, similar to other trypanosomatids. Taken together, these data
330 indicate that the flow of carbon atoms for glycolytic components in *T. congolense* is very similar
331 to that in *T. brucei*. However, the metabolic outputs differ drastically from BSF *T. brucei* and
332 appear to be more similar to PCF *T. brucei*.

333 To determine whether the elevated succinate in supernatants originated from glucose
334 catabolism, metabolite labelling was corrected for the 1:1 (50%) ratio of natural glucose to ¹³C-
335 U-D-glucose, which equated to a mean percentage labelling of 43.1% (the value is less than
336 50% due to D-glucose in the serum). All glycolytic metabolites up to pyruvate showed >90%

337 labelling when corrected (for glucose 6-phosphate and fructose-1,6-bisphosphate, both 3-
338 carbon and 6-carbon labels were taken into account), although glycerol and glycerol 3-
339 phosphate exhibited 57.2% and 64.4% labelling, respectively, as these metabolites can also
340 be obtained from catabolism of lipid precursors. Moreover, 40.1% (93.0% corrected) labelling
341 was detected in L-alanine, suggesting that the alanine aminotransferase reaction that utilizes
342 pyruvate to generate 2-oxoglutarate and L-alanine in both BSF and PCF *T. brucei*, also occurs
343 in BSF *T. congolense* [42, 66]. For both succinate and malate, 3 carbons are derived from
344 glucose and these metabolites showed 33.6% (78.1% corrected) and 26.0% (60.3%
345 corrected) labelling, respectively. These results suggest that glucose is not the only source of
346 intracellular succinate and malate in *T. congolense*. However, these values were higher than
347 those reported in *T. brucei* (70% and 52% for malate and succinate, respectively [42]).

348 Whilst PCF *T. brucei* exhibit citric acid (TCA) cycle activity, this pathway is not used to
349 catabolize glucose [35]. Similarly, no citric acid cycle intermediate isotopologues (e.g. citrate)
350 were found when BSF *T. congolense* were incubated with ¹³C-U-D-glucose, although small
351 amounts of 2-carbon labelled succinate and malate were observed (Fig 3H). This is similar to
352 BSF *T. brucei* [42], indicating that, like *T. brucei*, *T. congolense* does not appear to couple
353 glycolysis to TCA metabolism and instead directs high amounts of pyruvate through PDH into
354 acetyl-CoA and acetate. Taken together, these data suggest that BSF *T. congolense* both
355 from *in vitro* cultures and *in vivo* infection metabolically resemble an intermediate between
356 BSF and PCF *T. brucei*, with moderate glycolytic capacity and significant levels of succinate
357 shunt activity (glycosomal, rather than mitochondrial; S1 Table) as well as a highly active
358 mitochondrial acetate generating pathway.

359 Previous work has shown that reduction of glucose concentrations in BSF *T. brucei* culture
360 from 10 mM to 5 mM leads to decreased cellular motility, reduction in growth and cell body
361 rounding morphology within 8 hours [67]. Given that glucose was not substantially depleted in
362 *T. congolense* cultures after 56 h, we tested the effect of reduced glucose concentrations on
363 *T. congolense* viability. Unlike *T. brucei*, *T. congolense* was able to maintain a growth rate

364 equal to controls at concentrations as low as 2 mM (Fig 4A) when continuously passaged with
365 no observable change in morphology or motility. To test whether glycolysis was essential in
366 *T. congolense*, cells were incubated with D-glucose in addition to varying concentrations of 2-
367 deoxy-D-glucose (2DG), which can be internalised, but not metabolised further than 2-deoxy-
368 D-glucose 6-phosphate, thereby inhibiting glycolysis and pentose phosphate pathway
369 metabolism (Fig 4B). Incubation of *T. congolense* in medium supplemented with 2DG (in
370 addition to 10 mM glucose) led to growth defects in a dose dependent manner, likely due to
371 2DG being outcompeted by glucose at lower concentrations (Fig 4B). Although the growth
372 defect was minor in the presence of 1 mM 2DG, there was a more pronounced reduction with
373 5 mM 2DG. When equimolar concentrations of glucose and 2DG were used, growth was
374 repressed and cell death occurred within 48 hours (Fig 4B). *T. congolense* viability was also
375 tested in SCM-6 in the presence of N-acetyl-D-glucosamine (GlcNAc), a sugar that inhibits
376 glucose uptake [68] (S2 Fig). In the presence of 60 mM GlcNAc with 10 mM glucose, there
377 was a moderate, yet significant ($P < 0.0001$ at 96 h, *t*-test of cell densities) growth defect in *T.*
378 *congolense* (S2 Fig). Viability was further reduced when the same concentration of GlcNAc was
379 used alongside 2 mM glucose ($P < 0.0001$ at 96 h, *t*-test of cell densities), the lowest
380 concentration *T. congolense* could tolerate (S2 Fig). The rate of glucose consumption was
381 measured by assaying glucose concentrations in cell culture supplemented with 4 mM
382 glucose, and shown to be $47.17 \pm 27.91 \text{ nmol}^{-1} \text{ min}^{-1} 10^8 \text{ cells}$ in *T. congolense*, significantly
383 lower than the rate ($132.18 \pm 16.31 \text{ nmol}^{-1} \text{ min}^{-1} 10^8 \text{ cells}$) in *T. brucei* ($n = 4$, $P = 0.0039$; *t*-
384 test).

385 To further probe glycolytic metabolism in BSF *T. congolense*, several targets were selected
386 for RNAi-mediated knock-down, using a tetracycline-inducible *T. congolense* line expressing
387 T7 polymerase and Tet repressor under puromycin selection (TcoSM [69]). Given that the
388 majority of both malate and succinate appear to originate from glucose catabolism, the effect
389 of reducing expression levels of two proteins involved in the succinate shunt, PEPCK and
390 PPK (TcIL3000.A.H_000922100 – both expressed at high levels in *T. congolense*; Fig 3I),

391 was tested in separate experiments (Fig 4C, D). RNAi was induced by addition of 1 µg/mL
392 tetracycline, and cell growth in culture and transcript abundance measured by qPCR were
393 monitored every 24 hours (Fig 4C, D). Creek *et al* showed that PEPCK is essential in BSF *T.*
394 *brucei*, even though the levels of succinate generated through this pathway are negligible [42].
395 In BSF *T. congolense*, RNAi targeting the five copies of PEPCK reduced overall *PEPCK*
396 transcript abundance by approximately 50% (mean transcript levels of 60%, 46% and 63%
397 compared to uninduced controls at 24, 48 and 72 h post-induction, respectively; Fig 4E),
398 leading to a small but non-significant reduction in growth rate (Fig 4C; $P = 0.0689$, *t*-test at the
399 96 h time-point). PPDK expression is not detected in BSF *T. brucei* but is expressed in the
400 PCF stage [44]. Knock-down of PPDK in *T. congolense* did not affect parasite viability or
401 growth rate (Fig 4D), although similar levels of transcript knockdown were observed (mean
402 transcript levels of 67%, 64% and 50% compared to uninduced controls at 24, 48 and 72 h
403 post-induction, respectively; Fig 4F).


404 RNAi was also used to knock down expression of the hexose transporter (HT) array,
405 specifically those matching the THT1 and THT2 array in *T. brucei* (TcIL3000.A.H_000260500,
406 TcIL3000.A.H_000260600, TcIL3000.A.H_000794500, TcIL3000.A.H_000794600,
407 TcIL3000.A.H_000794700), which has been shown to significantly restrict growth of BSF *T.*
408 *brucei* [70]. Whilst growth rate was unaffected in BSF *T. congolense* (Fig 4G), induction of HT
409 RNAi led to a reduction in transcript abundance at all time points (mean transcript levels of
410 83%, 75%, 68% and 65% compared to uninduced controls at 24, 48, 72 and 96 h post-
411 induction, respectively; Fig 4H). Glucose uptake was decreased (mean reduction of 37% in
412 uptake compared to uninduced controls after 72 h; Fig 4I), suggesting that either lower levels
413 of glucose are sufficient for energy generation in *T. congolense*, or the parasite can utilize
414 other carbon sources for ATP production. These alternatives sources could include serum
415 components such as fatty acids or amino acids, both of which trypanosomatids have been
416 reported to utilise [71, 72].

417 PCF *T. brucei* express most components of the electron transport chain (ETC) to generate
418 ATP through oxidative phosphorylation, in contrast to BSF *T. brucei*, which do not detectably
419 express any ETC components with the exception of the reversed F_1F_0 -ATPase and alternative
420 oxidase [73]. As mentioned previously, BSF *T. congolense* is thought to express a complex I
421 NADH dehydrogenase, but it is not known whether BSF *T. congolense* has capacity for
422 oxidative phosphorylation. Transcriptomics analysis of the ETC was attempted, using a gene
423 list generated by Zikova and colleagues [73], but no significant patterns could be discerned
424 (S1 Table, S3 Fig).

425 **Nucleotide metabolism**

426 Metabolomic analysis of BSF *T. congolense* culture supernatants indicated a significant
427 uptake of exogenous ribose, a contributor to nucleotide metabolism via uptake, or via the
428 pentose phosphate pathway (PPP; Fig 5A and Fig 2A). Whilst guanosine was not detected in
429 the supernatant, significant accumulation of guanine (Fig 5B) was observed, suggesting either
430 excretion of this metabolite, or, hydrolysis of guanosine through parasite-secreted
431 hydrolases/nucleosidases (previously identified in BSF *T. brucei* secretomes [74, 75]). This
432 mechanism would enable uptake of guanine and other nucleobases through nucleobase
433 transporters, for which multiple orthologues have been identified in the *T. congolense* genome
434 [18] through homology with known *T. brucei* nucleobase transporters TbNT8.1 and TbNBT1
435 [76, 77]. In addition, there was an accumulation of xanthine, a product of xanthosine
436 hydrolysis, and depletion of inosine, an important nucleoside composed of hypoxanthine and
437 ribose (Fig 5C and 5D). The nucleoside cytidine and the nucleobase hypoxanthine were also
438 detected, but appeared to remain unchanged during the time course, although the latter was
439 a medium supplement potentially added in excess (S4 Table). It is noteworthy that only a
440 single nucleoside transporter gene (TbTc_1072; *T. congolense* gene IDs:
441 TcIL3000.A.H_000665800 and the pseudogene TcIL3000.A.H_000679300; S2 Table) can be
442 identified in *T. congolense*, a syntenic homologue of TbNT10 [18], functionally characterized
443 as a P1-type purine nucleoside transporter [78], and is thus unlikely to transport cytidine [79].

444 Purine salvage is an essential process in trypanosomatids, as they lack the *de novo* synthesis
445 pathway for the purine ring [80], and previous analysis of cell pellets to investigate intracellular
446 nucleotide metabolism utilizing ¹³C-U-D-glucose in BSF *T. brucei* showed purine salvage
447 pathways incorporating 5-carbon labelled ribose derived from glucose [42] (Fig. 5F). Whilst
448 the ribose incorporated into these nucleosides originates almost exclusively from glucose in
449 *T. brucei* (Fig 5F), *T. congolense* appears to use far less glucose-derived ribose to make
450 purine nucleosides such as adenosine, guanosine and inosine (Fig 5F).

451 Transcriptomics analyses indicated upregulation of genes associated with generation of
452 adenosine nucleotides (Fig 5G; red vertical bar), especially in *ex vivo* *T. congolense*, as well
453 as hypoxanthine-guanine phosphoribosyltransferase and uracil phosphoribosyltransferase.
454 Upregulation of nucleoside hydrolases and phosphoribosyltransferases supports previous
455 the  findings based upon genome content that *T. congolense* has a capacity for nucleobase uptake
456 [18].

457 The purines guanosine and inosine, which incorporate glucose-derived ribose in *T. brucei*,
458 were almost entirely unlabelled in *T. congolense* (Fig 5F). However, the phosphorylated
459 nucleosides GMP, GDP and GTP all incorporate glucose-derived carbon atoms, presumably
460 through ribose. Given the labelling patterns seen in adenosine, one possible explanation could
461 be conversion of AMP to inosine monophosphate (IMP; adenosine monophosphate
462 deaminase; TbTc_0145), IMP to xanthosine monophosphate (IMP dehydrogenase;
463 TbTc_1648) and XMP to GMP (GMP synthase; TbTc_1452). However, only one of these
464 enzymes, GMP synthase, was expressed at higher abundance in *T. congolense* (Log₂ fold
465 change: 1.56 and 2.02 for *ex vivo* and *in vitro*, respectively). Overall, incorporation of glucose-
466 derived carbons into purine nucleosides is reduced in *T. congolense* compared to *T. brucei*. It
467 should be noted that in both experiments, there was no ribose supplementation in the media
468 Of the pyrimidines, uracil and its derivatives were detected during the glucose labelling
469 experiment (S4 Fig). Uracil is known to be the main pyrimidine salvaged by other
470 kinetoplastids including *T. brucei* [81-83]. Whilst the majority of the uridine, UMP, UDP and

471 UTP pools incorporate glucose-derived ribose (five ¹³C labels), 5-carbon isotopologues of
472 these pyrimidines were reduced in abundance in *T. congolense* compared to *T. brucei*.
473 Instead, 2-carbon labelled isotopologues appeared to comprise the majority of uridine, uracil
474 and their nucleotides (S4 Fig).

475 Whilst uracil biosynthesis is not essential in *T. brucei* [84], the uracil pool in *T. congolense*
476 appears to derive almost entirely from glucose, when corrected for 50% glucose labelling (76%
477 in *T. congolense* vs 44% in *T. brucei* [42]; S4 Fig), suggesting that this species predominantly
478 synthesizes uracil from orotate to UMP (orotate phosphoribosyltransferase/orotidine 5-
479 phosphate decarboxylase; TbTc_0735) and from UMP to uracil (uracil
480 phosphoribosyltransferase; TbTc_4220), as can occur in *T. brucei* [42]. Both these genes are
481 expressed at higher abundance in *T. congolense*, both *in vitro* and *ex vivo*, compared to *T.*
482 *brucei* (Fig 5G, S1 Table), which could explain the increased isotopologue labelling. Uridine
483 nucleosides (UMP, UDP, UTP) all show a similar pattern, with significant 2-carbon labelling,
484 as well as moderate levels of 5-carbon labelling from incorporation of glucose-derived ribose
485 (S4 Fig).

486 These data indicate that, at least under the growth conditions used here, BSF *T. congolense*
487 favours purine nucleoside/nucleotide synthesis from nucleobases with a reduced dependence
488 on glucose-derived ribose 5-phosphate, in addition to *de novo* synthesis of orotate, uracil and
489 uridine nucleosides. However, the difference in serum requirements for the two organisms is
490 a confounding factor to the interpretation of this difference.

491 **Amino acid metabolism**

492 It is well established that trypanosomatid parasites scavenge amino acids, key nutrients for
493 survival, from their hosts [85, 86]. Therefore, comparative analyses of *T. congolense* and *T.*
494 *brucei* amino acid metabolism were undertaken. Whilst the majority of amino acids were
495 detected during the supernatant time course, relative abundances in the medium did not vary
496 greatly after 56 hours of *in vitro* culture (Fig 6A–C, S4 Table). The greatest reductions were
497 observed in threonine (Log₂ FC after 56 hours: -0.89; Fig 6A), tryptophan (Log₂ FC: -0.74; Fig

498 6B), glutamine (Log₂ FC: -0.39), asparagine (Log₂ FC: -0.35) and phenylalanine (Log₂ FC: -
499 0.35). Interestingly, cysteine, an essential factor for the *in vitro* culture of *T. brucei*, was not
500 significantly consumed by 56 hours (Log₂ FC: -0.07; Fig 6C). However, at least low-level
501 exogenous cysteine is still required to sustain parasite growth *in vitro*, as viability was
502 significantly affected in the absence of cysteine (for both 1.5 mM and 1 mM vs 0 mM cysteine,
503 $P < 0.0001$, *t*-test of cells densities at 96 h; S5 Fig). Experiments were carried out to test the
504 essentiality of all other individual amino acids (with the exception of glutamine, known to be
505 an important amino donor in trypanosomatid metabolism). Using the minimal medium SCM-6,
506 cell viability was monitored for 72 hours in the absence of specific amino acids. Removal of
507 the following amino acids from culture medium led to defects in growth over 72 hours:
508 asparagine, histidine, isoleucine, leucine, methionine, proline, serine, tyrosine and valine (Fig
509 6D–G). Whilst aspartate appeared to be depleted in spent culture supernatants (S4 Table),
510 this also occurred in the medium only control. Furthermore, removal of aspartate did not lead
511 to reduced cell viability or growth rate in culture (Fig 6F). Long term culture was impossible
512 without the addition of phenylalanine and threonine, leading to a final culture formulation,
513 SCM-7 (S6 Table) containing a total of 14 amino acids. Therefore, BSF *T. congolense* appears
514 to require a higher number of amino acids than BSF *T. brucei*, at least *in vitro*, with CMM
515 containing only 8 amino acids in total, including cysteine and glutamine [56]. To further probe
516 amino acid metabolism, pathway analysis was carried out on the transcriptome (S6 Fig) and
517 metabolome (Fig 6; S6, S7 Fig).

518 BSF *T. brucei* utilizes exogenous L-glutamine as the primary source of intracellular glutamate
519 and 2-oxoglutarate and produce significant levels of glutamine-derived succinate [42, 85] (Fig
520 6I). Given the high levels of succinate excreted by *T. congolense*, stable isotope labelling was
521 used to determine the contribution of L-glutamine to this pool. *T. congolense* was incubated
522 for 48 hours with 1 mM ¹³C-U-L-glutamine and cell pellets analysed by LC-MS. Results
523 indicated the presence of biochemical activities consistent with those observed in *T. brucei*.
524 Significant glutamine-derived carbon labelling was detected after 48 h incubation for succinate

525 (41.3%, 48.5% corrected), glutamate (76.1%, 89.2% corrected), 2-oxoglutarate (80.5%,
526 94.3% corrected) and succinate semialdehyde (94.7% corrected; Fig 6I). As would be
527 anticipated, labelling of glutathione (86.1%) and trypanothione (98.4%) from glutamine
528 through glutamate were also observed (S7 Fig). No labelling of malate or aspartate was seen
529 in this study, despite the use of high concentrations of ^{13}C -U-L-glutamine compared to the
530 equivalent study performed in *T. brucei* with a 50:50 ratio of ^{13}C -U-L-glutamine [85].

531 The apparent essentiality of several amino acids was also investigated using stable isotope
532 labelling. Proline is an essential carbon source for PCF but not BSF *T. brucei* [87]. However,
533 removal of proline from BSF *T. congolense* medium led to reduced growth (Fig 6F). RNAi-
534 mediated knock-down of proline metabolism (specifically pyrroline-5-carboxylate
535 dehydrogenase, TbP5CDH) in PCF *T. brucei* has highlighted the requirement of proline
536 metabolism for mitochondrial function [87]. Indeed, both P5CDH (TbTc_1695) and proline
537 dehydrogenase (TbTc_1591) expression were upregulated in *ex vivo T. congolense*,
538 compared to *T. brucei*, suggesting that proline catabolism was more active (S1 Table and S6
539 Fig). However, ^{13}C -U-L-proline labelling showed that this amino acid did not contribute to the
540 biosynthesis of other metabolites (S8 Fig). Therefore, the apparent requirement for proline in
541 BSF *T. congolense* may be for the purposes of polypeptide synthesis only.

542 As in *T. brucei*, glucose-derived carbon usage was detected in several amino acids in *T.*
543 *congolense* (S6A Fig). Aspartate (a precursor for pyrimidine nucleotide biosynthesis) and
544 alanine (a by-product of a pyruvate-utilising aminotransferase reaction) (S6A Fig) exhibited 3-
545 carbon isotopologues derived from ^{13}C -U-D-glucose. However, in *T. brucei*, a small proportion
546 of L-asparagine labelling was observed (1.2% 3-carbon labelling) [42], whilst none was
547 observed in *T. congolense* (S6A Fig). The metabolism of asparagine has not been studied in
548 African trypanosomes; given the reduction of cell growth in the absence of this amino acid (Fig
549 6F), labelling with ^{13}C -U-L-asparagine was performed, but no other labelled metabolites were
550 detected (S8 Fig). This indicates that, as with proline, protein synthesis is the sole role of
551 asparagine in *T. congolense*. The reduced expression of asparagine synthetase (TbTc_4894;

552 TcIL3000.A.H_000497800), which converts aspartate to asparagine (S6 Fig), suggests that
553 BSF *T. congolense* may rely upon scavenging of exogenous asparagine.

554 Serine was also shown to be essential to *T. congolense* (Fig 6F), in contrast to minimal
555 culturing requirements for *T. brucei* [56]. ¹³C-U-L-serine labelling indicated that *T. congolense*
556 L-serine metabolism mirrors that of *T. brucei* in several aspects, such as *de novo* sphingolipid
557 biosynthesis, with 70.0% 2-carbon labelling of sphinganine and downstream labelling of
558 ceramide and sphingomyelin species (S8 Fig). Similarly, phosphatidylserine decarboxylase
559 activity was evidenced at both transcript and metabolite levels, with 40.1% 2-carbon labelling
560 of glycerol-phospho-ethanolamine (S1 Table; S8 Fig). However, L-serine also has a minor role
561 in S-adenosyl-L-homocysteine detoxification, where serine-derived carbon ultimately
562 contributes to cysteine biosynthesis. In *T. congolense*, serine-derived carbon labelling can be
563 detected in cystathionine (18.1%) and cysteine (16.7%), through to glutathione (4.1%) and
564 trypanothione disulfide (3-carbon labelled, 6.8%; 6-carbon labelled, 0.02%; S7 Fig). Therefore,
565 the inability to exclude L-serine from *T. congolense in vitro* culture media may primarily be
566 attributable to lipid metabolism and an increased demand for serine-derived cysteine,
567 potentially over exogenously obtained cysteine, depending on bioavailability. Indeed,
568 metabolomics analysis of culture medium indicates that the ability of *T. congolense* to take up
569 cysteine from its environment may be lower than in *T. brucei* (Fig 6C).

570 Although L-cysteine is primarily a source of sulphur for trypanosomatids, we also investigated
571 the carbon contribution of this amino acid in *T. congolense*, and in particular, whether L-
572 cysteine-derived carbon atoms contribute to the biosynthesis of glutathione and trypanothione.
573 ¹³C-U-L-cysteine stable isotope labelling experiments were performed (S7 and S8 Fig). Direct
574 replacement of the 1.5 mM L-cysteine present in SCM with ¹³C-U-L-cysteine led to high levels
575 of labelling in glutathione and trypanothione disulfide (S7B Fig). This indicates that *T.*
576 *congolense* can readily take up and metabolize exogenous cysteine, even though abundance
577 of the amino acid is not reduced significantly over 56 hours of parasite *in vitro* culture. Although
578 no clear pattern could be observed in transcriptomic analysis of the trypanothione biosynthesis

579 pathway, both trypanothione synthase (TRY5; TbTc_1359) and trypanothione reductase
580 (TRYR; TbTc_4239) were expressed at high levels in *in vitro* *T. congolense* cells relative to
581 *ex vivo* cells, indicating that under *in vitro* conditions, cells may be subjected to higher levels
582 of oxidative stress (S7C Fig).

583 **Fatty acid metabolism in *T. congolense***

584 Lipids have a variety of crucial roles in trypanosomes, as a major constituent of membranes
585 and under certain conditions, for energy [72]. BSF *T. brucei* require large quantities of myristic
586 acid in particular, for the synthesis of glycosylphosphatidylinositol (GPI) that anchors the
587 parasite's major surface glycoprotein antigens [88]. To do this, BSF *T. brucei* both synthesises
588 and scavenges myristic acid. Glucose labelling experiments in *T. brucei* have shown that
589 myristic acid is partially synthesized from glucose-derived carbon through acetyl-CoA, using
590 a system of fatty acid elongases [89] (Fig 7A). However, no fatty acid carbon labelling was
591 detected after incubation of *T. congolense* with ¹³C-U-D-glucose (Fig 7A), unlike *T. brucei* [42].
592 Carbon dissemination was also investigated from threonine, which is used as a source of
593 acetate, and thus, lipids [90] (Fig 7B). Similarly, no saturated lipid carbon labelling was
594 observed, suggesting that *T. congolense* either uses alternative sources of carbon for lipid
595 biosynthesis, or does not rely on acetate as a source of lipids in the same way as *T. brucei*
596 [30].

597 While acetate/acetyl-CoA metabolism is highly active at the level of gene expression in *T.*
598 *congolense* compared to *T. brucei* (Fig 7C), consistent with metabolic data, expression of
599 acetyl-CoA synthetase (TbTc_0318), a key enzyme in lipid biosynthesis from acetate, is
600 reduced in both *ex vivo* and *in vitro* *T. congolense* (Fig 7C). Furthermore, an acetyl-CoA
601 thioesterase (TbTc_5515) that is involved in ATP synthesis-uncoupled acetate production in
602 PCF *T. brucei* [91] is also expressed at lower levels in *T. congolense* (Fig 7B). Other enzymes
603 involved in fatty acid biosynthesis, namely acetyl-CoA carboxylase (TbTc_0754), β -ketoacyl-
604 CoA synthase (TbTc_3372) and β -ketoacyl-CoA reductase (TbTc_1241), were all expressed
605 at lower abundance in *T. congolense* than *T. brucei*, in particular in *ex vivo* cells (Fig 7C). Of

606 the four elongases, ELO1 (TbTc_0159) and ELO2 (TbTc_1882) were expressed at equal
607 levels in BSF *T. congolense*, compared to BSF *T. brucei* (S1 Table). Whilst expression of
608 ELO3 (TbTc_0235) appeared to be reduced in *T. congolense* (Log₂ fold change of -1.98 and
609 -1.62 compared to *T. brucei* for *in vitro* and *ex vivo*, respectively; S1 Table), *T. congolense*
610 cells expressed higher levels of ELO4 (TbTc_0737) in both *in vitro* and *ex vivo* conditions,
611 compared to *T. brucei* (Log₂ fold change: 1.39 and 1.38 for *in vitro* and *ex vivo* comparisons,
612 respectively)

613 The variation in observed gene expression associated with the sterol pathway appeared to
614 correlate with sample condition rather than species (Fig 7C). However, *T. congolense*
615 transcripts for genes involved in lanosterol synthesis were reduced, especially under *in vitro*
616 conditions (squalene synthase, SQase, TbTc_2577; squalene monooxygenase, SM,
617 TbTc_3357; lanosterol synthase, LSS, TbTc_4540; Fig 7C).

618 Fatty acid oxidation was recently confirmed to be an energy source for *T. brucei* residing in
619 adipose tissue [72]. Transcripts associated with this pathway were less abundant in *T.*
620 *congolense* compared to *T. brucei* under both conditions (Fig 7C), suggesting this may not be
621 an energy-generating pathway in glucose-rich culture medium, or under the *in vivo* conditions
622 from which they were sampled. However, capacity for ATP generation from fatty acid oxidation
623 should not be ruled out.

624 **Exploiting differences in metabolism for pharmacological intervention**

625 Differences in metabolism between *T. congolense* and *T. brucei* have implications for
626 differential drug efficacy between the two species. To validate our findings in key areas of
627 metabolism, pharmacological inhibition was attempted for specific targets in trypanosome
628 metabolism, in order to compare inhibitory concentrations (EC₅₀).

629 To assess whether areas of mitochondrial metabolism were required more in BSF *T.*
630 *congolense* than in BSF *T. brucei*, both species were treated with FCCP, an uncoupling agent
631 that depolarises the mitochondrial membrane. However, there was no difference in sensitivity

632 between the species (EC_{50} : $13.0 \pm 5.0 \mu\text{M}$ and $12.6 \pm 5.3 \mu\text{M}$ for *T. brucei* and *T. congolense*,
633 respectively; Table 1). Given both metabolic and transcriptomic data indicated no increased
634 electron transport chain activity, we also treated with the complex III inhibitor antimycin A,
635 again with no significant differences seen between the species (Table 1). In addition, there
636 was no change in sensitivity to azide, an inhibitor of ATP hydrolysis by the F_1 -ATPase (Table
637 1). However, *T. congolense* appeared to be less sensitive to rotenone, a complex I NADH
638 dehydrogenase inhibitor (Table 1). Previous data inferred complex I activity in BSF *T.*
639 *congolense* based on nitroblue tetrazolium staining [48]. Rotenone resistance could indicate
640 NADH dehydrogenase activity of a rotenone-insensitive NADH dehydrogenase, such as the
641 inner membrane space-facing NDH2 [92]. *T. congolense* also showed enhanced sensitivity to
642 salicylhydroxamic acid (SHAM), an inhibitor of the trypanosome alternative oxidase (TAO;
643 Table 1). Taken together, these data indicate that, like *T. brucei*, *T. congolense* does not rely
644 on oxidative phosphorylation for ATP production, as indicated by transcriptomics analysis, and
645 that, as previously reported, TAO is the terminal oxidase [48, 51].

Compound	Target	<i>T. congolense</i> EC_{50} Mean \pm SEM	<i>T. brucei</i> EC_{50} Mean \pm SEM	Fold change (Tc/Tb)	P value (t-test)
Antimycin	Complex III	$271.2 \pm 143.5 \mu\text{M}$	$144.2 \pm 18.1 \mu\text{M}$	1.9	0.4295
FCCP	Uncoupling agent	$12.6 \pm 5.3 \mu\text{M}$	$13.0 \pm 5.0 \mu\text{M}$	1.0	0.9592
Azide	F_1 -ATPase	$432.3 \pm 127.9 \mu\text{M}$	$235.0 \pm 6.0 \mu\text{M}$	1.8	0.1982
Oligomycin	Complex V (F_0 ATPase)	$33.9 \pm 14.1 \text{ nM}$	$197.6 \pm 39.0 \text{ nM}$	0.2	0.0169
Rotenone	Complex I	$27.4 \pm 1.4 \mu\text{M}$	$7.4 \pm 0.9 \mu\text{M}$	3.7	0.0003
SHAM	TAO	$14.4 \pm 0.5 \mu\text{M}$	$26.0 \pm 1.5 \mu\text{M}$	0.6	0.0004
UK5099	Pyruvate transport	$82.1 \pm 8.8 \mu\text{M}$	$130.0 \pm 5.0 \mu\text{M}$	0.6	0.0091
ACS inhibitor	Acetyl-CoA synthetase	$57.7 \pm 15.2 \mu\text{M}$	$7.1 \pm 2.4 \mu\text{M}$	8.1	0.0304
Orlistat	Fatty acid synthase/lipases	$15.6 \pm 2.5 \mu\text{M}$	$0.02 \pm 0.01 \mu\text{M}$	780.0	0.0033
Diminazene	Kinetoplast	$50.0 \pm 5.6 \text{ nM}$	$32.0 \pm 0.5 \text{ nM}$	1.6	0.0425

646 **Table 1: Comparative analysis of sensitivity to metabolic inhibitors in *T. congolense***
647 **and *T. brucei*.** Abbreviations: SHAM, salicylhydroxamic acid; LCFA, long-chain fatty acid

648

649 Metabolomics and transcriptomics data indicated that *T. congolense* direct pyruvate towards
650 mitochondrial metabolism, with high transcript levels in PDH and enzymes involved in acetate
651 generation, compared to *T. brucei* (Fig 3 and 7). We therefore hypothesised *T. congolense* to
652 be more sensitive to inhibition of mitochondrial pyruvate uptake and to investigate this further,
653 we tested drug sensitivities for UK5099, an inhibitor of mitochondrial pyruvate transport [93].
654 As expected, *T. congolense* (EC₅₀: 82.1 μM) was significantly more sensitive ($P = 0.0091$,
655 unpaired *t*-test) to UK5099 compared to *T. brucei* (130.0 μM; Table 1).

656 Whilst acetate generation appears to be important in *T. congolense*, our data suggest that the
657 acetate does not appear to be utilised for the biosynthesis of fatty acids, in contrast to what
658 has been shown for *T. brucei*. To probe this further, we compared drug sensitivity of the two
659 species with compounds targeting fatty acid synthesis (Fig 8). Indeed, *T. congolense* was
660 significantly more resistant than *T. brucei* to an acetyl-CoA synthetase inhibitor (ACS inhibitor;
661 1-(2,3-di(thiophen-2-yl)quinoxalin-6-yl)-3-(2-methoxyethyl)urea, [94]; Fig 8A; Table 1),
662 indicating that acetyl-CoA synthetase is far less essential to this species. ACS is essential to
663 both BSF and PCF *T. brucei* [30, 95], thus indicating a key metabolic difference between the
664 species.

665 We next compared drug sensitivity to Orlistat, an inhibitor of fatty acid synthase and
666 phospholipase [32]. Here, a striking difference was found, with *T. congolense* exhibiting
667 significantly less sensitivity (780-fold increase in EC₅₀) to the compound compared to *T. brucei*
668 (Fig 8B; Table 1), providing further evidence that *T. congolense* primarily relies on fatty acid
669 scavenging, instead of synthesis, as predicted by the combination of metabolomics and
670 transcriptomics.

671 **Discussion**

672 The protozoan parasite *T. congolense* is a principal cause of AAT, but crucially, *T. brucei*
673 remains the dominant model for laboratory-led studies of African trypanosomes, even in the
674 face of mounting evidence that *T. brucei* and *T. congolense* differ profoundly in many facets

675 of their biology. In order to facilitate the identification and development of potential drug targets
676 for *T. congolense*, a detailed understanding of the fundamental cellular metabolism, leading
677 to an understanding of both the differences and commonalities between *T. congolense* and *T.*
678 *brucei*, would be a significant step forward. Thus, this study aimed to generate a detailed
679 comparison of metabolism in *T. congolense* and *T. brucei*, through a combination of
680 metabolomics, transcriptomics and gene knockdown approaches. Based on these
681 comparisons, areas of metabolism were further probed with chemical inhibition, in order to
682 validate findings.

683 Transcriptomic data was generated from *T. congolense* and *T. brucei* with parasite samples
684 isolated from both *in vitro* culture and purified from *in vivo* murine infections (*ex vivo*). Crucially,
685 there were high levels of correlation between *ex vivo* and *in vitro* *T. congolense* samples,
686 indicating that the cultured form of the parasite closely resembles the *in vivo* situation, at a
687 transcriptomic level. In contrast, there was lower inter-species correlation between *T. brucei*
688 and *T. congolense*.

689 To complement the transcriptomic data, several metabolomic analyses were carried out to
690 gain an understanding of specific areas of metabolism. These data demonstrate that BSF *T.*
691 *congolense*, while possessing some metabolic similarities with BSF *T. brucei* (as expected),
692 differs substantially in several core components, including in having a reduced reliance on
693 glucose, excretion of distinct glycolytic end products (acetate, malate and succinate in *T.*
694 *congolense* compared to pyruvate in *T. brucei*), and increased gene expression and metabolic
695 signatures of specific mitochondrial pathways, in particular pyruvate to acetate conversion.
696 Additionally, we show increased reliance on exogenous substrates such as ribose for
697 nucleotide synthesis as demonstrated by reduced glucose-derived carbon labelling in
698 nucleoside species in addition to upregulation of hydrolases and phosphoribosyltransferases.
699 Furthermore, while there is overlap in amino acid utilisation (e.g. glutamine), *T. congolense*
700 relies on more exogenous amino acids than *T. brucei*. Surprisingly, this included serine which,
701 in the case of *T. congolense*, appears to be important in the transsulfuration pathway that is

702 geared towards trypanothione biosynthesis. This may also explain the observed decreased
703 reliance on exogenous cysteine. Unlike *T. brucei*, *T. congolense* also requires asparagine and
704 proline for viable *in vitro* culture, although carbon usage from these amino acids is minimal.
705 Finally, *T. congolense* exhibits increased acetate/acetyl-CoA metabolism compared to *T.*
706 *brucei*, despite a reduction in fatty acid biosynthesis through the classical trypanosomatid
707 pathways involving acetyl-CoA synthase, acetyl-CoA carboxylase, β -ketoacyl-CoA synthase
708 and β -ketoacyl-CoA reductase, the expression of which are reduced in *T. congolense* (both in
709 *ex vivo* and *in vitro* conditions). This is further underlined by lack of glucose-derived 2-carbon
710 labelling of fatty acids, most notably myristic acid, a key GPI anchor component of variant
711 surface glycoproteins of *T. brucei* and *T. congolense* [96]. However, fatty acid elongase 4,
712 previously shown to extend exogenously scavenged arachidonic acid (C22:4) to
713 docosatetraenoic acid (C22:4) [97], is upregulated under *in vitro* conditions, compared to *T.*
714 *brucei*, which may indicate a reliance on long-chain polyunsaturated fatty acids. These findings
715 are shown in a summary figure of *in vitro* transcriptomics data (Fig 9)

716 Analyses of culture supernatants showed that 10 mM glucose was not substantially depleted
717 after *T. congolense* cultures reached high cell density, as would be expected from an
718 equivalently dense *T. brucei* culture [56]. *T. brucei* requires at least 5 mM glucose in culture
719 [67], whereas BSF *T. congolense* were viable and maintained doubling times in levels as low
720 as 2 mM. Furthermore, confirming conclusions from one previous study on BSF *T. congolense*
721 [43], the primary metabolic outputs *in vitro* were (S)-malate, succinate and acetate, in contrast
722 to *T. brucei*, in which the main output is pyruvate, which is excreted in large amounts [42, 56].
723 Interestingly, we observed a reproducible reduction in pyruvate levels in *T. congolense*
724 supernatants over time, before abundance of this metabolite returned to levels similar to those
725 observed in negative controls. A recent study in PCF *T. brucei* demonstrated that these
726 parasites can re-metabolize glycolytic end products such as pyruvate and succinate [37].
727 Stable isotope labelling patterns in catabolic products derived from glucose do not support
728 cyclical TCA activity, nor re-uptake of excreted metabolites in BSF *T. congolense*. However,

729 it would be of interest to determine whether this species can recycle the aforementioned
730 metabolites.

731 *T. congolense* exhibits high levels of expression in genes involved in the glycosomal succinate
732 shunt (PEPCK, glycosomal malate dehydrogenase and fumarate hydratase; Fig 9). In *T.*
733 *brucei* these phenotypes are associated with PCF rather than BSF; thus, to further dissect
734 glycolytic metabolism, RNAi was employed to investigate the essentiality of PPDK and PEPCK
735 in *T. congolense*. In *T. brucei*, PPDK is only expressed in the PCF stage, and is absent in the
736 BSF stage. In contrast, BSF *T. congolense* expresses PPDK at both transcript (Fig 3) and
737 protein [44] levels, although our initial analyses suggest that the protein is not essential for
738 growth *in vitro*. PEPCK was previously found to be essential in BSF *T. brucei* [42]; though in
739 BSF *T. congolense*, PEPCK knock-down only led to a mild reduction in growth rate. Previous
740 studies in PCF *T. brucei* demonstrated that individual null mutants of PEPCK and PPDK
741 showed no change in growth rate, with moderate reductions in glycolytic flux [40]. However, a
742 PEPCK/PPDK null mutant did exhibit reduced growth rates, with further data showing that
743 PPDK functions in a glycolytic direction and contributes to glycosomal ATP/ADP balance [40].
744 Further work is required to establish the roles of PEPCK and PPDK in BSF *T. congolense*.
745 Gene knock-out has not been previously attempted for *T. congolense*, and consistent with
746 other studies RNAi penetrance does not appear as efficient as in *T. brucei* [69]. Techniques
747 such as CRISPR/Cas9 and conditional knock-out would greatly enhance our capabilities to
748 study this parasite.

749 Whilst the major PGK isoform in BSF *T. brucei* is expressed in the glycosome, a previous
750 study suggested that the major isoform of phosphoglycerate kinase in BSF *T. congolense*
751 lacks the glycosomal targeting signal present in *T. brucei*, and is thus expressed in the cytosol,
752 akin to PCF *T. brucei* [46]. This has significant implications for glycosomal ADP/ATP balance,
753 as the expression of cytosolic PGK in BSF *T. brucei* is lethal [39]. Taken together, these data
754 suggest that *T. congolense* appears to carry out glycolytic metabolism in the same fashion as
755 PCF, not BSF *T. brucei*, including in *ex vivo* cells.

756 Whilst 2-deoxy-D-glucose does cause *T. congolense* death *in vitro* and supplementation of
757 cultures with GlcNAc also has a detrimental impact on viability, knock-down of the glucose
758 transporter array did not affect growth, even though glucose uptake appeared to be reduced
759 by 37% subsequent to 72 h of RNAi induction. These experiments highlight a crucial difference
760 between BSF *T. congolense* and *T. brucei* in a pathway that has become a metabolic
761 paradigm in the latter species. Whilst *T. brucei* requires high levels of glucose to sustain a
762 significant glycolytic flux, *T. congolense* remains viable in significantly lower glucose
763 concentrations, with a reduced flux, more similar to PCF *T. brucei*. However, glucose remains
764 an essential carbon source in this species, as growth is abolished in the absence of glucose.
765 Of particular interest is whether the parasite generates the majority of ATP from this reduced
766 glucose intake, or if it can thrive on other carbon sources such as amino acids or even fatty
767 acids. If the latter, this adaptation could be due to the reduced bioavailability of glucose in the
768 ruminant host bloodstream. Blood concentrations of glucose in humans are approximately 5.5
769 mM [98]. Glucose concentrations in ruminants are typically lower (2–4 mM [99-101]), and
770 primary sources of energy are typically volatile fatty acids in the form of acetic, propionic and
771 butyric acid [102, 103]. To date, products of volatile fatty acid metabolism, such as 2-
772 methylcitrate and 2-methyl-cis-aconitase have not been reported in *T. congolense*. However,
773 it is thought *T. brucei* can metabolise ketone bodies such as β -hydroxybutyrate through the
774 action of a β -hydroxybutyrate dehydrogenase (Tb927.10.11930) to generate acetoacetate. *T.*
775 *congolense* possesses an orthologue of this gene (TcIL3000.A.H_000824100), and therefore,
776 the ability of *T. congolense* to utilise other products available in adult ruminant blood merits
777 further investigation.

778 RNAseq analyses of *T. congolense* indicate high levels of expression of mitochondrial
779 pathways associated with glucose catabolism, specifically acetate and acetyl-CoA metabolism
780 involving PDH, ASCT and succinyl-CoA synthetase (SCS; Fig 9). Given that the large amounts
781 of acetate generated by the parasite appear not to be required for fatty acid synthesis, these
782 findings could suggest significant reliance on mitochondrial substrate level phosphorylation for

783 growth, similar to PCF *T. brucei* cultured in glucose-rich medium [104, 105]. Interestingly, *T.*
784 *congolense* does not appear to encode a homologue of MPC1, and therefore likely relies on
785 MPC2 for pyruvate transport into the mitochondrion. The lack of multiple pyruvate transporters
786 combined with the importance of mitochondrial pyruvate catabolism likely explains the
787 increased sensitivity of *T. congolense* to UK5099, a mitochondrial pyruvate transport inhibitor,
788 compared to *T. brucei*.

789 Our data are consistent with the absence of oxidative phosphorylation, based on
790 transcriptomics and lack of sensitivity to chemical inhibition, compared to *T. brucei*.
791 Interestingly, a previous study reported NADH dehydrogenase (complex I) activity in *T.*
792 *congolense*, offering the possibility of ATP generation via complex V [48]. However, there was
793 no change in rotenone sensitivity in *T. congolense*, suggesting that the NADH dehydrogenase
794 activity may originate from a rotenone-insensitive NADH dehydrogenase such as NDH2,
795 known to be important for acetate production in BSF *T. brucei* [92, 106, 107]. Furthermore,
796 sensitivity to the TAO inhibitor, SHAM suggests that TAO is the terminal oxidase, with no
797 significant complex III or IV activity. These conclusions support one previous study of BSF *T.*
798 *congolense* [48].

799 Rather than oxidative phosphorylation, we propose it is more likely that considerable ATP
800 production occurs in the ASCT – SCS cycle, which would explain the high levels of acetate
801 generated by *T. congolense*, in addition to increased sensitivity to inhibition of mitochondrial
802 uptake of pyruvate, the key metabolic precursor. Given that 2-oxoglutarate dehydrogenase
803 complex expression appears to be less than, or equal to, that in *T. brucei* (under *in vitro*
804 culturing conditions; Fig 9), it is likely that SCS activity occurs in the acetate-generating
805 pathway rather than in the TCA cycle, which is not thought to be fully functional in BSF African
806 trypanosomes [35], although recent data have challenged this paradigm in PCF *T. brucei* [37].
807 The mechanisms proposed here bear some similarities to the scheme proposed by Dewar
808 and colleagues for stumpy-form *T. brucei* metabolism, which also exhibit increased
809 mitochondrial metabolism compared to BSF *T. brucei* [108].

810 In *T. brucei*, carbon atoms from glucose disseminate through multiple pathways in the cell [42]
811 and, using stable isotope-labelled glucose, our data demonstrate that this pattern is also seen
812 in *T. congolense*, in particular through the glycolytic pathway, suggesting some of the key
813 metabolic differences observed are quantitative, rather than qualitative. However, there were
814 key differences in glucose-derived carbon usage. In particular, a reduction in labelling was
815 observed in purine nucleotides in *T. congolense*. In both species, carbon labelling is likely due
816 to generation of ribose phosphate sugars via the PPP and these data suggest that *T.*
817 *congolense* does not obtain its ribose through the PPP (from glucose), to the same extent that
818 *T. brucei* does. Interestingly, *T. congolense* appears to express higher levels of APRT1
819 (cytosolic) compared to APRT2 (glycosomal) to synthesise adenosine (Fig 5). This
820 discrepancy could underpin the reduced fraction of glucose-derived purine labelling, with a
821 reliance on ribose from alternative sources (for example, exogenously).

822 Whilst the majority of pyrimidine labelling is 5-carbons in *T. brucei*, indicating labelled ribose,
823 there is decreased 5-carbon labelling and higher abundance of 2-carbon labelling in *T.*
824 *congolense*, likely through uridine generated from aspartate through orotate, again
825 highlighting a reduction in glucose-derived ribose, but conversely, an increase in glucose-
826 derived UMP and its derivatives.

827 There was also a reduced abundance of glucose-derived fatty acid labelling in *T. congolense*
828 relative to *T. brucei*. Coupled with a decreased abundance of acetyl-CoA synthetase mRNA,
829 these results suggest that *T. congolense* may scavenge exogenous lipids in favour of carrying
830 out fatty acid biosynthesis, for which it must break down extracellular lipids to their constituent
831 parts. Indeed, supernatant metabolomics showed accumulation of both choline and choline
832 phosphate, with a corresponding decrease in the LysoPC lipids, which appears to indicate
833 activity of the phospholipases which *T. congolense* is known to secrete [58, 109]. It is unknown
834 whether *T. congolense* is able to generate cytosolic acetyl-CoA for fatty acid biosynthesis
835 through the action of citrate lyase, although transcript abundance of this gene was reduced
836 compared to *T. brucei*. Analysis of drug sensitivity supports these conclusions, as *T.*

837 *congolense* is significantly less sensitive to acetyl-CoA synthetase inhibition, as well as
838 Orlistat, and inhibitor of fatty acid synthase, suggesting that fatty acid scavenging (e.g. lipid or
839 fatty acid transporters) could be a viable therapeutic target for this species. However, the
840 efficacy of orlistat *in vivo* has not been reported to our knowledge.

841 BSF *T. brucei* growth in CMM required only cysteine and glutamine when supplemented with
842 FBS gold, although a further 6 amino acids (Tyr, Phe, Trp, Leu, Met and Arg) were required
843 when supplemented with standard FBS [56]. As part of this study, 14 amino acids essential
844 for *T. congolense* growth were identified. Tryptophan and arginine, essential to *T. brucei*, were
845 not required to sustain *T. congolense* growth in 10% goat serum. Conversely, several amino
846 acids considered not essential to *T. brucei* were crucial for *T. congolense* growth *in vitro* (Asp,
847 His, Ile, Pro, Ser and Val). Proline is a well-established carbon source for PCF *T. brucei* [87].
848 However, based on stable isotope labelling experiments, this amino acid is solely used for
849 protein synthesis in BSF *T. congolense*, as there was no evidence of carbon dissemination
850 from proline into the metabolome (likewise for asparagine). Unlike BSF *T. congolense*, BSF
851 *T. brucei* must be able to synthesise sufficient amounts of these amino acids from alternative
852 sources, or obtain them from the serum supplement.

853 One metabolic area of interest in trypanosomatids is trypanothione biosynthesis, a crucial
854 pathway for parasite response to oxidative stress. Indeed, trypanothione synthase, as well as
855 proteins involved in the trypanothione biosynthesis pathway, such as ornithine decarboxylase
856 (targeted by Eflornithine), have long been considered prime chemotherapeutic targets due to
857 their absence from other organisms [110]. Whilst cysteine was previously known to be a main
858 carbon contributor to trypanothione synthesis in *T. brucei* along with glutamine and methionine
859 [85], we show here that serine, an amino acid essential to *T. congolense*, also contributes to
860 the generation of this metabolite in addition to the aforementioned amino acids. These data
861 indicate that *T. congolense* can both synthesise and transport cysteine. Interestingly, cysteine
862 was not significantly depleted from *T. congolense* culture supernatants and future work should

863 ascertain whether the presence of L-serine in medium can compensate for reduced cysteine
864 levels in *T. congolense* culture.

865 The data presented here have led to the generation of a novel semi-defined medium for
866 culturing the strain IL3000, which must be further optimized for the culture of multiple strains
867 of *T. congolense*. Of interest is the peculiar requirement of adult bovine or goat serum for *in*
868 *vitro* culture of *T. congolense*, rather than foetal bovine serum (FBS) which is typically used to
869 culture *T. brucei* [15, 59]. Whilst this study made no attempts to adapt *T. congolense* to FBS-
870 supplemented medium (indeed, even in SCM-7, growth rate is drastically reduced in the
871 presence of FBS after 2-3 passages), this is of crucial importance, as it would allow the study
872 of multiple species of African trypanosome under the same *in vitro* conditions. Analysis of
873 metabolism presented here indicates that this phenomenon is likely to centre on the lipid
874 requirements of *T. congolense*, although it remains to be seen if this requirement is for energy
875 generation or synthesis of lipids in general. Furthermore, adult ruminant serum composition
876 drastically differs from that of non-ruminants and of foetal ruminants [102, 103], and this likely
877 has significant implications on the extracellular environment faced by livestock trypanosomes.

878 The information presented here is a significant step in laying the foundation for fundamental
879 understanding of metabolism for an important livestock parasite. Understanding essential
880 areas of metabolism in both *T. brucei* and *T. congolense* enables the development of drugs
881 effectively targeting both species. Conversely, understanding the key differences between the
882 two species aids in dissecting drug mechanisms of action and resistance, as well as enabling
883 a greater understanding of host-pathogen dynamics.

884 **Materials and Methods**

885 **Compounds and reagents**

886 All compounds were obtained from Sigma/Merck with the exception of: Orlistat (Cambridge
887 Bioscience), oligomycin A (VWR International), diminazene aceturate (Cambridge
888 BioScience) and FCCP (Abcam).

889 **Cell lines and *in vitro* culture**

890 In all cases, *T. congolense* strain IL3000 [48] was used (originally received from Theo Baltz,
891 University of Bordeaux). For RNAi experiments a *T. congolense* IL3000 single marker line,
892 TcoSM, was used [69]. For *in vitro* experiments, cells were grown at 34°C, 5% CO₂ and
893 routinely cultured in either TcBSF3 [14] or HMI-93 [15], in both cases without a serum plus
894 supplement, with 20% goat serum (Gibco). For global metabolite analysis of culture
895 supernatant, an experimental medium (SCM-3) was used with the following components: 77
896 mM NaCl, 1.5 mM CaCl₂, 4.5 mM KCl, 0.8 mM MgSO₄, 36 mM NaHCO₃, 25 mM HEPES, 0.05
897 mM bathocuproinedisulfonic acid, 0.22 mM 2-mercaptoethanol, 50 U/mL
898 penicillin/streptomycin, 2.5 mM glucose, 1 mM pyruvate, 10 % goat serum, 10% TcBSF3 [14],
899 1 mM each of L-cysteine and L-glutamine, and 100 µM L-tyrosine, L-phenylalanine, L-
900 tryptophan, L-leucine, L-methionine and L-arginine. BSF *T. congolense* in exponential growth
901 phase were centrifuged at 1,500 × *g* for 10 minutes, washed with PBS and inoculated into this
902 medium (0 h time point).

903 For stable isotope labelling experiments, as well as experiments involving the removal or
904 addition of specific medium components, a custom medium, Steketee's Congolense Medium-
905 6 (SCM-6) was used (S6 Table). The final medium formulation based on this study's findings,
906 SCM-7, is provided in S6 Table. This medium is essentially HMI-93, although i) vitamins (with
907 the exception of folate) were removed, ii) D-glucose concentrations were modified depending
908 on experimental procedure, but was routinely kept at 10 mM, iii) goat serum levels were
909 reduced to 10% and, iv) of the 20 amino acids, 14 were added. Increasing the temperature to
910 37°C led to a detrimental effect on cell viability after several passages, as previously reported
911 [15].

912 For experiments involving *T. brucei*, either the monomorphic Lister 427 (*in vitro* experiments
913 and growth curves) or pleomorphic STIB 247 (RNAseq experiments, both *in vitro* and *ex vivo*
914 sample groups) strains were used. Lister 427 cells were grown in HMI-11 [111], whilst STIB

915 247 were grown in modified HMI-9 containing 1.1% methylcellulose and 20% serum plus
916 (Sigma) [112, 113]. In both cases, cells were incubated at 37°C, 5% CO₂.

917 For both species, cell counts were carried out using a haemocytometer, and in the case of *T.*
918 *congolense*, cells were mechanically detached from the culturing plasticware by pipetting prior
919 to counting. Growth curves were routinely carried out in 2 mL samples incubated in 24-well
920 plates, resuspended using a P1000. For detachment of cells from flasks, 10 mL plastic pipettes
921 were used. In cases where cells were harvested for experiments other than those involving
922 metabolomics, cells could also be detached by replacing the medium with PBS for incubating
923 at room temperature for several minutes, prior to vigorously tapping the flask to detach
924 parasites.

925 RNAi experiments using TcoSM were carried out in HMI-93 in 20 mL cultures. Cells were
926 seeded at 7×10^5 cells/mL and RNAi induction was initiated with the addition of 1 µg/mL
927 tetracycline (Sigma) and 1×10^7 cells were isolated every 24 hours for RNA analysis (outlined
928 below) before cells were passaged

929 **Ethics statement**

930 All animal experiments were performed in accordance with the Animals (Scientific Procedures)
931 Act 1986 and the University of Glasgow care and maintenance guidelines. All animal protocols
932 and procedures were approved by The Home Office of the UK government and the University
933 of Glasgow Ethics Committee.

934 **Animal experiments**

935 Adult female CD-1 mice (20–30 g body weight; Charles River Laboratories) were infected with
936 5×10^4 wild-type *T. brucei* STIB 247 or 1×10^5 wild-type *T. congolense* IL3000 by
937 intraperitoneal injection. Parasitaemia was monitored daily by venesection of the lateral tail
938 vein [114]. At first peak of parasitaemia ($>10^7$ cells/mL) mice were euthanised and blood
939 isolated. Parasites of both species were purified from blood by anion exchange using DEAE
940 cellulose [115]. Purified cells were counted, and a total of 1×10^8 cells were centrifuged for 10
941 minutes at $1,500 \times g$ prior to RNA extraction.

942 **RNA extraction**

943 For RNAseq experiments, 10^8 cells were isolated either from *in vitro* culture or from mouse
944 infections. RNA was extracted using the QIAgen RNeasy kit (Qiagen) with an on-column
945 DNase treatment step. Sample concentrations were analysed by Nanodrop and QuBit, and
946 concentrations adjusted to 37 ng/ μ L of which 80 μ L (2.96 μ g) was submitted for RNAseq.

947 For RNAi time course experiments, cell pellets (10^7 cells) were resuspended in 1 mL TRIzol
948 (Invitrogen) and stored at -80°C . Samples were thawed, 200 μ L chloroform was added,
949 samples were shaken vigorously for 15 seconds and incubated at room temperature for 3
950 minutes, prior to centrifugation at $12,000 \times g$ for 15 minutes, 4°C . The aqueous layer was
951 transferred to a fresh tube and 500 μ L isopropanol and 1 μ L Glycoblue (Invitrogen) were
952 added. Samples were mixed by inverting, incubated at room temperature for 10 minutes and
953 centrifuged at $12,000 \times g$ for 10 minutes at 4°C . RNA pellet was washed in ice-cold 75%
954 ethanol and centrifuged at $12,000 \times g$ for 10 minutes at 4°C . After air-drying, RNA was
955 resuspended in 20 μ L RNase-free water and concentration adjusted to 100 ng/ μ L. DNase
956 treatment was carried out using the Ambion TURBO DNase kit (Applied Biosystems) as per
957 manufacturer's instructions.

958 **Metabolomics sample preparation**

959 For metabolomics analysis of supernatants, 10 mL *T. congolense* cultures were incubated in
960 T25 flasks in relevant media. Cells were centrifuged at $1,500 \times g$ for 10 minutes, washed with
961 PBS, resuspended in relevant media and density adjusted to 1×10^5 cells/mL. At each time-
962 point, 500 μ L medium was transferred to a 1.5 mL Eppendorf tube and briefly quenched in a
963 dry ice/ethanol bath, before centrifuging at $1,500 \times g$ for 10 minutes at 4°C . A 5 μ L aliquot was
964 then transferred to a new Eppendorf containing 200 μ L metabolite extraction solvent
965 (chloroform:methanol:water in a 1:3:1 ratio) and samples vortexed at 4°C for one hour.
966 Samples were centrifuged for 5 minutes at $13,000 \times g$ (4°C) and supernatants transferred to
967 new Eppendorf tubes. Samples were stored at -80°C prior to analysis.

968 For analysis of intracellular metabolites, cells were grown to a final density of 2×10^6 cells/mL
969 and a total of 10^8 cells isolated. Cells were quenched in 50 mL falcon tubes to 4°C using a dry
970 ice/ethanol bath (stirred and measured by thermometer) and all subsequent steps were carried
971 out at 4°C. Cells were centrifuged at $1,500 \times g$ for 10 minutes and if supernatant samples were
972 required in addition to cell pellets, 5 μ L was transferred to an Eppendorf containing 200 μ L
973 extraction solvent. Cells were resuspended in residual medium before transfer to Eppendorf
974 tubes. Cells were then centrifuged ($1,500 \times g$, 5 minutes) and washed twice with ice-cold
975 phosphate buffered saline (PBS) before resuspension in 200 μ L extraction solvent
976 (chloroform:methanol:water in a 1:3:1 ratio). Samples were vortexed at 4°C for 1 hour, and
977 then centrifuged for 5 minutes at $13,000 \times g$. Supernatants were transferred to clean
978 Eppendorf tubes. For all experiments, a quality control sample was generated by pooling 10
979 μ L from each sample and samples were stored under argon gas at -80°C.

980 **Primers and plasmids**

981 RNAi experiments were carried out using a *T. congolense* single marker line, TcoSM [69] that
982 expresses Tet repressor and T7 polymerase, maintained in 0.5 μ g/mL puromycin, and gene
983 specific RNAi constructs were introduced with a *T. congolense* specific plasmid, p3T7-TcoV
984 [69]. Primers carrying a HindIII (5'-AAGCTT-forward) or an FseI (5'-GGCCGGCC-reverse)
985 restriction site were used to amplify *TcoPEPCK*, *TcoPPDK* and *TcoHT* (S7 Table). Gene
986 fragments were amplified using a HiFi polymerase master mix (NEB) and cloned into pGEM-
987 T easy (Promega) and sequenced to confirm correct sequence identity of each fragment. The
988 constructs were then digested with HindIII and FseI and ligated into the p3T7-TcoV vector
989 using T4 DNA ligase (Promega). The final plasmid was linearised with NotI before purification
990 by ethanol precipitation prior to electroporation into TcoSM cells.

991 **Transfections/electroporations**

992 *T. congolense* IL3000 electroporation experiments and selection experiments were performed
993 as developed by [69]. A total of 4×10^7 cells were used per transfection, including a negative
994 (buffer only) control. A transfection buffer previously published for use with *T. brucei* was used

995 for *T. congolense* transfections [116]. Cells were centrifuged at 1,500 × *g* for 10 minutes,
996 pellets resuspended in residual medium and transferred to Eppendorf tubes for a further
997 centrifugation step. Cells were subsequently washed in transfection buffer prior to final
998 resuspension in 100 µL buffer per transfection. Up to 12 µg linearised plasmid DNA was added
999 to an electroporation cuvette (Sigma), and 100 µL cells were subsequently added.
1000 Electroporation was carried out using a Nucleofector II (Lonza) programme Z-001.
1001 Transfected cells were then incubated overnight in 25 mL warm medium in the absence of
1002 selective antibiotics, prior to their addition and plating out at dilutions of 1:50, 1:100 and 1:200
1003 in 96-well plates. Antibiotics were added at the following concentrations: Puromycin: 0.5
1004 µg/mL; Neomycin (G418): 0.4 µg/mL. Clones were retrieved after 7-10 days, and these were
1005 maintained in 0.25 µg/mL puromycin and 0.2 µg/mL G418.

1006 **Drug sensitivity assays**

1007 Drug sensitivity assays were carried out using the alamar blue method developed by Raz and
1008 colleagues [117]. Briefly, Compounds were diluted to 2× starting concentration in SCM-6 (with
1009 10% goat serum for *T. congolense* IL3000 or 10% FBS for *T. brucei* Lister 427) and 200 µL
1010 was transferred to the first well of a solid white flat-bottomed 96-well plate. 100 µL medium
1011 was then added to 23 further wells and compounds were diluted 1:2 over this series of wells,
1012 with the exception of the last well, for a negative control. Subsequently, 100 µL cells were
1013 added at 2× starting density (4×10^4 cells/mL for *T. brucei* and 5×10^5 cells/mL for *T.*
1014 *congolense*). Plates were incubated for 48 hours (37°C or 34°C for *T. brucei* and *T.*
1015 *congolense*, respectively, 5% CO₂ in both cases), prior to addition of 20 µL resazurin sodium
1016 salt (0.49 mM in 1× PBS, pH 7.4) to each well. Plates were then incubated for a further 24
1017 hours before measurements of cell viability.

1018 Reduction of the resazurin salt was measured as a function of cell viability. Fluorescence of
1019 each plate was read using a Cytation 5 imaging reader (BioTek) and GEN5 software.
1020 Parameters were as follows: $\lambda_{\text{excitation}} = 540$ nm and $\lambda_{\text{emission}} = 590$ nm. Raw values were plotted
1021 against concentrations (converted to Log₁₀ values) and normalised (0% defined as smallest

1022 mean in the dataset; 100% defined as largest mean in the dataset) using Graphpad Prism
1023 version 8.4.0. EC₅₀ values for each compound were calculated using a non-linear sigmoidal
1024 dose-response curve. Each assay was performed in duplicate and each EC₅₀ value represents
1025 a mean of three independent experiments.

1026 **Real-time quantitative PCR (RT-qPCR)**

1027 RNA was extracted as described above, and reverse transcription was carried out in 20 µL
1028 using 1 µg RNA, using a high capacity cDNA kit (Applied Biosystems). Primers for RT-qPCR
1029 analysis were designed using Primer 3 [118], and primer efficiency was tested using serial
1030 dilutions of *T. congolense* IL3000 genomic DNA by plotting Ct value against Log₁₀(DNA
1031 concentration). Real-time PCR was carried out using the SensiFAST SYBR Hi-ROX kit
1032 (Bioline, BIO92005). Briefly, a 20 µL reaction was set up using 10 µL SYBR mix, RT template
1033 and 400 nM of each primer. Cycling conditions were: 96°C, 120 seconds, followed by 40 cycles
1034 of 95°C for 5 seconds, 62°C for 10 seconds and 72°C for 20 seconds. Previously published
1035 endogenous control primers for TcoTERT were used for within sample normalisation [119],
1036 and normalised transcript level was calculated using the delta delta Ct method [120].

1037 **Glucose uptake assays**

1038 For analysis of wild-type *T. congolense* and *T. brucei* glucose uptake, cells were seeded in 10
1039 mL cultures of SCM-6 at an initial density of 2×10^5 cells/mL (four cultures per species), with
1040 10 mM glucose added separately at the start of the experiment. Upon the addition of glucose,
1041 1 mL supernatant was immediately centrifuged ($1,500 \times g$, 10 minutes) and supernatant stored
1042 at -80°C. This process was repeated at 12, 15, 18, 21 and 24 h, and cell density measured by
1043 haemocytometer. A medium-only control (4 replicates) was also incubated alongside *in vitro*
1044 cultures. Glucose concentration of each supernatant sample was analysed using the Glucose
1045 (GO) assay kit (GAGO-20; Sigma) in a 96-well format. Briefly, 40 µL supernatant sample
1046 (diluted if necessary) was incubated with 80 µL assay reagent for 30 minutes at 37°C, after
1047 which 80 µL 12 N sulphuric acid was added and absorbance measured at 540 nm using a

1048 spectrophotometer. A standard curve was also run to calculate glucose concentration. Rate
1049 of glucose consumption was calculated using a custom script [57].

1050 For glucose consumption of the TcoHT RNAi line, the Glucose Uptake-Glo kit (Promega) was
1051 used. RNAi was induced for 72 hours prior to carrying out the assay. Cells were centrifuged,
1052 washed in PBS and resuspended in assay buffer (77 mM NaCl, 1.5 mM CaCl₂·2H₂O, 4.5 mM
1053 KCl, 0.8 mM MgSO₄·7H₂O, 36 mM NaHCO₃, 25 mM HEPES and 0.02 mM
1054 bathocuproinedisulfonic acid), as it was determined *T. congolense* viability is reduced in PBS
1055 alone. Density was adjusted to 10⁸ cells/mL, and three 100 µL replicates of each sample were
1056 added to wells of a black flat-bottomed 96-well plate. The uptake reaction was started by the
1057 addition of 50 µL 1 mM 2-deoxy-D-glucose. Plate was shaken for 15 minutes at 34°C prior to
1058 addition of 25 µL stop buffer, 25 µL neutralisation buffer and 100 µL pre-prepared 2DG6P
1059 detection reagent. Plates were shaken in between addition of the buffers. Finally, the plate
1060 was read with 0.3–1 second integration on a luminometer (Cytation 5 Imaging reader, BioTek).
1061 Wild-type *T. congolense*, and *T. congolense* supplemented with glucose were used as
1062 controls, in addition to cells without 2-deoxy-D-glucose and assays in the absence of cells.

1063 **Acetate concentration assay**

1064 Acetate was not detectable by mass spectrometry and therefore, a commercial colorimetric
1065 acetate assay kit (MAK086, Merck) was used to analyse changes in supernatant acetate
1066 concentrations in trypanosome cultures over time. *T. congolense* IL3000 were seeded in 10
1067 mL SCM-6 at a density of 1 × 10⁵ cells/mL as outlined in the supernatant metabolomics
1068 experiment. At each time-point, 500 µL supernatant was taken from each flask and transferred
1069 to an Eppendorf tube. Samples were centrifuged at 1,500 × g, the supernatant was transferred
1070 to a fresh Eppendorf tube, and samples were stored at -80°C until samples from all time-points
1071 had been collected. Acetate concentration assays were carried out according to the
1072 manufacturer's instructions. Briefly, for each sample, 5 µL was added to the wells of a 96-well
1073 plate in duplicate and 45 µL assay buffer was added to each sample. Subsequently, 50 µL
1074 reaction mix was added to each well, and the plate was mixed and incubated for 40 minutes

1075 at room temperature before absorbance was read at 450 nm. Acetate concentrations were
1076 calculated using the standard curve comprised of six concentrations run alongside the
1077 experimental samples.

1078 **Metabolomics – Liquid chromatography mass spectrometry**

1079 Hydrophilic interaction liquid chromatography (HILIC) was carried out by Glasgow Polyomics
1080 (Glasgow, UK), using a Dionex UltiMate 3000 RSLC system (Thermo Fischer Scientific)
1081 coupled to a ZIC-pHILIC column (150 mm × 4.6 mm, 5 µm column, Merck Sequant). The
1082 column was maintained at 30°C and samples were eluted with a linear gradient (20 mM
1083 ammonium carbonate in water and acetonitrile) over 26 minutes with a flow rate of 0.3
1084 mL/minute.

1085 Sample injection volume was 10 µL and samples were maintained at 4°C before injection. A
1086 Thermo Orbitrap Exactive (Thermo Fischer Scientific) was used to generate mass spectra,
1087 and was operated in polarity switching mode with the following settings: Resolution: 50,000;
1088 AGC: 106; *m/z* range: 70–1,400; sheath gas: 40; auxiliary gas: 5; sweep gas: 1; probe
1089 temperature: 150°C; capillary temperature: 275°C. Samples were run in both positive and
1090 negative polarity with the following ionisation: source voltage +4.5 kV, capillary voltage +50 V,
1091 tube voltage +70 kV and skimmer voltage +20 V for positive mode; source voltage -3.5 kV,
1092 capillary voltage -50 V, tube voltage -70 V and skimmer voltage -20 V for negative mode. Mass
1093 calibration was performed for each polarity immediately prior to each analysis batch. The
1094 calibration mass range was extended to cover small metabolites by inclusion of low-mass
1095 contaminants with the standard Thermo calmix masses (below *m/z* 1400), C₂H₆NO₂ for
1096 positive ion electrospray ionisation (PIESI) mode (*m/z* 76.0393) and C₃H₅O₃ for negative ion
1097 electrospray ionisation (NIESI) mode (*m/z* 89.0244). To enhance calibration stability, lock-
1098 mass correction was also applied to each analytical run using these ubiquitous low-mass
1099 contaminants. A set of authentic standards was run prior to the sample set for each
1100 experiment.

1101 **Metabolomics data analysis**

1102 RAW spectra were converted to mzXML files (mzML files for fragmentation data) using XCMS
1103 for untargeted peak detection [121]. The resultant files were further processed using mzMatch
1104 [122] for peak matching and annotation, resulting in a tabular output that was analysed using
1105 IDEOM with default settings [123]. For stable-isotope assisted metabolomics experiments,
1106 mzMatch output (in .peakml format) was analysed using mzMatch-ISO to extract all carbon
1107 isotopologue abundances from putative metabolites [124]. Data analysis of stable isotope-
1108 labelled metabolomics was based on a 48 hour time-point in all experiments. Data was further
1109 analysed using Microsoft Excel or Metaboanalyst v4.0 [125]. The raw data from all
1110 metabolomics analyses are available in Metabolights (accession number: MTBLS2372; URL:
1111 www.ebi.ac.uk/metabolights/MTBLS2372).

1112 **RNA sequencing and data processing**

1113 RNA sequencing was carried out by Edinburgh Genomics (Edinburgh, UK). Libraries were
1114 prepared from 8 samples (4x *T. brucei*, 4x *T. congolense*) using the TruSeq Stranded mRNA
1115 kit (Illumina) and 2 × 75 bp paired-end sequencing was carried out using a HiSeq 4000 system
1116 (Illumina). Sequencing reads were aligned to the corresponding genome sequence using
1117 HiSat2 (--no-spliced-alignment) [126]. For *T. brucei*, the TREU 927 reference genome
1118 sequence was used (v34.0 from TriTrypDB [127]), whilst a PacBio assembly of *T. congolense*
1119 IL3000 was used for *T. congolense* [65]. The resulting SAM files were converted to BAM files
1120 using samtools [128], and subsequently filtered for quality and primary alignment (-q 1 -F
1121 0x100), the latter to reduce the effects of multimapping. Read counts were extracted from the
1122 filtered BAM files using HTSeq-count (-s reverse -f bam -t CDS -i ID -m union -a 0 --nonunique
1123 all).

1124 For all samples, transcripts per million (TPM) values for each gene were calculated manually
1125 using Microsoft Excel as follows: 1) Reads per kilobase (RPK) were calculated by dividing the
1126 read counts by the length of gene in kilobases; 2) All RPK values in a sample were summed
1127 and divided by 1 million as a scaling factor; 3) Each RPK value was divided by the scaling

1128 factor to yield TPM values [53]. To compare transcript abundances between the two species,
1129 Orthofinder [54] was used to infer orthologue genes or gene groups. Default parameters were
1130 used to compare the TriTrypDB v34.0 TREU 927 annotated proteins and the PacBio *T.*
1131 *congolense* IL3000 annotated proteins (S2 Table). A custom MATLAB (version R2019a) was
1132 used to combine the Orthofinder dataset and the TPM values for 1-to-1 orthologues, as well
1133 as “sum of TPM” values for groups containing multiple genes, where TPM value for each gene
1134 was summed, resulting in a final dataset (S1 Table). Raw RNA-seq data is deposited at GEO
1135 (accession number: GSE165290). Transcriptomics data were cross-referenced with the
1136 TrypanoCyc database (vm-trypanocyc.toulouse.inra.fr/; [60]) to enable pathway analysis of
1137 the data.

1138 **Computation**

1139 Figures were generated using Graphpad Prism version 8.4.0 (www.graphpad.com) with the
1140 exception of scatter plots and heatmaps, which were generated using R [129]. Heatmaps were
1141 generated using the R packages pheatmap and ComplexHeatmap [130]; scatter plots were
1142 generated using GGplot2 and GGally; and pathway maps were generated with Inkscape v1.0.

1143 **Acknowledgements**

1144 The authors would like to thank the following people: Steve Kelly, Paul Michels & Simon Young
1145 for very useful discussion. We thank Anne-Marie Donachie for help with *in vivo* experiments.
1146 In addition, the authors would like to thank the following institutes: Glasgow Polyomics for LC-
1147 MS work, Edinburgh Genomics for RNAseq, MRC PPU DNA Sequencing and Services,
1148 Dundee, for plasmid sequencing. LM, PS, EP, HdK and MPB were funded by BBSRC grant
1149 BB/N007492/1, and LM, PS, EP, RR and MPB by BB/S00243X/1. CG and BW were funded
1150 by University of Nottingham Strategic Support Funds (Wellcome Trust), and GAM by Sir Halley
1151 Stewart Medical Research Grant (R410). MPB is funded by a Wellcome Trust core grant to
1152 the Wellcome Centre for Integrative Parasitology (grant 104111/Z/14/Z). This article is based
1153 on research funded in part by the Bill & Melinda Gates Foundation (Investment ID
1154 OPP1176784) and with UK aid from the UK Government (Project 300504) through GALVmed.

1155 The findings and conclusions contained within are those of the authors and do not necessarily
1156 reflect positions or policies of the Bill & Melinda Gates Foundation or the UK Government. The
1157 Roslin Institute is core funded by the BBSRC (BS/E/D/20002173).

1158 **Figure legends**

1159 **Figure 1: Overview of comparative transcriptomics analysis of *T. brucei* and *T.***
1160 ***congolense*, isolated from *ex vivo* and *in vitro* conditions.** RNAseq data from *T.*
1161 *congolense* (IL3000) and *T. brucei* (STIB247) in both *in vitro* and *ex vivo* (from mouse
1162 infections) conditions was aligned to the species' respective genome sequence and read
1163 counts were normalised by the transcripts per million (TPM) method. To directly compare the
1164 species, a pseudogenome was generated using the Orthofinder tool [54]. TPM values from
1165 the 4 sample groups were plotted against each other to analyse correlation between conditions
1166 (A and B) and between species in the same conditions (C and D). Correlation was assessed
1167 using both Spearman's rank correlation (ρ) and Pearson correlation (ρ ; Pearson's r)
1168 coefficients.

1169 **Figure 2: Analysis of supernatant metabolites after *T. congolense* culture.** A heatmap
1170 covering the 80 putative medium components judged to be significantly altered after 56 hours
1171 of *in vitro* cell culture containing *T. congolense* strain IL3000, as calculated by a one-way
1172 repeated measures ANOVA ($P < 0.05$). Peak abundances were log transformed and mean
1173 centred and metabolites were clustered based on Pearson correlation. Two clusters of interest
1174 were identified, which are shown in a larger format on the right. Metabolites in the top cluster
1175 were observed to increase significantly over time, whilst those in the bottom cluster decreased.
1176 Metabolite names follow by [*] were matched to an authentic standard. B) Comparison of
1177 metabolite changes in medium supernatants after 56 hours between *T. brucei* [56] and *T.*
1178 *congolense* (S4 Table). Relative changes in metabolite abundance were calculated as Log_2
1179 fold change of 56 h vs 0 h. Key differences are highlighted numerically: 1, guanine; 2, *N*6-
1180 acetyl-L-lysine; 3, succinate; 4, 4-hydroxy-4-methylglutamate; 5, *N*6,*N*6,*N*6-trimethyl-L-lysine;
1181 6, choline; 7, 2-oxoglutarate; 8, L-1-pyrroline-3-hydroxy-5-carboxylate; 9, D-glycerate; 10,

1182 pyruvate; 11, 12-hydroxydodecanoic acid; 12, L-cystine; 13, diacetyl; 14, [PC (18:0)] 1-
1183 octadecanoyl-sn-glycero-3-phosphocholine; 15, LysoPC(17:0); 16, [PC (16:0)] 1-
1184 hexadecanoyl-sn-glycero-3-phosphocholine; 17, inosine; 18, [PC (16:1)] 1-(9Z-
1185 hexadecenoyl)-sn-glycero-3-phosphocholine; 19, [FA trihydroxy(18:1)] 9S,12S,13S-
1186 trihydroxy-10E-octadecenoic acid; 20, inosine.

1187 **Figure 3: Energy metabolism in *T. congolense*.** A-E) Supernatant metabolomics analysis
1188 of metabolites involved in glycolytic metabolism in *T. congolense*. Grey bars indicate a
1189 negative medium control incubated for 56 hours. F) A commercial kit was used to measure
1190 acetate concentration during *T. congolense* culture, with supernatant samples analysed at the
1191 same time points as the supernatant metabolomics experiment. G) A simplified overview of
1192 the glycolytic pathway. Typically, the succinate shunt is only active in PCF *T. brucei*, with low
1193 levels of activity in BSF *T. brucei*. Numbers refer to the following proteins: 1, glucose
1194 transporters; 2, hexokinase; 3, glucose 6-phosphate isomerase; 4, phosphofructokinase; 5,
1195 aldolase; 6, triosephosphate isomerase; 7, glycerol 3-phosphate dehydrogenase; 8, glycerol
1196 kinase; 9, glyceraldehyde 3-phosphate dehydrogenase; 10, phosphoglycerate kinase; 11,
1197 phosphoglycerate mutase and enolase; 12, phosphoenolpyruvate carboxykinase; 13, malate
1198 dehydrogenase; 14, fumarate hydratase; 15, NADH-dependent fumarate reductase; 16,
1199 pyruvate kinase; 17, alanine aminotransferase; 18, pyruvate dehydrogenase complex; 19,
1200 acetate:succinate CoA-transferase and acetyl-CoA thioesterase. H) Tracing glucose derived
1201 carbon usage through glycolytic metabolism. *T. congolense* were incubated with a 50:50 mix
1202 of ¹²C-D-glucose:¹³C-U-D-glucose before cell pellets were isolated for metabolomics analysis.
1203 Results were compared to those generated in *T. brucei* by Creek and colleagues [42]. Colours
1204 indicate the number of ¹³C atoms in each metabolite. I) Comparative analysis of transcript level
1205 activity of glycolysis in *T. brucei* and *T. congolense* from both *in vitro* and *ex vivo* conditions.
1206 Gene IDs: HK1 & 2, hexokinase, TbTc_0341; GPI, glucose 6-phosphate isomerase,
1207 TbTc_1840; PFK, phosphofructokinase, TbTc_1399; ALDA, aldolase, TbTc_0358; TPI,
1208 Triosephosphate isomerase, TbTc_1075; GPDH, glycerol 3-phosphate dehydrogenase,

1209 TbTc_2722; GK, glycerol kinase, TbTc_0392; GAPDH, glyceraldehyde 3-phosphate
1210 dehydrogenase, TbTc_0377; PGK, phosphoglycerate kinase, TbTc_6030; PGKA,
1211 phosphoglycerate kinase A, TbTc_0241; PGKB/C, phosphoglycerate kinase B & C,
1212 TbTc_0240, ENO1, enolase, TbTc_0465; ENO2, enolase, putative, TbTc_3614, PK1,
1213 pyruvate kinase 1, TbTc_0372; FBPase, fructose-1,6-bisphosphatase, TbTc_1967; PEPCK,
1214 phosphoenolpyruvate carboxykinase, TbTc_0348; gMDH, glycosomal malate
1215 dehydrogenase, TbTc_0642, FH, fumarate hydratase, TbTc_0242; Frd, NADH-dependent
1216 fumarate reductase, TbTc_0141; PPK, pyruvate phosphate dikinase, TbTc_1304; AAT,
1217 alanine aminotransferase, TbTc_0675; PDH E1 α , pyruvate dehydrogenase E1 alpha subunit,
1218 TbTc_4169; PDH E1 β , pyruvate dehydrogenase E1 beta subunit, TbTc_5437.

1219 **Figure 4: *In vitro* analysis of glycolytic metabolism.** To further probe glycolytic metabolism
1220 in *T. congolense*, novel RNAi technology was employed to knock-down key glycolytic and
1221 gluconeogenic steps. A) *T. congolense* remains viable in reduced glucose concentrations. A
1222 growth defect was only observed when glucose concentrations were reduced to <2 mM. B)
1223 Supplementation with increased concentrations of 2-deoxy-D-glucose leads to *T. congolense*
1224 cell death (red dotted line indicates detection limit by haemocytometer). C) Growth analysis of
1225 RNAi-mediated knock-down of PEPCK in *T. congolense* IL3000 single marker induced with 1
1226 μ g/mL tetracycline. D) Growth analysis of RNAi-mediated knock-down of PPK in *T.*
1227 *congolense* IL3000 single marker induced with 1 μ g/mL tetracycline. E-F) Transcript
1228 abundance over time, following tetracycline-mediated RNAi induction of PEPCK and PPK.
1229 G) Knock-down of the entire glucose transporter (HT) array does not affect *in vitro* cell viability.
1230 H) Normalised HT mRNA abundance over time after RNAi induction. I) Changes in glucose
1231 uptake in RNAi-induced cells were detected via an enzyme-linked luminescence assay
1232 coupled to 2-deoxy-D-glucose uptake over a period of 30 minutes. The assay was carried out
1233 72-hours post-induction. Of the three RNAi lines, 2 showed a significant reduction in glucose
1234 uptake capability (* $P < 0.05$; *** $P < 0.001$)

1235 **Figure 5: Nucleotide metabolism in *T. congolense*.** Supernatant analysis of *T. congolense*
1236 *in vitro* cultures showing changes in abundance of D-ribose (A), guanine (B), xanthine (C) and
1237 inosine (D) over 56 hours. Grey bar indicates a negative medium control group E) Simplified
1238 overview of purine salvage and synthesis in trypanosomatids adapted from [131]. Numbers
1239 indicate the following enzymes: 1, APRT; 2, AD; 3, HGPRT; 4, IMPD; 5, HGXPRT; 6, GMPR;
1240 7, GMPS; 8, HGPRT. Red cross indicates guanine deaminase, which is not
1241 encoded/annotated in the *T. congolense* genome. F) Comparison of glucose-derived purine
1242 carbon labelling in *T. congolense* and *T. brucei* [42]. Colours indicate the number of ¹³C atoms
1243 in each metabolite. D) Comparative RNAseq analysis of *T. congolense* and *T. brucei* under
1244 both *in vitro* and *ex vivo* conditions. Gene IDs from top to bottom: P121-PWY
1245 (adenine/adenosine salvage): IMPDH1, inosine-5'-monophosphate dehydrogenase,
1246 TbTc_1648; ADSS, adenylosuccinate synthetase, TbTc_1142; APRT-1, cytosolic adenine
1247 phosphoribosyltransferase, TbTc_3522; HGPRT, hypoxanthine-guanine
1248 phosphoribosyltransferase, TbTc_0726; GMPR, GMP reductase, TbTc_4627; HGXPRT,
1249 hypoxanthine-guanine-xanthine phosphoribosyltransferase, TbTc_3696; APRT-2, glycosomal
1250 adenine phosphoribosyltransferase, TbTc_5918; ADSL, adenylosuccinate lyase, TbTc_1986.
1251 PWY0-162 (pyrimidine biosynthesis): DHODH, dihydroorotate dehydrogenase (fumarate),
1252 TbTc_0620; PYR1A-B, glutamine hydrolysing carbomoyl phosphate synthase, TbTc_1631;
1253 PYR2, aspartate carbamoyltransferase, TbTc_1630; PYR3, dihydroorotase, TbTc_3801;
1254 CTPS, cytidine triphosphate synthase, TbTc_0920; OMPDC/OPRT, orotidine-5-
1255 monophosphate decarboxylase/orotate phosphoribosyltransferase, TbTc_0735; CMF40a,
1256 nucleoside diphosphate kinase, TbTc_5784. PWY0-163 (pyrimidine salvage): UP, uridine
1257 phosphorylase, TbTc_5794; CDA, cytidine deaminase, TbTc_3318; UPRT, uracil
1258 phosphoribosyltransferase, TbTc_4220; NDPK, nucleoside diphosphate kinase, TbTc_0593;
1259 CMF40a, nucleoside diphosphate kinase, TbTc_5784; NDPK3, nucleoside diphosphate
1260 kinase 3, TbTc_2560.

1261 **Figure 6: Amino acid metabolism in *T. congolense* IL3000.** A-C) Analysis of indicated
1262 amino acids in *T. congolense* IL3000 culture supernatants over a 56 h time course. Grey bars
1263 indicate a negative medium control group. D-F) Growth curves in SCM-6 excluding one amino
1264 acid at a time, to determine those essential to *T. congolense* viability. In each experiment, full
1265 SCM-6 was used as a positive control. Legends indicate which amino acid was removed in
1266 each experiment. G) Growth analysis of SCM-6 and SCM-7, the latter containing only amino
1267 acids deemed essential, compared to HMI-93 [111]. H) Simplified map of intracellular
1268 glutamine metabolism. Numbers refer to the following enzymes: 1, glutaminase; 2, glutamate
1269 decarboxylase; 3, 4-aminobutyrate aminotransferase; 4, succinate semialdehyde
1270 dehydrogenase; 5, glutamate dehydrogenase; 6, 2-oxoglutarate dehydrogenase; 7, Succinyl-
1271 CoA synthetase; 8, isocitrate dehydrogenase; 9 & 10, aconitase. I) Carbon utilisation from L-
1272 glutamine was analysed in *T. congolense* (100% ¹³C-U-L-glutamine) and compared to that in
1273 *T. brucei* (50:50 ratio of L-glutamine and ¹³C-U-L-glutamine) [85].

1274 **Figure 7: Fatty acid metabolism in *T. congolense*.** A) Glucose-derived ¹³C carbon labelling
1275 of saturated fatty acids in *T. congolense* and *T. brucei* [42]. Colours correspond to the number
1276 of ¹³C labels detected in each metabolite. B) L-threonine-derived saturated fatty acid ¹³C
1277 labelling in *T. congolense*. Fatty acid systematic names and numbers: lauric acid: dodecanoic
1278 acid, C12:0; myristic acid: tetradecanoic acid, C14:0; palmitic acid: hexadecanoic acid, C16:0;
1279 nonadecyclic acid: nonadecanoic acid, C19:0. C) Transcriptomics analysis of acetate and lipid
1280 metabolism. Gene names and IDs: ACH, acetyl-CoA hydrolase, TbTc_5515; ACS, acetyl-CoA
1281 synthetase, TbTc_0318; AKCT, 2-amino-3-ketobutyrate-CoA ligase, TbTc_6236; TDH, L-
1282 threonine 3-dehydrogenase, TbTc_5991; PDHe1 α , pyruvate dehydrogenase E1 α subunit,
1283 TbTc_4169; PDHe1 β , pyruvate dehydrogenase E1 β subunit; SCS α , succinyl-CoA synthetase
1284 α subunit, TbTc_0813; PPDK, pyruvate phosphate dikinase, TbTc_1304; PDHe2,
1285 dihydrolipoamide acetyltransferase, TbTc_1015; PDHe3, pyruvate dehydrogenase E3,
1286 TbTc_4765; PYK1, pyruvate kinase, TbTc_0372; BKR, β -ketoacyl-ACP reductase,
1287 TbTc_1241; BKS, β -ketoacyl synthase, TbTc_3372; ACC, acetyl-CoA carboxylase,

1288 TbTc_0754; HMGCL, hydroxymethylglutaryl-CoA lyase, TbTc_6160; FPPS, farnesyl
1289 pyrophosphate synthase, TbTc_5375; LSS, lanosterol synthase, TbTc_4540; MVK,
1290 mevalonate kinase, TbTc_3761; SM, squalene monooxygenase, TbTc_3357; MDD,
1291 mevalonate diphosphate decarboxylase, TbTc_0546; SMT, sterol 24-c methyltransferase,
1292 TbTc_0387; CYP51A1, lanosterol 14 α demethylase, TbTc_4837; SQase, squalene synthase,
1293 TbTc_2577; SPPS, solanesyl-diphosphate synthase, TbTc_3025; IDI, isopentenyl-
1294 diphosphate delta-isomerase, TbTc_1099; PTase, prenyltransferase, TbTc_1352; GGTase-
1295 II β , geranylgeranyl transferase type II β subunit, TbTc_0680; SCP2, 3-ketoacyl-CoA thiolase,
1296 TbTc_4024; PMVK, phosphomevalonate kinase, TbTc_3039; HMGR, 3-hydroxy-3-
1297 methylglutaryl-CoA reductase, TbTc_3189; LACS5, fatty acyl-CoA synthetase, TbTc_0099;
1298 ACSL_0688, long-chain-fatty-acid-CoA ligase, TbTc_0688; ECHD, enoyl-CoA hydratase,
1299 TbTc_3283; ACS3/ACS4, fatty acyl-CoA synthetase 3 & 4, TbTc_0101; ACS1, fatty acyl-CoA
1300 synthetase 1, TbTc_0100; ACS2, fatty acyl-CoA synthetase 2, TbTc_0102; ECI_4184, 3,2-
1301 trans-enoyl-CoA isomerase, TbTc_4184; ACSL_2381, long-chain-fatty-acid-CoA ligase,
1302 TbTc_2381; TFE α 1, enoyl-CoA hydratase/enoyl-CoA isomerase, TbTc_3362; SCP2, 3-
1303 ketoacyl-CoA thiolase, TbTc_4024; ECI_0360, 3,2-trans-enoyl-CoA isomerase, TbTc_0360;
1304 ACAD, acyl-CoA dehydrogenase, TbTc_4954.

1305 **Figure 8: Pharmacological inhibition of fatty acid synthesis in *T. brucei* and *T.***
1306 ***congolense*.** Dose-response curves to determine differential sensitivity of the two species of
1307 parasite to inhibition of an ACS inhibitor (panel A) and Orlistat (B).

1308 **Figure 9: Summary of *T. congolense* and *T. brucei* *in vitro* transcriptome.** Log₂ fold
1309 change (*T. congolense*/*T. brucei*) was calculated for each gene (for ratio changes, see the key
1310 on the bottom-left). Dashed lines represent transport processes. Genes: 1, hexose
1311 transporters, TbTc_0095; 2, hexokinase, TbTc_0341; 3, glucose-6-phosphate isomerase,
1312 TbTc_1840; 4, phosphofructokinase, TbTc_1399; 5, fructose-1,6-bisphosphatase,
1313 TbTc_1967; 6, aldolase, TbTc_0358; 7, triosephosphate isomerase, TbTc_1075; 8, glycerol-
1314 3-phosphate dehydrogenase, TbTc_2722; 9, glycerol kinase, TbTc_0392; 10, glyceraldehyde

1315 3-phosphate dehydrogenase, TbTc_0377; 11, phosphoglycerate kinase, TbTc_0240; 12,
1316 phosphoglycerate mutase, TbTc_5039; 13, enolase, TbTc_0465; 14, pyruvate kinase 1,
1317 TbTc_0372; 15, alanine aminotransferase, TbTc_0675; 16, pyruvate phosphate dikinase,
1318 TbTc_1304; 17, Phosphoenolpyruvate carboxykinase, TbTc_0348; 18, glycosomal malate
1319 dehydrogenase, TbTc_0642; 19, glycosomal fumarate hydratase, TbTc_0242; 20, glycosomal
1320 NADH-dependent fumarate reductase, TbTc_0140; 21, glucose-6-phosphate dehydrogenase,
1321 TbTc_0931; 22, 6-phosphogluconolactonase, TbTc_4165; 23, 6-phosphogluconate
1322 dehydrogenase, TbTc_2025; 24, ribulose-5-phosphate epimerase, TbTc_4356; 25, ribose 5-
1323 phosphate isomerase, TbTc_3090; 26, transketolase, TbTc_1701; 27, transaldolase,
1324 TbTc_1823; 28, ribokinase, TbTc_5212; 29, malic enzyme, TbTc_0296; 30, Mitochondrial
1325 pyruvate carrier 2, TbTc_2668; 31, FAD-dependent glycerol-3-phosphate dehydrogenase,
1326 TbTc_2282; 32, NADH dehydrogenase (NDH2), TbTc_5033; 33, Alternative oxidase,
1327 TbTc_6589; 34, mitochondrial fumarate hydratase, TbTc_0243; 35, mitochondrial NADH-
1328 dependent fumarate reductase, TbTc_0141; 36, mitochondrial malate dehydrogenase,
1329 TbTc_0256; 37, citrate synthase, TbTc_0486; 38, aconitase, TbTc_5765; 39, isocitrate
1330 dehydrogenase, TbTc_0510; 40, 2-oxoglutarate dehydrogenase E1 component, TbTc_2864;
1331 41, 2-oxoglutarate dehydrogenase E1 component, TbTc_3111; 42, 2-oxoglutarate
1332 dehydrogenase E2 component, TbTc_3057; 43, succinyl-CoA synthetase α , TbTc_0813; 44,
1333 succinyl-CoA ligase β , TbTc_3392; 45, glutamine synthetase, TbTc_2226; 46, glutamate
1334 dehydrogenase, TbTc_0872; 47, pyruvate dehydrogenase E1 α subunit, TbTc_4169; 48,
1335 pyruvate dehydrogenase E1 β subunit, TbTc_5437; 49, dihydrolipoamide acetyltransferase,
1336 TbTc_1015; 50, pyruvate dehydrogenase complex E3, TbTc_4765; 51, L-threonine 3-
1337 dehydrogenase, TbTc_5991; 52, 2-amino-3-ketobutyrate coenzyme A ligase, TbTc_6236; 53,
1338 Acetyl-CoA hydrolase (ACH), TbTc_5515; 54, Succinyl-CoA:3-ketoacid coenzyme A
1339 transferase (ASCT), TbTc_0236; 55, Acyl carrier protein, TbTc_5262; 56, beta-ketoacyl-ACP
1340 synthase, TbTc_3372; 57, beta-ketoacyl-ACP reductase, TbTc_1241; 58, Trans-2-enoyl-ACP
1341 reductase 1, TbTc_5269; 59, acetyl-CoA synthetase, TbTc_0318; 60, acetyl-CoA
1342 carboxylase, TbTc_0754; 61, Fatty acid elongase (ELO1), TbTc_0159; 62, Fatty acid

1343 elongase (ELO2), TbTc_1882; 63, Fatty acid elongase (ELO3), TbTc_0235; 64, elongation of
1344 very long chain fatty acids protein (ELO4), TbTc_0737; 65, aspartate aminotransferase,
1345 TbTc_0799; 66, aspartate carbamoyltransferase, TbTc_1630; 67, dihydroorotase,
1346 TbTc_3801; 68, dihydroorotate dehydrogenase, TbTc_0620; 69, orotidine-5-phosphate
1347 decarboxylase/orotate phosphoribosyltransferase, TbTc_0735; 70, uracil
1348 phosphoribosyltransferase, TbTc_4220; 71, Adenine phosphoribosyltransferase (APRT-2),
1349 TbTc_3522; 72, inosine-adenosine-guanosine-nucleoside hydrolase, TbTc_4998; 73,
1350 adenosine kinase, TbTc_1024; 74, AMP deaminase, TbTc_5808; 75, hypoxanthine-guanine
1351 phosphoribosyltransferase (HGPRT), TbTc_0726; 76, inosine-guanine nucleoside hydrolase,
1352 TbTc_0808; 77, inosine-5'-monophosphate dehydrogenase, TbTc_1648; 78, Hypoxanthine-
1353 guanine-xanthine phosphoribosyltransferase (HGXPRT), TbTc_3696; 79, GMP reductase,
1354 TbTc_4627; 80, GMP synthase, TbTc_1452. Abbreviations: PUFA, polyunsaturated fatty acid.

1355 **S1 figure: comparative analysis of published *T. congolense* RNAseq data and data**
1356 **generated in this study.** Scatter matrix of *T. congolense* datasets from this study compared
1357 to ascending and peak parasitaemia *in vivo* transcriptomics data generated by Silvester and
1358 colleagues [55]. TPM values were calculated for each gene in the *T. congolense* genome and
1359 Log₂ TPM was plotted. Lower panels: Scatter plots of individual comparisons of the 4 datasets.
1360 Red dots correspond to genes associated with glycolysis; Diagonal panels: sample names;
1361 Upper panels: Pearson correlation coefficients for comparisons of entire datasets (black),
1362 glycolytic pathway (“Glyc”, green) and proteins with predicted transmembrane domains
1363 (“Trans”, red).

1364 **S2 figure: Growth of *T. congolense* IL3000 in absence or presence of N-acetyl-D-**
1365 **glucosamine.** Parasites were cultured in SCM-6 supplemented with 10 mM or 2 mM glucose
1366 in the presence or absence of 60 mM GlcNAc and density monitored by haemocytometer
1367 every 24 hours.

1368 **S3 figure: Comparative transcriptomics analysis of the electron transport chain in *T.***
1369 ***congolense* and *T. brucei*.** A heatmap of all ETC complexes based on a table generated by

1370 Zikova and colleagues [73]. Heatmaps are divided into the alternative oxidases (AOX), NADH
1371 dehydrogenase 2 (NDH2), complex I, II, III, IV and ATPase (complex V).

1372 **S4 figure: Stable isotope labelled (¹³C)-glucose derived pyrimidine labelling.**
1373 Comparative analysis of glucose-derived pyrimidine labelling in *T. congolense* and *T. brucei*
1374 (taken from [42]).

1375 **S5 figure: Effect of cysteine exclusion on *T. congolense* growth.** Parasites were grown in
1376 SCM-6 supplemented with 1.5 mM, 1.0 mM or absence of L-cysteine. Cell density was
1377 monitored every 24 hours.

1378 **S6 figure: Comparison of amino acid metabolism in *T. congolense* and *T. brucei*.** A)
1379 glucose-derived carbon labelling of amino acids B) Transcriptomics pathway analysis. Gene
1380 IDs: A) ARG+POLYAMINE-SYN: AdoMetDC_3193, AdoMet decarboxylase, TbTc_3193;
1381 ODC, ornithine decarboxylase, TbTc_5903; AdoMetDC_0696, AdoMet decarboxylase,
1382 TbTc_0696; SpSyn, spermidine synthase, TbTc_1034. B) ASPASN-PWY: cASAT, cytosolic
1383 aspartate aminotransferase, TbTc_0799; ASNS, asparagine synthetase, TbTc_4894;
1384 mASAT, mitochondrial aspartate aminotransferase, TbTc_5877. C) GLUCAT-PWY: OGDH-
1385 E1, 2-oxoglutarate dehydrogenase E1, TbTc_2864; GDH, glutamate dehydrogenase,
1386 TbTc_0872; SCS α , succinyl-CoA synthetase, TbTc_0813; SUCLG2, succinyl-CoA ligase,
1387 TbTc_3392; OGDH-E2, 2-oxoglutarate dehydrogenase E2, TbTc_3057. D) ILEUDEG-PWY:
1388 ECH, enoyl-CoA hydratase, TbTc_3283; BCAAT, branched-chain amino acid
1389 aminotransferase, TbTc_0559; SCP2, 3-ketoacyl-CoA thiolase, TbTc_4024. E) LEUDEG-
1390 PWY: ECH, enoyl-CoA hydratase, TbTc_3283; BCKDH α , 2-oxoisovalerate dehydrogenase α ,
1391 TbTc_1182; BCKDH β , 2-oxoisovalerate dehydrogenase β , TbTc_0682; AUH,
1392 methylglutaconyl-CoA hydratase, TbTc_5348; HMGCL, hydroxymethylglutaryl-CoA lyase,
1393 TbTc_6160; BCAAT, branched-chain amino acid aminotransferase, TbTc_0559; MCC β , 3-
1394 methylcrotonyl-CoA carboxylase β , TbTc_5385; MCC α , 3-methylcrotonyl-CoA carboxylase α ,
1395 TbTc_1670; SCP2, 3-ketoacyl-CoA thiolase, TbTc_4024; IVDH, isovaleryl-CoA
1396 dehydrogenase, TbTc_3112. F) PWY0-781: cASAT, cytosolic aspartate aminotransferase,

1397 TbTc_0799; MTR - 5-methyltetrahydropteroyltriglutamate-homocysteine S-methyltransferase,
1398 TbTc_5805; NMNAT, nicotinamide/nicotinic acid mononucleotide adenylyltransferase,
1399 TbTc_4133; NADSYN, NAD⁺ synthase, TbTc_2404; mASAT, mitochondrial aspartate
1400 aminotransferase, TbTc_5877; METK1, AdoMet synthase, TbTc_0178. G) PWY1V8-11:
1401 AKCT, 2-amino-3-ketobutyrate-CoA ligase, TbTc_6236; TDH, L-threonine dehydrogenase,
1402 TbTc_5991. H) VALDEG-PWY: ECH, enoyl-CoA hydratase, TbTc_3283; HOPR, 2-hydroxy-
1403 3-oxopropionate reductase, TbTc_2903; BCAAT, branched-chain amino acid
1404 aminotransferase, TbTc_0559. I) PROLINE-DEG2-PWY: P5CDH, delta-1-pyrroline-5-
1405 carboxylate dehydrogenase, TbTc1695; GDH, glutamate dehydrogenase, TbTc_0872;
1406 ProDH, proline dehydrogenase, TbTc_1591.

1407 **S7 figure: Carbon utilisation for trypanothione biosynthesis in *T. congolense*.**

1408 Metabolomics and transcriptomics analyses were carried out to analyse trypanothione
1409 biosynthesis. A) A simplified map of trypanothione biosynthesis as known in *T. brucei*.
1410 Numbers refer to the following enzymes: 1, S-adenosyl-L-methionine synthase, METK1; 2, S-
1411 adenosyl-L-methionine decarboxylase, AdoMetDC; 3, spermidine synthase, SpSyn; 4,
1412 methyltransferase reaction, MTase; 5, S-adenosyl-L-homocysteine dehydrolase, AdoHycase;
1413 6, cystathionine beta synthase, CBS; 7, cystathione gamma lyase, CTH; 8,
1414 glutaminase/amidase, AM; 9, gamma-glutamylcysteine synthetase, GCS; 10, glutathione
1415 synthetase, GSS; 11, ornithine decarboxylase, ODC; 12, spermidine synthase, SpSyn; 13,
1416 glutathionylspermidine synthase, GSP; 14, trypanothione synthetase, TRYS; 15, tryparedoxin
1417 peroxidase, TXN1b; 16, trypanothione reductase, TRYR. B) Isotopologue labelling
1418 experiments using 100% ¹³C-L-serine, ¹³C-L-glutamine, ¹³C-L-methionine or ¹³C-L-cysteine,
1419 showing the abundance of carbon labelling derived from these amino acids in components of
1420 the trypanothione biosynthesis pathway. C) Transcriptomics analysis using the following
1421 TrypanoCyc pathways: PWY1V8-6 (trypanothione biosynthesis), HOMOCYSDESGR-PWY1
1422 (homocysteine degradation/cysteine biosynthesis) & METHIONINE-DEG1-PWY (methionine
1423 degradation I). GeneIDs: TNX1b, tryparedoxin 1b, TbTc_0324; TRYS, trypanothione

1424 synthetase, TbTc_1359; SpSyn, Spermidine synthase, TbTc_1034; TRYR, trypanothione
1425 reductase, TbTc_4239; AdoMetDC_0696, S-adenosylmethionine decarboxylase, TbTc0696;
1426 GCS, gamma-glutamylcysteine synthetase, TbTc_3424; METK1, S-adenosylmethionine
1427 synthetase, TbTc_0178; GSS, glutathione synthetase, TbTc_3678; AdoMetDC_3193, S-
1428 adenosylmethionine decarboxylase, TbTc_3193; AM, amidase, TbTc_5549; ODC, ornithine
1429 decarboxylase, TbTc_5903; CTH, cystathione gamma lyase, TbTc_1051; CBS, cystathionine
1430 beta synthase, TbTc_0413; AdoHcyase, S-adenosylhomocysteine hydrolase, TbTc_0685;
1431 METK1, S-adenosylmethionine synthase, TbTc_0178.

1432 **S8 Figure: Analysis of LC-MS utilising stable isotope labelled amino acids.** Percentage
1433 total labelling of metabolites identified in data from 6 stable isotope labelling experiments using
1434 ¹³C-L-asparagine, ¹³C-L-cysteine, ¹³C-L-glutamine, ¹³C-L-methionine, ¹³C-L-proline and ¹³C-L-
1435 serine. Colour intensity correlates to the total fraction of the metabolite that was ¹³C-labeled.

1436 **Supplementary Data**

1437 **S1 Table:** RNAseq dataset – *T. congolense ex vivo*, *T. congolense in vitro*, *T. brucei ex vivo*,
1438 *T. brucei in vitro*, Silvester *et al* dataset

1439 **S2 Table:** Orthofinder output comparing *T. congolense* TriTrypDB (v34.0), *T. congolense*
1440 Liverpool pacbio, *T. brucei* TriTrypDB (v34.0) and other trypanosomatids

1441 **S3 Table:** RNAseq dataset – *T. congolense* only, Pacbio assembly, single genes.

1442 **S4 Table:** Supernatant metabolomics dataset for *in vitro* cultured *T. congolense* over a period
1443 of 56 hours. Metabolites highlighted in yellow were confidently predicted using a set of
1444 metabolite standards run alongside the experimental samples. Results of statistical analysis
1445 by means of a one-way repeated measures ANOVA (false discovery rate-adjusted P value,
1446 FDR) is also shown for metabolites that were taken forward for downstream analysis

1447 **S5 Table:** TrypanoCyc pathways and linked Orthogroup gene IDs

1448 **S6 Table:** Formulation of Steketee's congolense medium (SCM)-6 & -7

1449 **S7 table:** List of primers used in this study

1450

1451

1452 **References**

1453 1. Morrison LJ, Vezza L, Rowan T, Hope JC. Animal African Trypanosomiasis: Time to Increase Focus
1454 on Clinically Relevant Parasite and Host Species. *Trends Parasitol.* 2016;32(8): 599-607. doi:
1455 10.1016/j.pt.2016.04.012.

1456 2. Auty H, Torr SJ, Michael T, Jayaraman S, Morrison LJ. Cattle trypanosomosis: the diversity of
1457 trypanosomes and implications for disease epidemiology and control. *Rev Sci Tech.* 2015;34(2):
1458 587-98.

1459 3. Giordani F, Morrison LJ, Rowan TG, HP DEK, Barrett MP. The animal trypanosomiasis and their
1460 chemotherapy: a review. *Parasitology.* 2016;143(14): 1862-89. doi:
1461 10.1017/S0031182016001268.

1462 4. Shaw AP, Cecchi G, Wint GR, Mattioli RC, Robinson TP. Mapping the economic benefits to
1463 livestock keepers from intervening against bovine trypanosomosis in Eastern Africa. *Prev Vet*
1464 *Med.* 2014;113(2): 197-210. doi: 10.1016/j.prevetmed.2013.10.024.

1465 5. Chitanga S, Marcotty T, Namangala B, Van den Bossche P, Van Den Abbeele J, Delespaux V. High
1466 prevalence of drug resistance in animal trypanosomes without a history of drug exposure. *PLoS*
1467 *Negl Trop Dis.* 2011;5(12): e1454. doi: 10.1371/journal.pntd.0001454.

1468 6. Delespaux V, Dinka H, Masumu J, Van den Bossche P, Geerts S. Five-fold increase in
1469 *Trypanosoma congolense* isolates resistant to diminazene aceturate over a seven-year period
1470 in Eastern Zambia. *Drug Resist Updat.* 2008;11(6): 205-9. doi: 10.1016/j.drug.2008.10.002.

1471 7. Geerts S, Holmes PH, Eisler MC, Diall O. African bovine trypanosomiasis: the problem of drug
1472 resistance. *Trends Parasitol.* 2001;17(1): 25-8.

- 1473 8. Diall O, Cecchi G, Wanda G, Argiles-Herrero R, Vreysen MJB, Cattoli G, et al. Developing a
1474 Progressive Control Pathway for African Animal Trypanosomosis. *Trends Parasitol.* 2017;33(7):
1475 499-509. doi: 10.1016/j.pt.2017.02.005.
- 1476 9. Barrett MP, Burchmore RJ, Stich A, Lazzari JO, Frasch AC, Cazzulo JJ, et al. The trypanosomiasis.
1477 *Lancet.* 2003;362(9394): 1469-80. doi: 10.1016/S0140-6736(03)14694-6.
- 1478 10. Alsford S, Kawahara T, Glover L, Horn D. Tagging a *T. brucei* rRNA locus improves stable
1479 transfection efficiency and circumvents inducible expression position effects. *Mol Biochem*
1480 *Parasitol.* 2005;144(2): 142-8. doi: 10.1016/j.molbiopara.2005.08.009.
- 1481 11. Rico E, Jeacock L, Kovarova J, Horn D. Inducible high-efficiency CRISPR-Cas9-targeted gene
1482 editing and precision base editing in African trypanosomes. *Sci Rep.* 2018;8(1): 7960. doi:
1483 10.1038/s41598-018-26303-w.
- 1484 12. Gibson W. The origins of the trypanosome genome strains *Trypanosoma brucei brucei* TREU
1485 927, *T. b. gambiense* DAL 972, *T. vivax* Y486 and *T. congolense* IL3000. *Parasit Vectors.* 2012;5:
1486 71. doi: 10.1186/1756-3305-5-71.
- 1487 13. Kay C, Peacock L, Gibson W. *Trypanosoma congolense*: In Vitro Culture and Transfection. *Curr*
1488 *Protoc Microbiol.* 2019;53(1): e77. doi: 10.1002/cpmc.77.
- 1489 14. Coustou V, Guegan F, Plazolles N, Baltz T. Complete in vitro life cycle of *Trypanosoma*
1490 *congolense*: development of genetic tools. *PLoS Negl Trop Dis.* 2010;4(3): e618. doi:
1491 10.1371/journal.pntd.0000618.
- 1492 15. Hirumi H, Hirumi K. In vitro cultivation of *Trypanosoma congolense* bloodstream forms in the
1493 absence of feeder cell layers. *Parasitology.* 1991;102 Pt 2: 225-36.
- 1494 16. Rotureau B, Van Den Abbeele J. Through the dark continent: African trypanosome development
1495 in the tsetse fly. *Front Cell Infect Microbiol.* 2013;3: 53. doi: 10.3389/fcimb.2013.00053.
- 1496 17. Silvester E, Young J, Ivens A, Matthews KR. Interspecies quorum sensing in co-infections can
1497 manipulate trypanosome transmission potential. *Nat Microbiol.* 2017;2(11): 1471-9. doi:
1498 10.1038/s41564-017-0014-5.

- 1499 18. Jackson AP, Allison HC, Barry JD, Field MC, Hertz-Fowler C, Berriman M. A cell-surface phylome
1500 for African trypanosomes. *PLoS Negl Trop Dis.* 2013;7(3): e2121. doi:
1501 10.1371/journal.pntd.0002121.
- 1502 19. Jackson AP, Berry A, Aslett M, Allison HC, Burton P, Vavrova-Anderson J, et al. Antigenic diversity
1503 is generated by distinct evolutionary mechanisms in African trypanosome species. *Proc Natl
1504 Acad Sci U S A.* 2012;109(9): 3416-21. doi: 10.1073/pnas.1117313109.
- 1505 20. Silva Pereira S, Casas-Sanchez A, Haines LR, Ogugo M, Absolomon K, Sanders M, et al. Variant
1506 antigen repertoires in *Trypanosoma congolense* populations and experimental infections can
1507 be profiled from deep sequence data using universal protein motifs. *Genome Res.* 2018;28(9):
1508 1383-94. doi: 10.1101/gr.234146.118.
- 1509 21. Silva Pereira S, de Almeida Castilho Neto KJG, Duffy CW, Richards P, Noyes H, Ogugo M, et al.
1510 Variant antigen diversity in *Trypanosoma vivax* is not driven by recombination. *Nat Commun.*
1511 2020;11(1): 844. doi: 10.1038/s41467-020-14575-8.
- 1512 22. Tihon E, Imamura H, Dujardin JC, Van Den Abbeele J, Van den Broeck F. Discovery and genomic
1513 analyses of hybridization between divergent lineages of *Trypanosoma congolense*, causative
1514 agent of Animal African Trypanosomiasis. *Mol Ecol.* 2017;26(23): 6524-38. doi:
1515 10.1111/mec.14271.
- 1516 23. Creek DJ, Barrett MP. Determination of antiprotozoal drug mechanisms by metabolomics
1517 approaches. *Parasitology.* 2014;141(1): 83-92. doi: 10.1017/S0031182013000814.
- 1518 24. Haanstra JR, Gerding A, Dolga AM, Sorgdrager FJH, Buist-Homan M, du Toit F, et al. Targeting
1519 pathogen metabolism without collateral damage to the host. *Sci Rep.* 2017;7: 40406. doi:
1520 10.1038/srep40406.
- 1521 25. Vincent IM, Ehmann DE, Mills SD, Perros M, Barrett MP. Untargeted Metabolomics To Ascertain
1522 Antibiotic Modes of Action. *Antimicrob Agents Chemother.* 2016;60(4): 2281-91. doi:
1523 10.1128/AAC.02109-15.

- 1524 26. Bringaud F, Biran M, Millerioux Y, Wargnies M, Allmann S, Mazet M. Combining reverse genetics
1525 and nuclear magnetic resonance-based metabolomics unravels trypanosome-specific metabolic
1526 pathways. *Mol Microbiol.* 2015;96(5): 917-26. doi: 10.1111/mmi.12990.
- 1527 27. Creek DJ, Anderson J, McConville MJ, Barrett MP. Metabolomic analysis of trypanosomatid
1528 protozoa. *Mol Biochem Parasitol.* 2012;181(2): 73-84. doi: 10.1016/j.molbiopara.2011.10.003.
- 1529 28. Allmann S, Bringaud F. Glycosomes: A comprehensive view of their metabolic roles in *T. brucei*.
1530 *Int J Biochem Cell Biol.* 2017;85: 85-90. doi: 10.1016/j.biocel.2017.01.015.
- 1531 29. Haanstra JR, van Tuijl A, Kessler P, Reijnders W, Michels PA, Westerhoff HV, et al.
1532 Compartmentation prevents a lethal turbo-explosion of glycolysis in trypanosomes. *Proc Natl
1533 Acad Sci U S A.* 2008;105(46): 17718-23. doi: 10.1073/pnas.0806664105.
- 1534 30. Mazet M, Morand P, Biran M, Bouyssou G, Courtois P, Daulouede S, et al. Revisiting the central
1535 metabolism of the bloodstream forms of *Trypanosoma brucei*: production of acetate in the
1536 mitochondrion is essential for parasite viability. *PLoS Negl Trop Dis.* 2013;7(12): e2587. doi:
1537 10.1371/journal.pntd.0002587.
- 1538 31. Millerioux Y, Mazet M, Bouyssou G, Allmann S, Kiema TR, Bertiaux E, et al. De novo biosynthesis
1539 of sterols and fatty acids in the *Trypanosoma brucei* procyclic form: Carbon source preferences
1540 and metabolic flux redistributions. *PLoS Pathog.* 2018;14(5): e1007116. doi:
1541 10.1371/journal.ppat.1007116.
- 1542 32. Yang PY, Wang M, Liu K, Ngai MH, Sheriff O, Lear MJ, et al. Parasite-based screening and
1543 proteome profiling reveal orlistat, an FDA-approved drug, as a potential anti *Trypanosoma
1544 brucei* agent. *Chemistry.* 2012;18(27): 8403-13. doi: 10.1002/chem.201200482.
- 1545 33. Lamour N, Riviere L, Coustou V, Coombs GH, Barrett MP, Bringaud F. Proline metabolism in
1546 procyclic *Trypanosoma brucei* is down-regulated in the presence of glucose. *J Biol Chem.*
1547 2005;280(12): 11902-10. doi: 10.1074/jbc.M414274200.
- 1548 34. Tielens AG, Van Hellemond JJ. Differences in energy metabolism between trypanosomatidae.
1549 *Parasitol Today.* 1998;14(7): 265-72.

- 1550 35. van Weelden SW, Fast B, Vogt A, van der Meer P, Saas J, van Hellemond JJ, et al. Procylic
1551 Trypanosoma brucei do not use Krebs cycle activity for energy generation. J Biol Chem.
1552 2003;278(15): 12854-63. doi: 10.1074/jbc.M213190200.
- 1553 36. van Hellemond JJ, Opperdoes FR, Tielens AG. The extraordinary mitochondrion and unusual
1554 citric acid cycle in Trypanosoma brucei. Biochem Soc Trans. 2005;33(Pt 5): 967-71. doi:
1555 10.1042/BST20050967.
- 1556 37. Villafraz O, Biran M, Pineda E, Plazolles N, Cahoreau E, Ornitz R, et al. Fly stage trypanosomes
1557 recycle glucose catabolites and TCA cycle intermediates to stimulate growth in near
1558 physiological conditions. 2020: 2020.12.17.423221. doi: 10.1101/2020.12.17.423221 %J
1559 bioRxiv.
- 1560 38. Colasante C, Robles A, Li CH, Schwede A, Benz C, Voncken F, et al. Regulated expression of
1561 glycosomal phosphoglycerate kinase in Trypanosoma brucei. Mol Biochem Parasitol.
1562 2007;151(2): 193-204. doi: 10.1016/j.molbiopara.2006.11.003.
- 1563 39. Blattner J, Helfert S, Michels P, Clayton C. Compartmentation of phosphoglycerate kinase in
1564 Trypanosoma brucei plays a critical role in parasite energy metabolism. Proc Natl Acad Sci U S
1565 A. 1998;95(20): 11596-600.
- 1566 40. Deramchia K, Morand P, Biran M, Millerioux Y, Mazet M, Wagnies M, et al. Contribution of
1567 pyruvate phosphate dikinase in the maintenance of the glycosomal ATP/ADP balance in the
1568 Trypanosoma brucei procyclic form. J Biol Chem. 2014;289(25): 17365-78. doi:
1569 10.1074/jbc.M114.567230.
- 1570 41. van Grinsven KW, Van Den Abbeele J, Van den Bossche P, van Hellemond JJ, Tielens AG.
1571 Adaptations in the glucose metabolism of procyclic Trypanosoma brucei isolates from tsetse
1572 flies and during differentiation of bloodstream forms. Eukaryot Cell. 2009;8(8): 1307-11. doi:
1573 10.1128/EC.00091-09.
- 1574 42. Creek DJ, Mazet M, Achcar F, Anderson J, Kim DH, Kamour R, et al. Probing the metabolic
1575 network in bloodstream-form Trypanosoma brucei using untargeted metabolomics with stable

1576 isotope labelled glucose. PLoS Pathog. 2015;11(3): e1004689. doi:
1577 10.1371/journal.ppat.1004689.

1578 43. Agosin M, Von Brand T. Studies on the carbohydrate metabolism of *Trypanosoma congolense*.
1579 Exp Parasitol. 1954;3(6): 517-24.

1580 44. Bringaud F, Baltz D, Baltz T. Functional and molecular characterization of a glycosomal PPI-
1581 dependent enzyme in trypanosomatids: pyruvate, phosphate dikinase. Proc Natl Acad Sci U S A.
1582 1998;95(14): 7963-8.

1583 45. Ohashi-Suzuki M, Yabu Y, Ohshima S, Nakamura K, Kido Y, Sakamoto K, et al. Differential kinetic
1584 activities of glycerol kinase among African trypanosome species: phylogenetic and therapeutic
1585 implications. J Vet Med Sci. 2011;73(5): 615-21.

1586 46. Parker HL, Hill T, Alexander K, Murphy NB, Fish WR, Parsons M. Three genes and two isozymes:
1587 gene conversion and the compartmentalization and expression of the phosphoglycerate kinases
1588 of *Trypanosoma (Nannomonas) congolense*. Mol Biochem Parasitol. 1995;69(2): 269-79.

1589 47. Vickerman K. The fine structure of *Trypanosoma congolense* in its bloodstream phase. J
1590 Protozool. 1969;16(1): 54-69.

1591 48. Bienen EJ, Webster P, Fish WR. *Trypanosoma (Nannomonas) congolense*: changes in respiratory
1592 metabolism during the life cycle. Exp Parasitol. 1991;73(4): 403-12.

1593 49. Ebiloma GU, Ayuga TD, Balogun EO, Gil LA, Donachie A, Kaiser M, et al. Inhibition of
1594 trypanosome alternative oxidase without its N-terminal mitochondrial targeting signal
1595 (Δ MTS-TAO) by cationic and non-cationic 4-hydroxybenzoate and 4-alkoxybenzaldehyde
1596 derivatives active against *T. brucei* and *T. congolense*. Eur J Med Chem. 2018;150: 385-402. doi:
1597 10.1016/j.ejmech.2018.02.075.

1598 50. Fueyo Gonzalez FJ, Ebiloma GU, Izquierdo Garcia C, Bruggeman V, Sanchez Villamanan JM,
1599 Donachie A, et al. Conjugates of 2,4-Dihydroxybenzoate and Salicylhydroxamate and
1600 Lipocations Display Potent Antiparasite Effects by Efficiently Targeting the *Trypanosoma brucei*

1601 and *Trypanosoma congolense* Mitochondrion. *J Med Chem.* 2017;60(4): 1509-22. doi:
1602 10.1021/acs.jmedchem.6b01740.

1603 51. Steiger RF, Steiger E, Trager W, Schneider I. *Trypanosoma congolense*: partial cyclic
1604 development in a *Glossina* cell system and oxygen consumption. *J Parasitol.* 1977;63(5): 861-7.

1605 52. Hsu HH, Araki M, Mochizuki M, Hori Y, Murata M, Kahar P, et al. A Systematic Approach to Time-
1606 series Metabolite Profiling and RNA-seq Analysis of Chinese Hamster Ovary Cell Culture. *Sci Rep.*
1607 2017;7: 43518. doi: 10.1038/srep43518.

1608 53. Wagner GP, Kin K, Lynch VJ. Measurement of mRNA abundance using RNA-seq data: RPKM
1609 measure is inconsistent among samples. *Theory Biosci.* 2012;131(4): 281-5. doi:
1610 10.1007/s12064-012-0162-3.

1611 54. Emms DM, Kelly S. OrthoFinder: solving fundamental biases in whole genome comparisons
1612 dramatically improves orthogroup inference accuracy. *Genome Biol.* 2015;16: 157. doi:
1613 10.1186/s13059-015-0721-2.

1614 55. Silvester E, Ivens A, Matthews KR. A gene expression comparison of *Trypanosoma brucei* and
1615 *Trypanosoma congolense* in the bloodstream of the mammalian host reveals species-specific
1616 adaptations to density-dependent development. *PLoS Negl Trop Dis.* 2018;12(10): e0006863.
1617 doi: 10.1371/journal.pntd.0006863.

1618 56. Creek DJ, Nijagal B, Kim DH, Rojas F, Matthews KR, Barrett MP. Metabolomics guides rational
1619 development of a simplified cell culture medium for drug screening against *Trypanosoma*
1620 *brucei*. *Antimicrob Agents Chemother.* 2013;57(6): 2768-79. doi: 10.1128/AAC.00044-13.

1621 57. Kim DH, Achcar F, Breitling R, Burgess KE, Barrett MP. LC-MS-based absolute metabolite
1622 quantification: application to metabolic flux measurement in trypanosomes. *Metabolomics.*
1623 2015;11(6): 1721-32. doi: 10.1007/s11306-015-0827-2.

1624 58. Nok AJ, Esievo KA, Ibrahim S, Ukoha AI, Ikediobi CO. Phospholipase A2 from *Trypanosoma*
1625 *congolense*: characterization and haematological properties. *Cell Biochem Funct.* 1993;11(2):
1626 125-30. doi: 10.1002/cbf.290110208.

- 1627 59. Duszenko M, Ferguson MA, Lamont GS, Rifkin MR, Cross GA. Cysteine eliminates the feeder cell
1628 requirement for cultivation of *Trypanosoma brucei* bloodstream forms in vitro. *J Exp Med.*
1629 1985;162(4): 1256-63.
- 1630 60. Shameer S, Logan-Klumpler FJ, Vinson F, Cottret L, Merlet B, Achcar F, et al. TrypanoCyc: a
1631 community-led biochemical pathways database for *Trypanosoma brucei*. *Nucleic Acids Res.*
1632 2015;43(Database issue): D637-44. doi: 10.1093/nar/gku944.
- 1633 61. Szoor B, Ruberto I, Burchmore R, Matthews KR. A novel phosphatase cascade regulates
1634 differentiation in *Trypanosoma brucei* via a glycosomal signaling pathway. *Genes Dev.*
1635 2010;24(12): 1306-16. doi: 10.1101/gad.570310.
- 1636 62. Mugo E, Clayton C. Expression of the RNA-binding protein RBP10 promotes the bloodstream-
1637 form differentiation state in *Trypanosoma brucei*. *PLoS Pathog.* 2017;13(8): e1006560. doi:
1638 10.1371/journal.ppat.1006560.
- 1639 63. Dean S, Marchetti R, Kirk K, Matthews KR. A surface transporter family conveys the
1640 trypanosome differentiation signal. *Nature.* 2009;459(7244): 213-7. doi: 10.1038/nature07997.
- 1641 64. Aranda A, Maugeri D, Uttaro AD, Opperdoes F, Cazzulo JJ, Nowicki C. The malate dehydrogenase
1642 isoforms from *Trypanosoma brucei*: subcellular localization and differential expression in
1643 bloodstream and procyclic forms. *Int J Parasitol.* 2006;36(3): 295-307. doi:
1644 10.1016/j.ijpara.2005.09.013.
- 1645 65. Abbas AH, Silva Pereira S, D'Archivio S, Wickstead B, Morrison LJ, Hall N, et al. The Structure of
1646 a Conserved Telomeric Region Associated with Variant Antigen Loci in the Blood Parasite
1647 *Trypanosoma congolense*. *Genome Biol Evol.* 2018;10(9): 2458-73. doi: 10.1093/gbe/evy186.
- 1648 66. Spitznagel D, Ebikeme C, Biran M, Nic a' Bhaird N, Bringaud F, Henehan GT, et al. Alanine
1649 aminotransferase of *Trypanosoma brucei*--a key role in proline metabolism in procyclic life
1650 forms. *FEBS J.* 2009;276(23): 7187-99. doi: 10.1111/j.1742-4658.2009.07432.x.

- 1651 67. Natesan SK, Peacock L, Leung KF, Gibson W, Field MC. Evidence that low endocytic activity is
1652 not directly responsible for human serum resistance in the insect form of African trypanosomes.
1653 BMC Res Notes. 2010;3: 63. doi: 10.1186/1756-0500-3-63.
- 1654 68. Ebikeme CE, Peacock L, Coustou V, Riviere L, Bringaud F, Gibson WC, et al. N-acetyl D-
1655 glucosamine stimulates growth in procyclic forms of *Trypanosoma brucei* by inducing a
1656 metabolic shift. Parasitology. 2008;135(5): 585-94. doi: 10.1017/S0031182008004241.
- 1657 69. Awuah-Mensah G, McDonald J, Steketee PC, Autheman D, Whipple S, D'Archivio S, et al.
1658 Reliable, scalable functional genetics in bloodstream-form *Trypanosoma congolense* in vitro
1659 and in vivo. PLoS Pathog. 2021;17(1): e1009224. doi: 10.1371/journal.ppat.1009224.
- 1660 70. Kovarova J, Nagar R, Faria J, Ferguson MAJ, Barrett MP, Horn D. Gluconeogenesis using glycerol
1661 as a substrate in bloodstream-form *Trypanosoma brucei*. PLoS Pathog. 2018;14(12): e1007475.
1662 doi: 10.1371/journal.ppat.1007475.
- 1663 71. Tielens AG, van Hellemond JJ. Surprising variety in energy metabolism within
1664 Trypanosomatidae. Trends Parasitol. 2009;25(10): 482-90. doi: 10.1016/j.pt.2009.07.007.
- 1665 72. Trindade S, Rijo-Ferreira F, Carvalho T, Pinto-Neves D, Guegan F, Aresta-Branco F, et al.
1666 *Trypanosoma brucei* Parasites Occupy and Functionally Adapt to the Adipose Tissue in Mice.
1667 Cell Host Microbe. 2016;19(6): 837-48. doi: 10.1016/j.chom.2016.05.002.
- 1668 73. Zikova A, Verner Z, Nenarokova A, Michels PAM, Lukes J. A paradigm shift: The mitoproteomes
1669 of procyclic and bloodstream *Trypanosoma brucei* are comparably complex. PLoS Pathog.
1670 2017;13(12): e1006679. doi: 10.1371/journal.ppat.1006679.
- 1671 74. Geiger A, Hirtz C, Becue T, Bellard E, Centeno D, Gargani D, et al. Exocytosis and protein
1672 secretion in *Trypanosoma*. BMC Microbiol. 2010;10: 20. doi: 10.1186/1471-2180-10-20.
- 1673 75. Manivel G, Meyyazhagan A, Durairaj DR, Piramanayagam S. Genome-wide analysis of
1674 Excretory/Secretory proteins in *Trypanosoma brucei brucei*: Insights into functional
1675 characteristics and identification of potential targets by immunoinformatics approach.
1676 Genomics. 2019;111(5): 1124-33. doi: 10.1016/j.ygeno.2018.07.007.

- 1677 76. Henriques C, Sanchez MA, Tryon R, Landfear SM. Molecular and functional characterization of
1678 the first nucleobase transporter gene from African trypanosomes. *Mol Biochem Parasitol.*
1679 2003;130(2): 101-10. doi: 10.1016/s0166-6851(03)00167-1.
- 1680 77. Burchmore RJ, Wallace LJ, Candlish D, Al-Salabi MI, Beal PR, Barrett MP, et al. Cloning,
1681 heterologous expression, and in situ characterization of the first high affinity nucleobase
1682 transporter from a protozoan. *J Biol Chem.* 2003;278(26): 23502-7. doi:
1683 10.1074/jbc.M301252200.
- 1684 78. Munday JC, Rojas Lopez KE, Eze AA, Delespaux V, Van Den Abbeele J, Rowan T, et al. Functional
1685 expression of TcoAT1 reveals it to be a P1-type nucleoside transporter with no capacity for
1686 diminazene uptake. *Int J Parasitol Drugs Drug Resist.* 2013;3: 69-76. doi:
1687 10.1016/j.ijpddr.2013.01.004.
- 1688 79. Al-Salabi MI, Wallace LJ, Luscher A, Maser P, Candlish D, Rodenko B, et al. Molecular interactions
1689 underlying the unusually high adenosine affinity of a novel *Trypanosoma brucei* nucleoside
1690 transporter. *Mol Pharmacol.* 2007;71(3): 921-9. doi: 10.1124/mol.106.031559.
- 1691 80. de Koning HP, Bridges DJ, Burchmore RJ. Purine and pyrimidine transport in pathogenic
1692 protozoa: from biology to therapy. *FEMS Microbiol Rev.* 2005;29(5): 987-1020. doi:
1693 10.1016/j.femsre.2005.03.004.
- 1694 81. Papageorgiou IG, Yakob L, Al Salabi MI, Diallinas G, Soteriadou KP, De Koning HP. Identification
1695 of the first pyrimidine nucleobase transporter in *Leishmania*: similarities with the *Trypanosoma*
1696 *brucei* U1 transporter and antileishmanial activity of uracil analogues. *Parasitology.* 2005;130(Pt
1697 3): 275-83. doi: 10.1017/s0031182004006626.
- 1698 82. Gudin S, Quashie NB, Candlish D, Al-Salabi MI, Jarvis SM, Ranford-Cartwright LC, et al.
1699 *Trypanosoma brucei*: a survey of pyrimidine transport activities. *Exp Parasitol.* 2006;114(2):
1700 118-25. doi: 10.1016/j.exppara.2006.02.018.

- 1701 83. de Koning HP, Jarvis SM. A highly selective, high-affinity transporter for uracil in *Trypanosoma*
1702 *brucei brucei*: evidence for proton-dependent transport. *Biochem Cell Biol.* 1998;76(5): 853-8.
1703 doi: 10.1139/bcb-76-5-853.
- 1704 84. Ali JA, Tagoe DN, Munday JC, Donachie A, Morrison LJ, de Koning HP. Pyrimidine biosynthesis is
1705 not an essential function for *Trypanosoma brucei* bloodstream forms. *PLoS One.* 2013;8(3):
1706 e58034. doi: 10.1371/journal.pone.0058034.
- 1707 85. Johnston K, Kim DH, Kerkhoven EJ, Burchmore R, Barrett MP, Achcar F. Mapping the metabolism
1708 of five amino acids in bloodstream form *Trypanosoma brucei* using U-(13)C-labelled substrates
1709 and LC-MS. *Biosci Rep.* 2019;39(5). doi: 10.1042/BSR20181601.
- 1710 86. Marchese L, Nascimento JF, Damasceno FS, Bringaud F, Michels PAM, Silber AM. The Uptake
1711 and Metabolism of Amino Acids, and Their Unique Role in the Biology of Pathogenic
1712 *Trypanosomatids*. *Pathogens.* 2018;7(2). doi: 10.3390/pathogens7020036.
- 1713 87. Mantilla BS, Marchese L, Casas-Sanchez A, Dyer NA, Ejeh N, Biran M, et al. Proline Metabolism
1714 is Essential for *Trypanosoma brucei brucei* Survival in the Tsetse Vector. *PLoS Pathog.*
1715 2017;13(1): e1006158. doi: 10.1371/journal.ppat.1006158.
- 1716 88. Paul KS, Jiang D, Morita YS, Englund PT. Fatty acid synthesis in African trypanosomes: a solution
1717 to the myristate mystery. *Trends Parasitol.* 2001;17(8): 381-7. doi: 10.1016/s1471-
1718 4922(01)01984-5.
- 1719 89. Stephens JL, Lee SH, Paul KS, Englund PT. Mitochondrial fatty acid synthesis in *Trypanosoma*
1720 *brucei*. *J Biol Chem.* 2007;282(7): 4427-36. doi: 10.1074/jbc.M609037200.
- 1721 90. Millerioux Y, Ebikeme C, Biran M, Morand P, Bouyssou G, Vincent IM, et al. The threonine
1722 degradation pathway of the *Trypanosoma brucei* procyclic form: the main carbon source for
1723 lipid biosynthesis is under metabolic control. *Mol Microbiol.* 2013;90(1): 114-29. doi:
1724 10.1111/mmi.12351.
- 1725 91. Millerioux Y, Morand P, Biran M, Mazet M, Moreau P, Wargnies M, et al. ATP synthesis-coupled
1726 and -uncoupled acetate production from acetyl-CoA by mitochondrial acetate:succinate CoA-

1727 transferase and acetyl-CoA thioesterase in *Trypanosoma*. *J Biol Chem*. 2012;287(21): 17186-97.
 1728 doi: 10.1074/jbc.M112.355404.

1729 92. Surve SV, Jensen BC, Heestand M, Mazet M, Smith TK, Bringaud F, et al. NADH dehydrogenase
 1730 of *Trypanosoma brucei* is important for efficient acetate production in bloodstream forms. *Mol*
 1731 *Biochem Parasitol*. 2017;211: 57-61. doi: 10.1016/j.molbiopara.2016.10.001.

1732 93. Stafkova J, Mach J, Biran M, Verner Z, Bringaud F, Tachezy J. Mitochondrial pyruvate carrier in
 1733 *Trypanosoma brucei*. *Mol Microbiol*. 2016;100(3): 442-56. doi: 10.1111/mmi.13325.

1734 94. Comerford SA, Huang Z, Du X, Wang Y, Cai L, Witkiewicz AK, et al. Acetate dependence of
 1735 tumors. *Cell*. 2014;159(7): 1591-602. doi: 10.1016/j.cell.2014.11.020.

1736 95. Riviere L, Moreau P, Allmann S, Hahn M, Biran M, Plazolles N, et al. Acetate produced in the
 1737 mitochondrion is the essential precursor for lipid biosynthesis in procyclic trypanosomes. *Proc*
 1738 *Natl Acad Sci U S A*. 2009;106(31): 12694-9. doi: 10.1073/pnas.0903355106.

1739 96. Lamont GS, Fox JA, Cross GA. Glycosyl-sn-1,2-dimyristylphosphatidylinositol is the membrane
 1740 anchor for *Trypanosoma equiperdum* and *T. (Nannomonas) congolense* variant surface
 1741 glycoproteins. *Mol Biochem Parasitol*. 1987;24(2): 131-6. doi: 10.1016/0166-6851(87)90099-5.

1742 97. Lee SH, Stephens JL, Paul KS, Englund PT. Fatty acid synthesis by elongases in trypanosomes.
 1743 *Cell*. 2006;126(4): 691-9. doi: 10.1016/j.cell.2006.06.045.

1744 98. Danaei G, Finucane MM, Lu Y, Singh GM, Cowan MJ, Paciorek CJ, et al. National, regional, and
 1745 global trends in fasting plasma glucose and diabetes prevalence since 1980: systematic analysis
 1746 of health examination surveys and epidemiological studies with 370 country-years and 2.7
 1747 million participants. *Lancet*. 2011;378(9785): 31-40. doi: 10.1016/S0140-6736(11)60679-X.

1748 99. Cozzi G, Ravarotto L, Gottardo F, Stefani AL, Contiero B, Moro L, et al. Short communication:
 1749 reference values for blood parameters in Holstein dairy cows: effects of parity, stage of
 1750 lactation, and season of production. *J Dairy Sci*. 2011;94(8): 3895-901. doi: 10.3168/jds.2010-
 1751 3687.

- 1752 100. Jackson PGG, Cockcroft PD. Appendix 2: Laboratory Reference Values: Haematology. Clinical
1753 Examination of Farm Animals 2002. p. 302-.
- 1754 101. Mair B, Drillich M, Klein-Jobstl D, Kanz P, Borchardt S, Meyer L, et al. Glucose concentration in
1755 capillary blood of dairy cows obtained by a minimally invasive lancet technique and determined
1756 with three different hand-held devices. BMC Vet Res. 2016;12: 34. doi: 10.1186/s12917-016-
1757 0662-3.
- 1758 102. Nafikov RA, Beitz DC. Carbohydrate and lipid metabolism in farm animals. J Nutr. 2007;137(3):
1759 702-5. doi: 10.1093/jn/137.3.702.
- 1760 103. Puppel K, Kuczynska B. Metabolic profiles of cow's blood; a review. J Sci Food Agric. 2016;96(13):
1761 4321-8. doi: 10.1002/jsfa.7779.
- 1762 104. Bochud-Allemann N, Schneider A. Mitochondrial substrate level phosphorylation is essential for
1763 growth of procyclic *Trypanosoma brucei*. J Biol Chem. 2002;277(36): 32849-54. doi:
1764 10.1074/jbc.M205776200.
- 1765 105. Mochizuki K, Inaoka DK, Mazet M, Shiba T, Fukuda K, Kurasawa H, et al. The ASCT/SCS cycle
1766 fuels mitochondrial ATP and acetate production in *Trypanosoma brucei*. Biochim Biophys Acta
1767 Bioenerg. 2020;1861(11): 148283. doi: 10.1016/j.bbabi.2020.148283.
- 1768 106. Verner Z, Skodova I, Polakova S, Durisova-Benkovicova V, Horvath A, Lukes J. Alternative NADH
1769 dehydrogenase (NDH2): intermembrane-space-facing counterpart of mitochondrial complex I
1770 in the procyclic *Trypanosoma brucei*. Parasitology. 2013;140(3): 328-37. doi:
1771 10.1017/S003118201200162X.
- 1772 107. Fang J, Beattie DS. Novel FMN-containing rotenone-insensitive NADH dehydrogenase from
1773 *Trypanosoma brucei* mitochondria: isolation and characterization. Biochemistry. 2002;41(9):
1774 3065-72. doi: 10.1021/bi015989w.
- 1775 108. Dewar CE, MacGregor P, Cooper S, Gould MK, Matthews KR, Savill NJ, et al. Mitochondrial DNA
1776 is critical for longevity and metabolism of transmission stage *Trypanosoma brucei*. PLoS Pathog.
1777 2018;14(7): e1007195. doi: 10.1371/journal.ppat.1007195.

- 1778 109. Tizard IR, Mellors A, Holmes WL, Nielsen K. The generation of phospholipase A and hemolytic
1779 fatty acids by autolysing suspensions of *Trypanosoma congolense*. *Tropenmed Parasitol.*
1780 1978;29(1): 127-33.
- 1781 110. Field MC, Horn D, Fairlamb AH, Ferguson MAJ, Gray DW, Read KD, et al. Anti-trypanosomatid
1782 drug discovery: an ongoing challenge and a continuing need. *Nat Rev Microbiol.* 2017;15(7):
1783 447. doi: 10.1038/nrmicro.2017.69.
- 1784 111. Hirumi H, Hirumi K. Axenic culture of African trypanosome bloodstream forms. *Parasitol Today.*
1785 1994;10(2): 80-4.
- 1786 112. Vassella E, Kramer R, Turner CM, Wankell M, Modes C, van den Bogaard M, et al. Deletion of a
1787 novel protein kinase with PX and FYVE-related domains increases the rate of differentiation of
1788 *Trypanosoma brucei*. *Mol Microbiol.* 2001;41(1): 33-46.
- 1789 113. Hirumi H, Hirumi K. Continuous cultivation of *Trypanosoma brucei* blood stream forms in a
1790 medium containing a low concentration of serum protein without feeder cell layers. *J Parasitol.*
1791 1989;75(6): 985-9.
- 1792 114. Herbert WJ, Lumsden WH. *Trypanosoma brucei*: a rapid "matching" method for estimating the
1793 host's parasitemia. *Exp Parasitol.* 1976;40(3): 427-31. doi: 10.1016/0014-4894(76)90110-7.
- 1794 115. Lanham SM, Godfrey DG. Isolation of salivarian trypanosomes from man and other mammals
1795 using DEAE-cellulose. *Exp Parasitol.* 1970;28(3): 521-34. doi: 10.1016/0014-4894(70)90120-7.
- 1796 116. Schumann Burkard G, Jutzi P, Roditi I. Genome-wide RNAi screens in bloodstream form
1797 trypanosomes identify drug transporters. *Mol Biochem Parasitol.* 2011;175(1): 91-4. doi:
1798 10.1016/j.molbiopara.2010.09.002.
- 1799 117. Raz B, Iten M, Grether-Buhler Y, Kaminsky R, Brun R. The Alamar Blue assay to determine drug
1800 sensitivity of African trypanosomes (*T.b. rhodesiense* and *T.b. gambiense*) in vitro. *Acta Trop.*
1801 1997;68(2): 139-47. doi: 10.1016/s0001-706x(97)00079-x.
- 1802 118. Untergasser A, Cutcutache I, Koressaar T, Ye J, Faircloth BC, Remm M, et al. Primer3--new
1803 capabilities and interfaces. *Nucleic Acids Res.* 2012;40(15): e115. doi: 10.1093/nar/gks596.

- 1804 119. Tihon E, Imamura H, Van den Broeck F, Vermeiren L, Dujardin JC, Van Den Abbeele J. Genomic
1805 analysis of Isometamidium Chloride resistance in *Trypanosoma congolense*. *Int J Parasitol Drugs*
1806 *Drug Resist.* 2017;7(3): 350-61. doi: 10.1016/j.ijpddr.2017.10.002.
- 1807 120. Livak KJ, Schmittgen TD. Analysis of relative gene expression data using real-time quantitative
1808 PCR and the 2⁻(Delta Delta C(T)) Method. *Methods.* 2001;25(4): 402-8. doi:
1809 10.1006/meth.2001.1262.
- 1810 121. Smith CA, Want EJ, O'Maille G, Abagyan R, Siuzdak G. XCMS: processing mass spectrometry data
1811 for metabolite profiling using nonlinear peak alignment, matching, and identification. *Anal*
1812 *Chem.* 2006;78(3): 779-87. doi: 10.1021/ac051437y.
- 1813 122. Scheltema RA, Jankevics A, Jansen RC, Swertz MA, Breitling R. PeakML/mzMatch: a file format,
1814 Java library, R library, and tool-chain for mass spectrometry data analysis. *Anal Chem.*
1815 2011;83(7): 2786-93. doi: 10.1021/ac2000994.
- 1816 123. Creek DJ, Jankevics A, Burgess KE, Breitling R, Barrett MP. IDEOM: an Excel interface for analysis
1817 of LC-MS-based metabolomics data. *Bioinformatics.* 2012;28(7): 1048-9. doi:
1818 10.1093/bioinformatics/bts069.
- 1819 124. Chokkathukalam A, Jankevics A, Creek DJ, Achcar F, Barrett MP, Breitling R. mzMatch-ISO: an R
1820 tool for the annotation and relative quantification of isotope-labelled mass spectrometry data.
1821 *Bioinformatics.* 2013;29(2): 281-3. doi: 10.1093/bioinformatics/bts674.
- 1822 125. Chong J, Xia J. Using MetaboAnalyst 4.0 for Metabolomics Data Analysis, Interpretation, and
1823 Integration with Other Omics Data. *Methods Mol Biol.* 2020;2104: 337-60. doi: 10.1007/978-1-
1824 0716-0239-3_17.
- 1825 126. Kim D, Langmead B, Salzberg SL. HISAT: a fast spliced aligner with low memory requirements.
1826 *Nat Methods.* 2015;12(4): 357-60. doi: 10.1038/nmeth.3317.
- 1827 127. Aslett M, Aurrecochea C, Berriman M, Brestelli J, Brunk BP, Carrington M, et al. TriTrypDB: a
1828 functional genomic resource for the Trypanosomatidae. *Nucleic Acids Res.* 2010;38(Database
1829 issue): D457-62. doi: 10.1093/nar/gkp851.

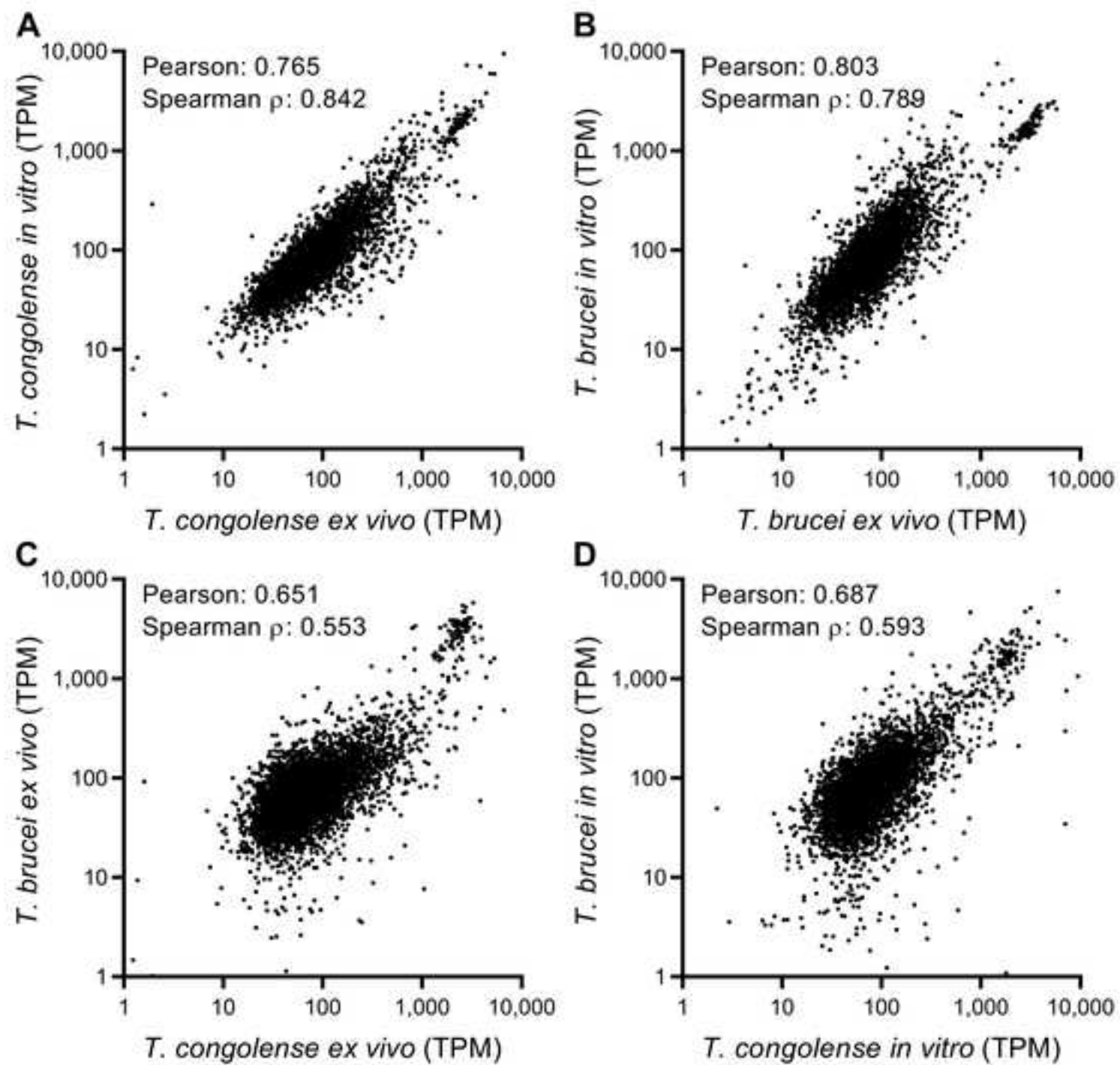
1830 128. Li H, Handsaker B, Wysoker A, Fennell T, Ruan J, Homer N, et al. The Sequence Alignment/Map
1831 format and SAMtools. *Bioinformatics*. 2009;25(16): 2078-9. doi:
1832 10.1093/bioinformatics/btp352.

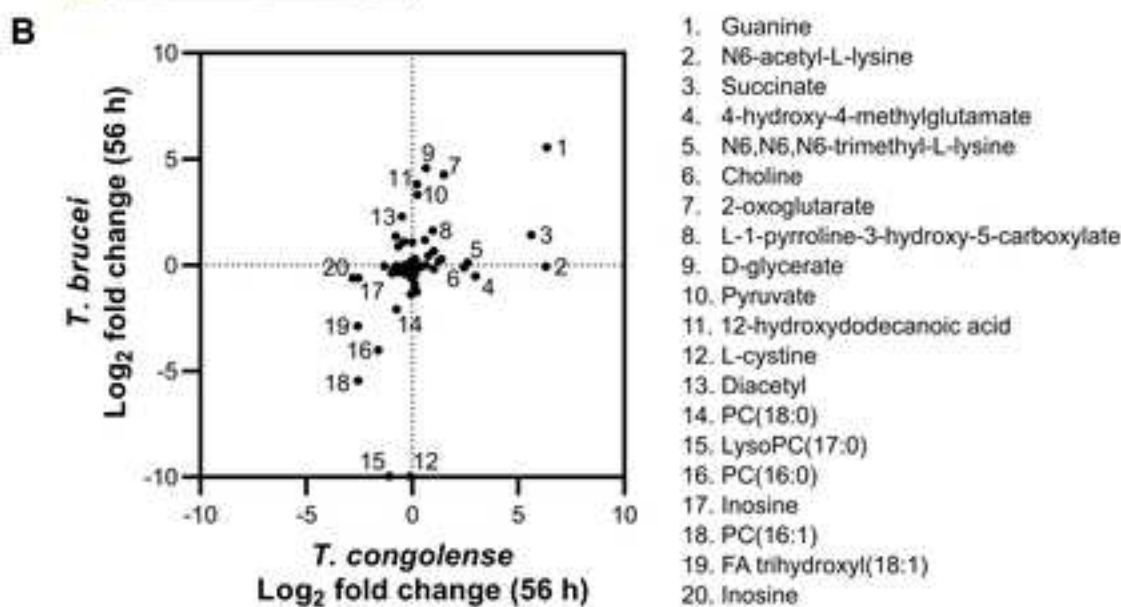
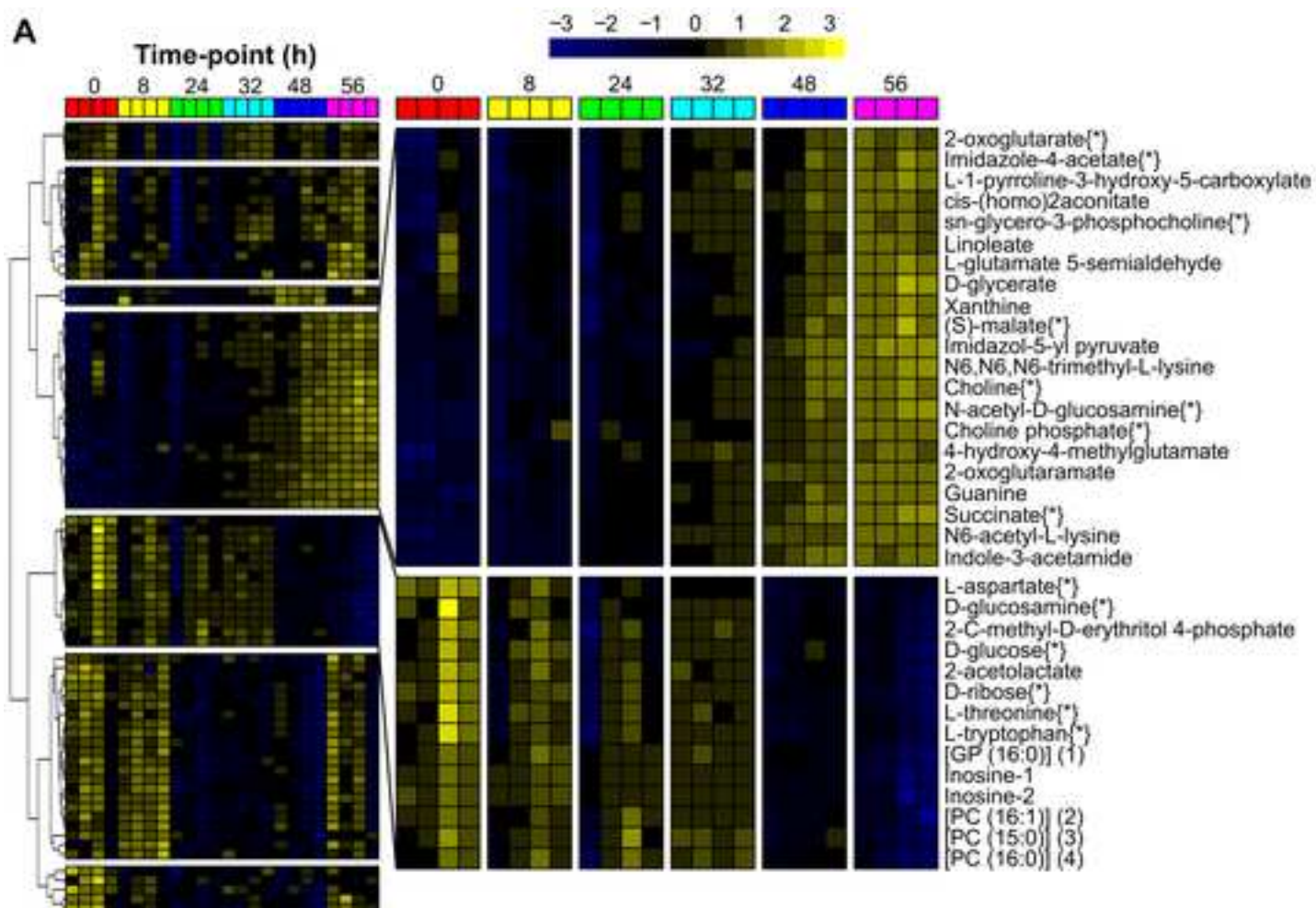
1833 129. Team. RC. R: A language and environment for statistical computing.: R Foundation for Statistical
1834 Computing, Vienna, Austria.; 2013.

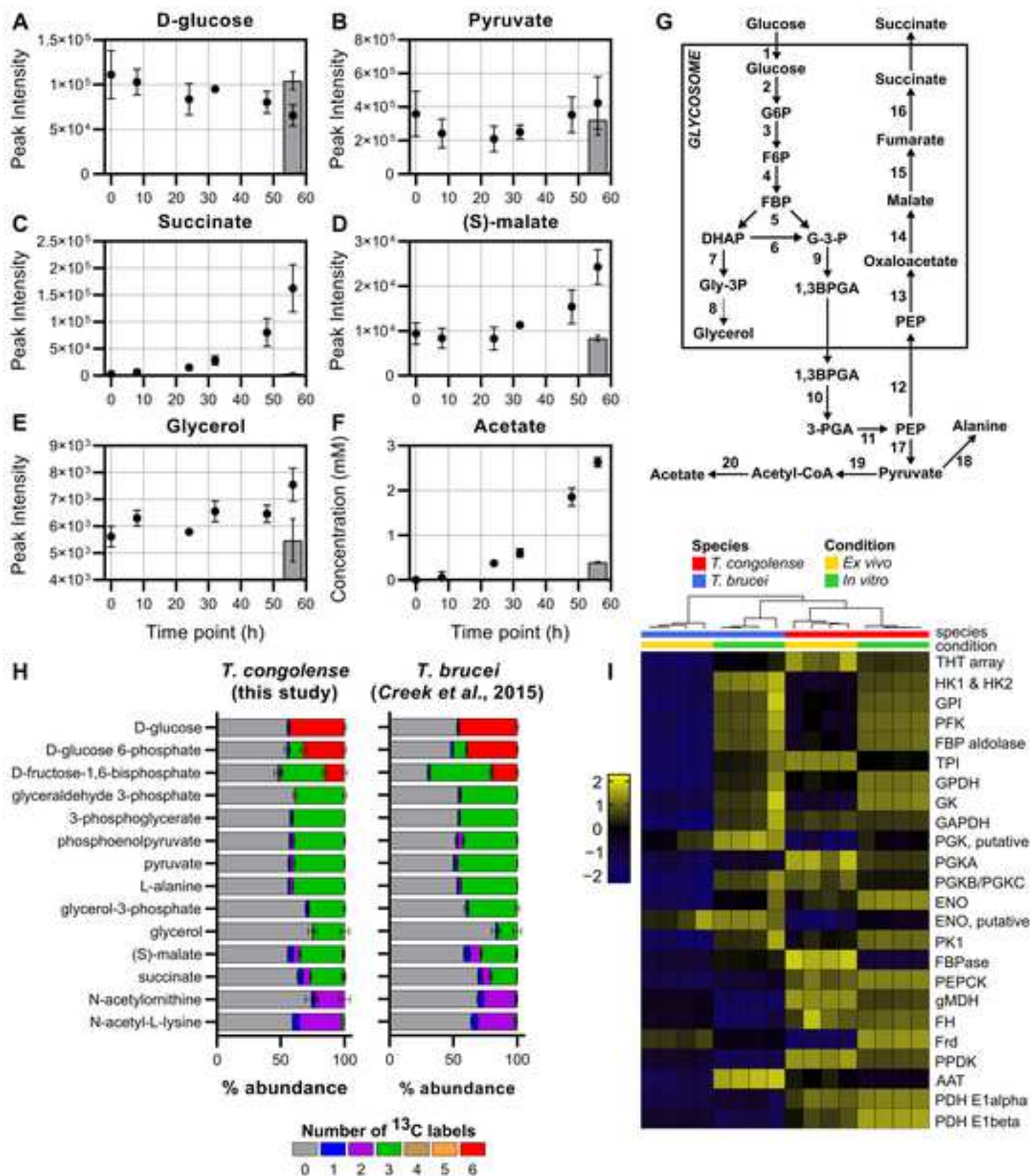
1835 130. Gu Z, Eils R, Schlesner M. Complex heatmaps reveal patterns and correlations in
1836 multidimensional genomic data. *Bioinformatics*. 2016;32(18): 2847-9. doi:
1837 10.1093/bioinformatics/btw313.

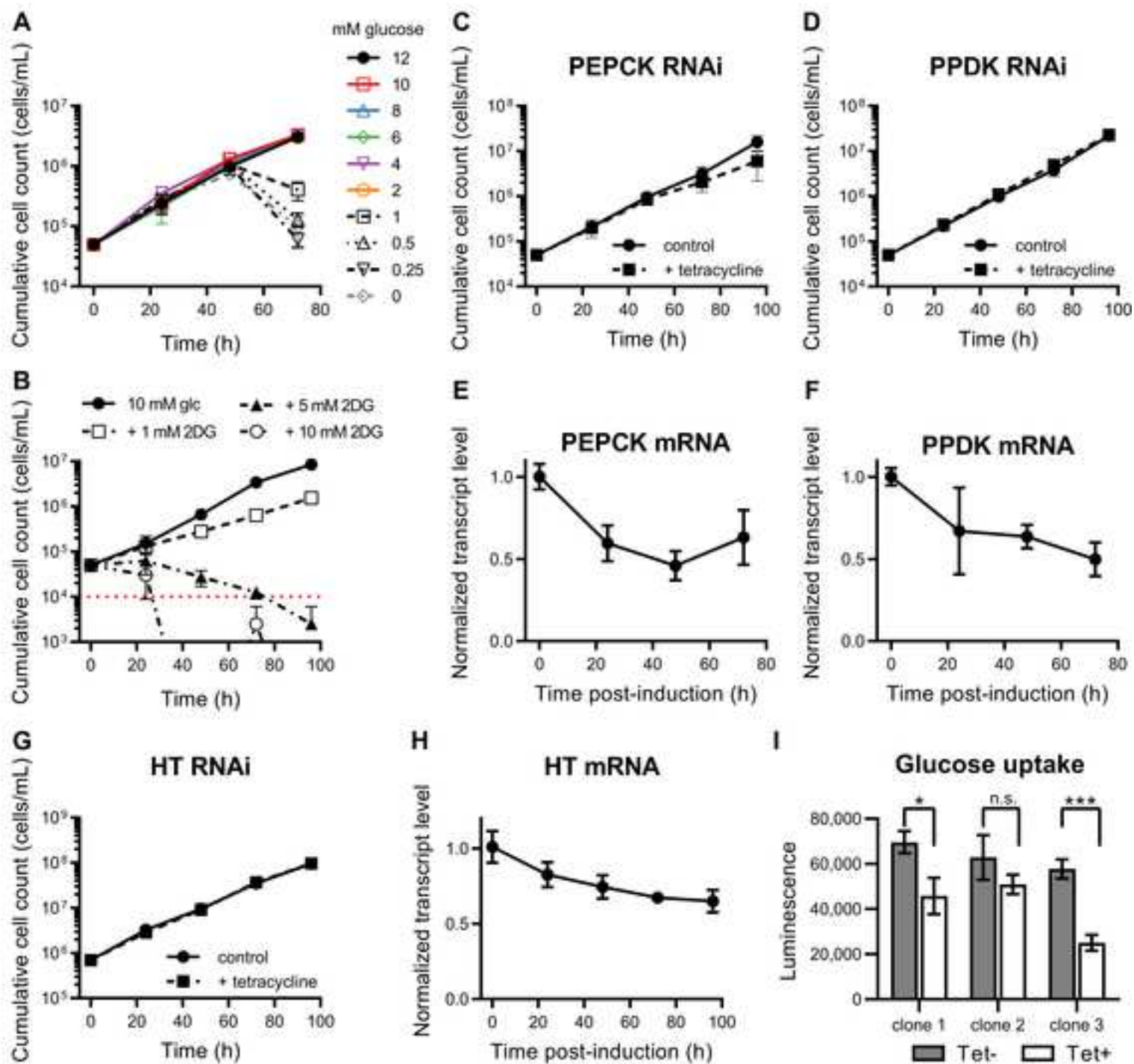
1838 131. Dolezelova E, Teran D, Gahura O, Kotrbova Z, Prochazkova M, Keough D, et al. Evaluation of the
1839 *Trypanosoma brucei* 6-oxopurine salvage pathway as a potential target for drug discovery. *PLoS*
1840 *Negl Trop Dis*. 2018;12(2): e0006301. doi: 10.1371/journal.pntd.0006301.

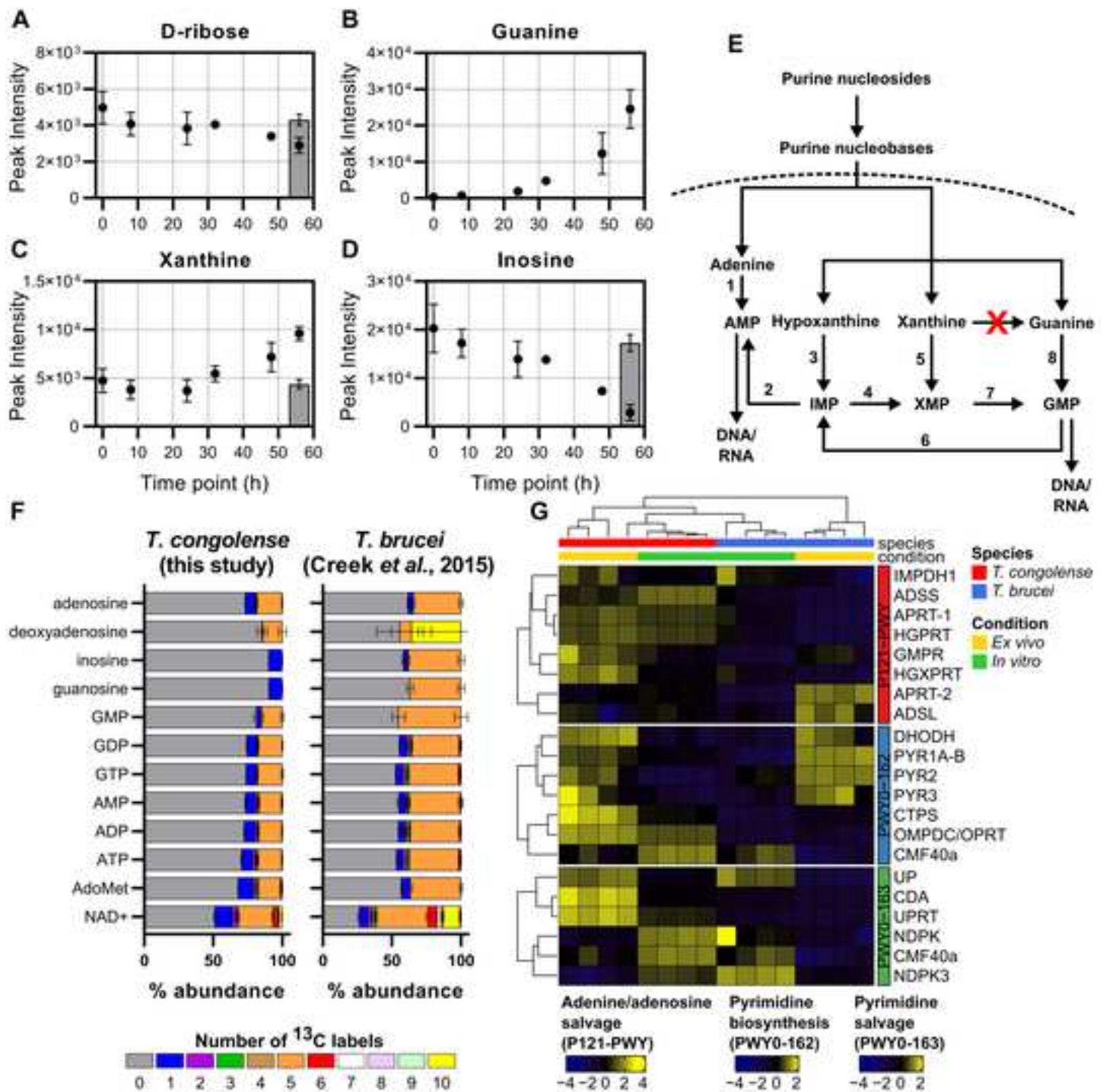
1841

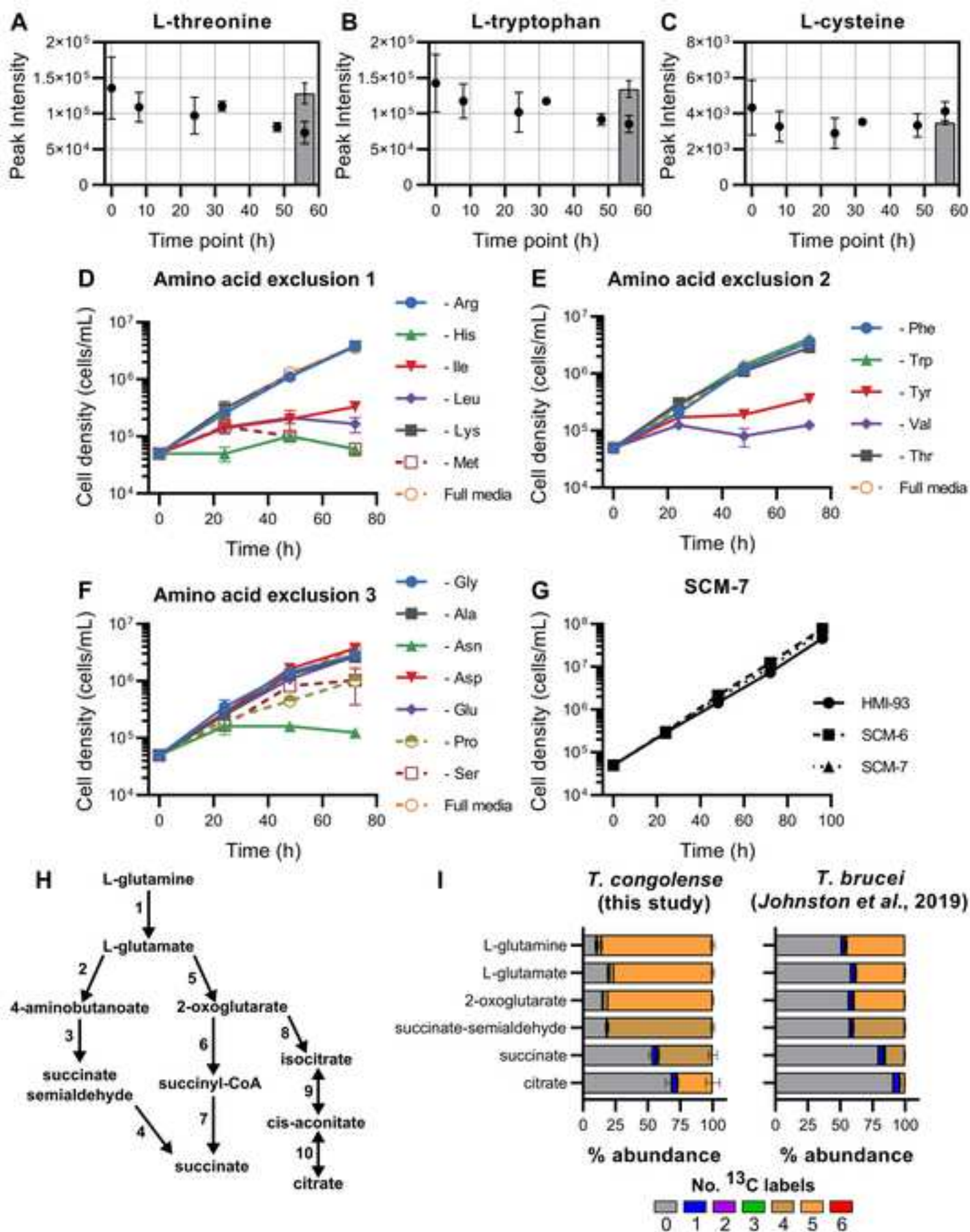


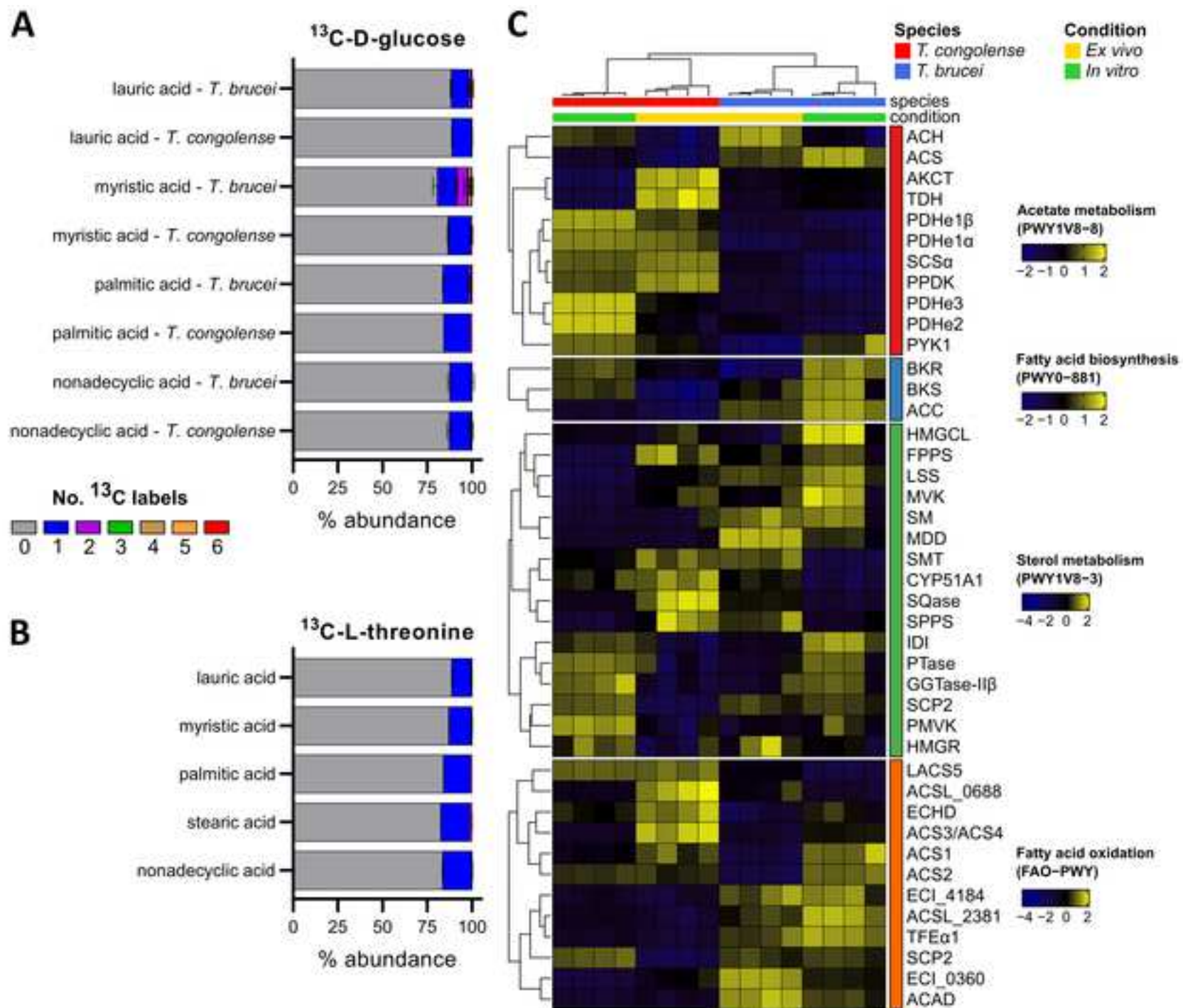












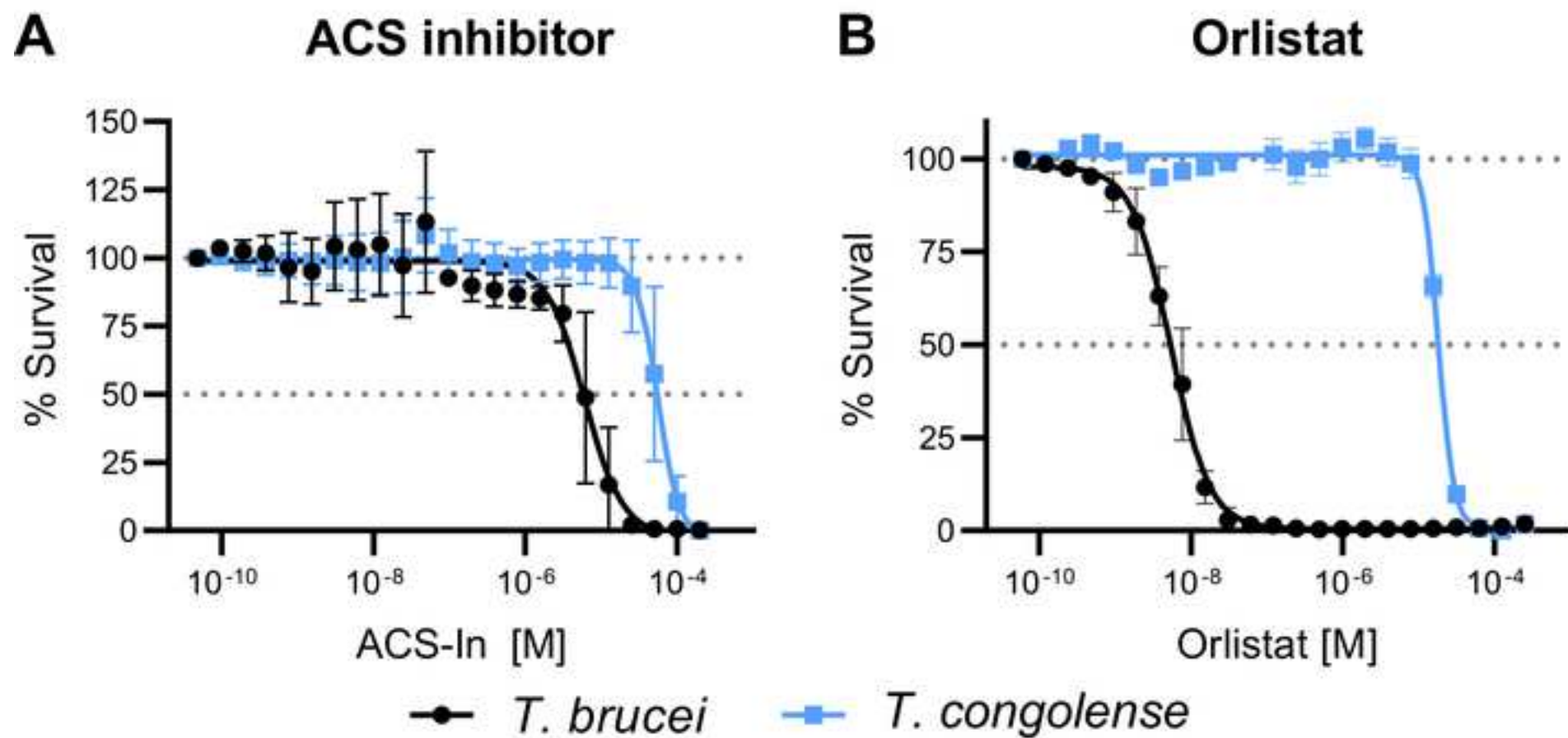
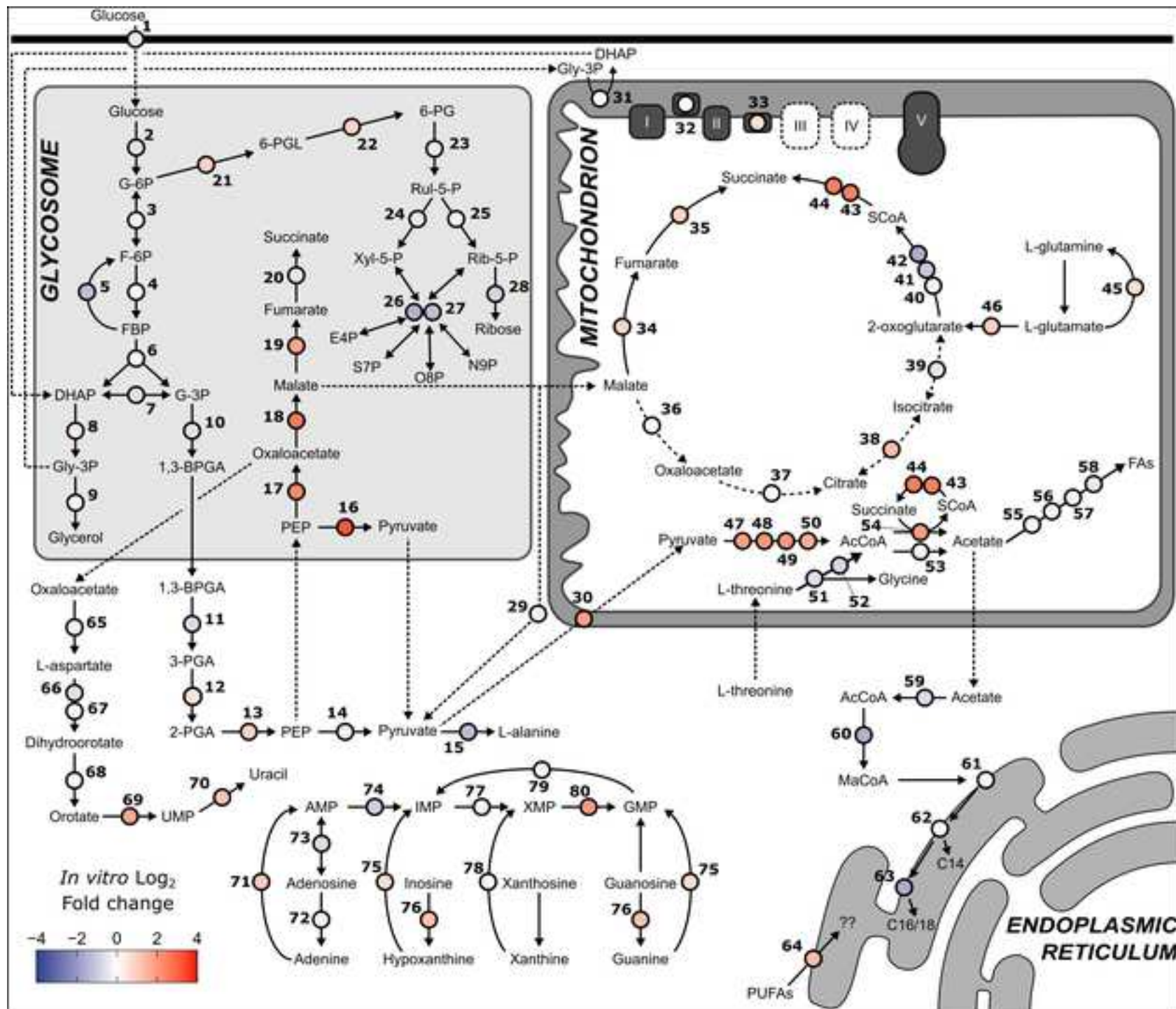
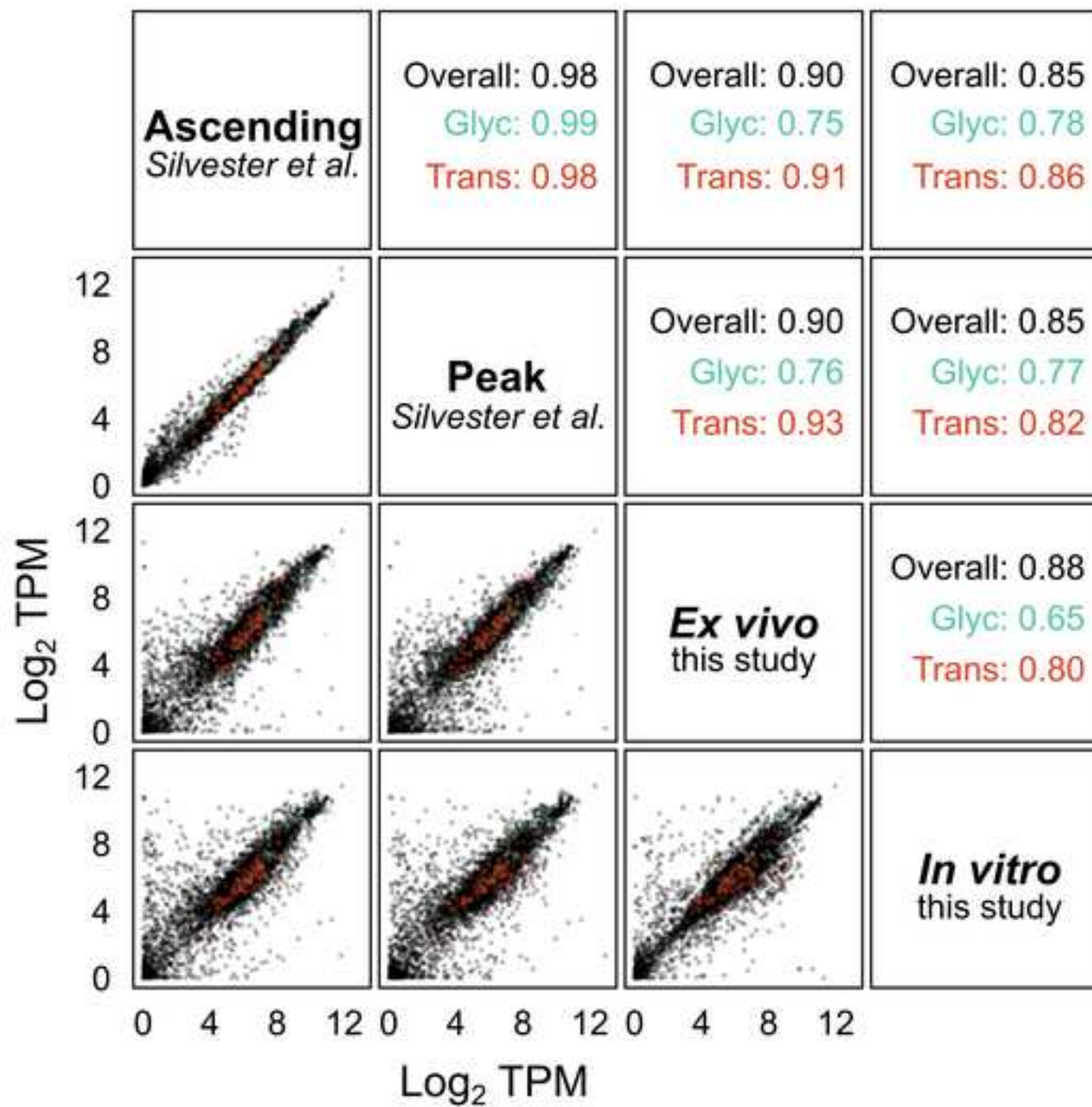
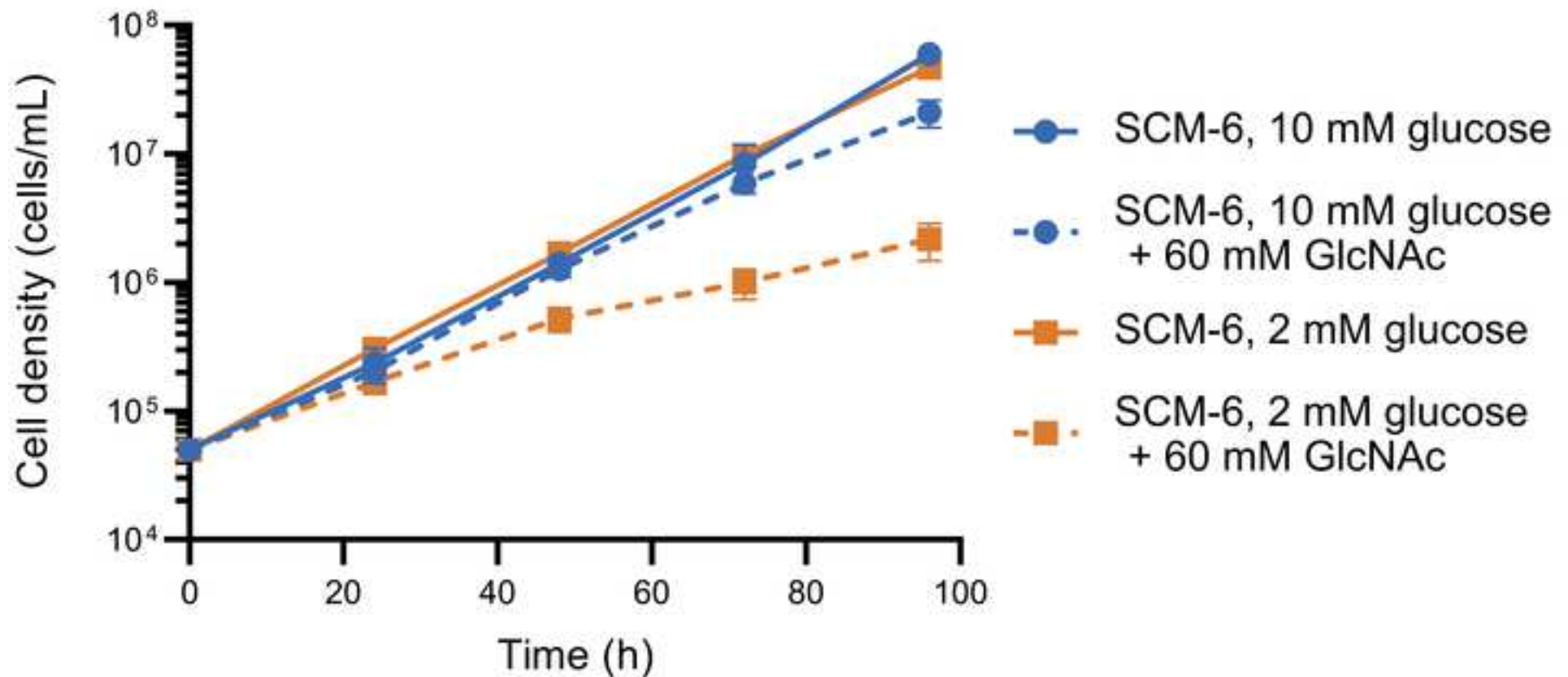


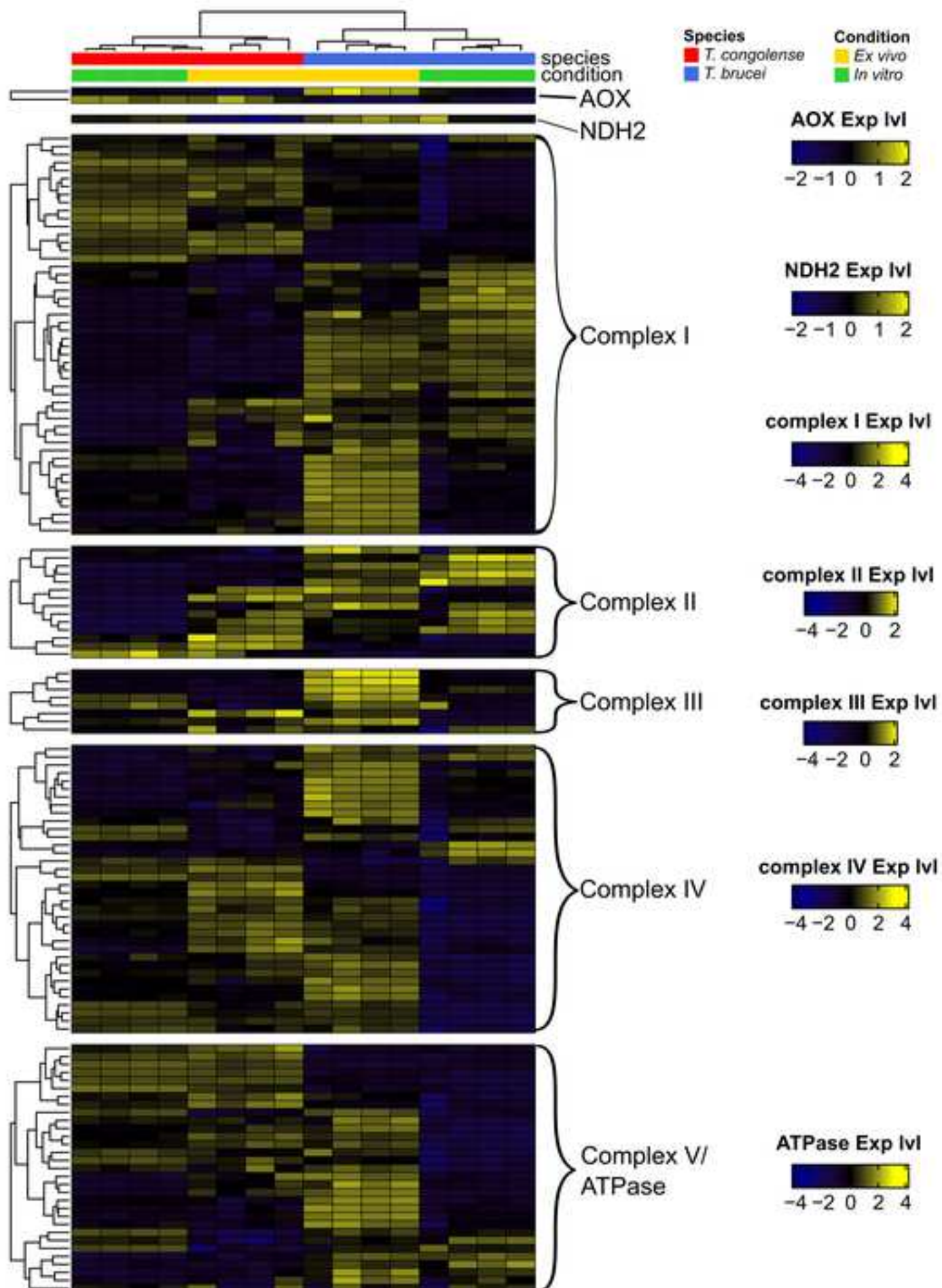
Figure 9

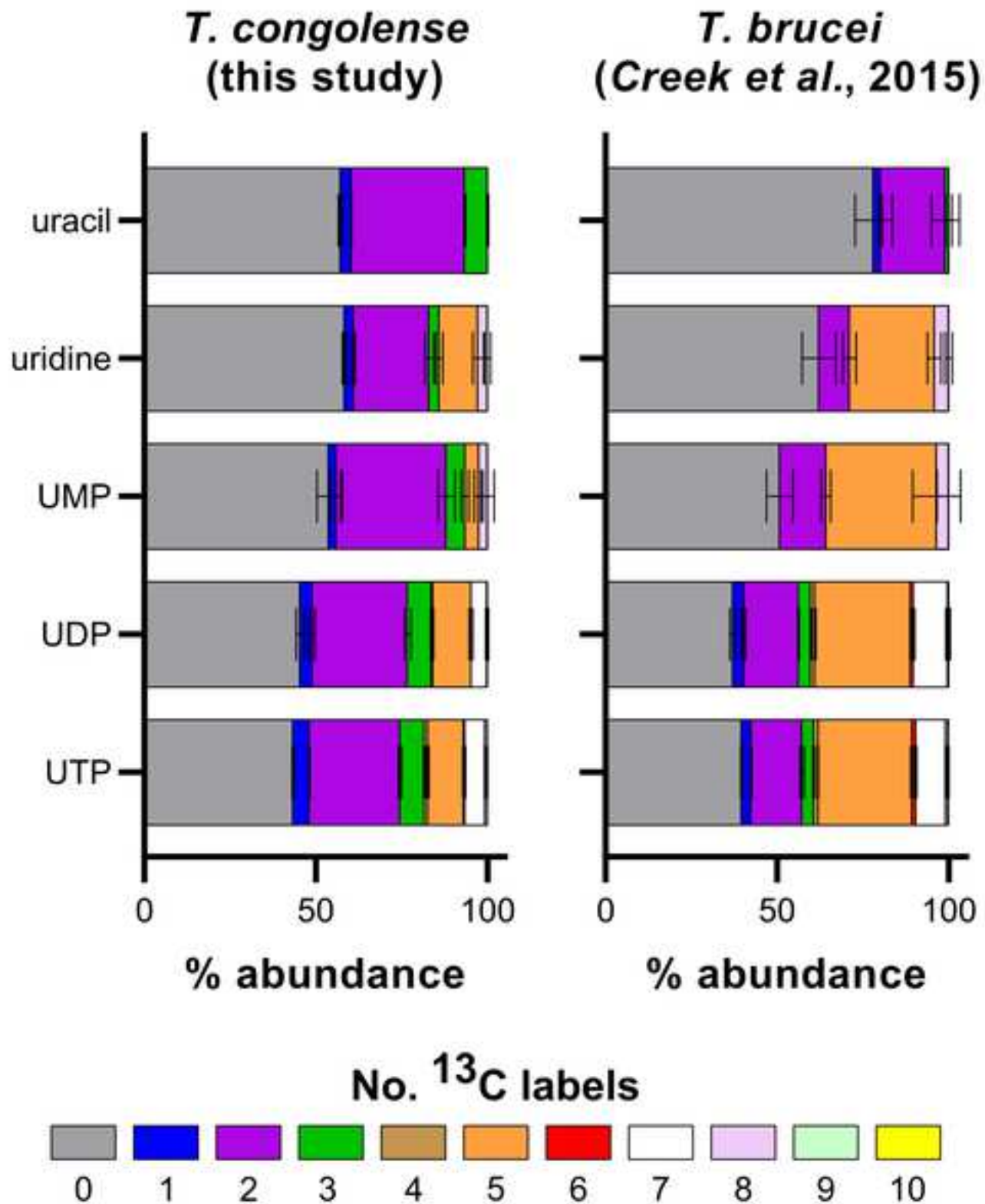




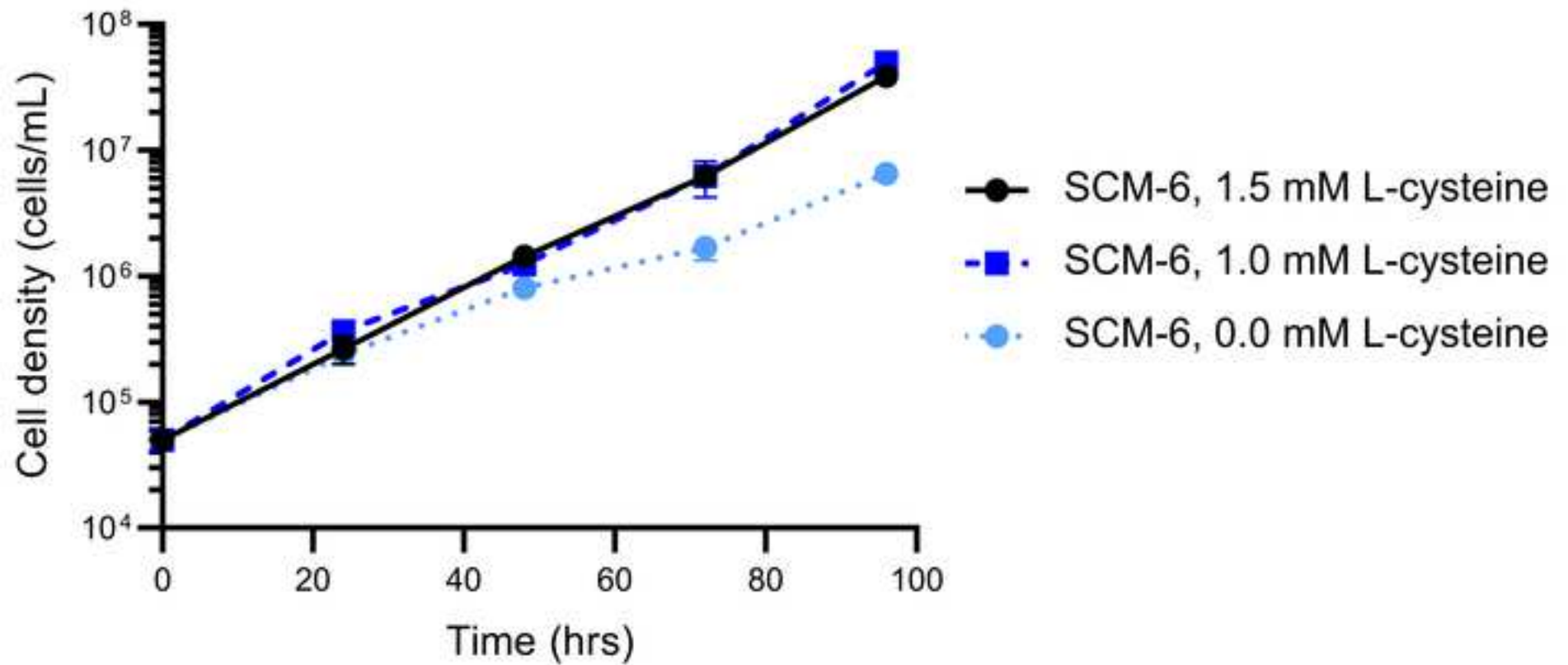
T. congolense growth ± N-acetyl-D-glucosamine

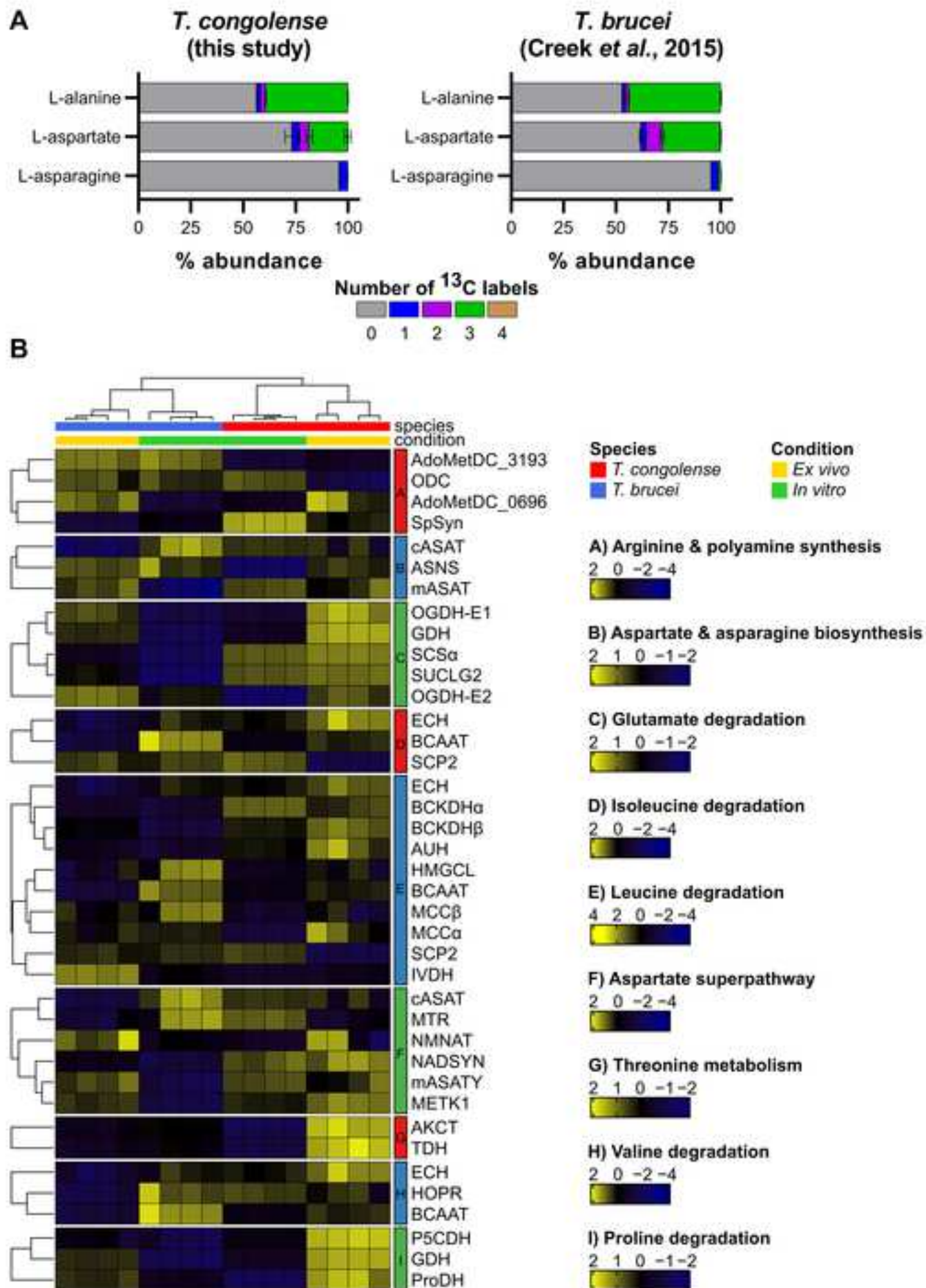


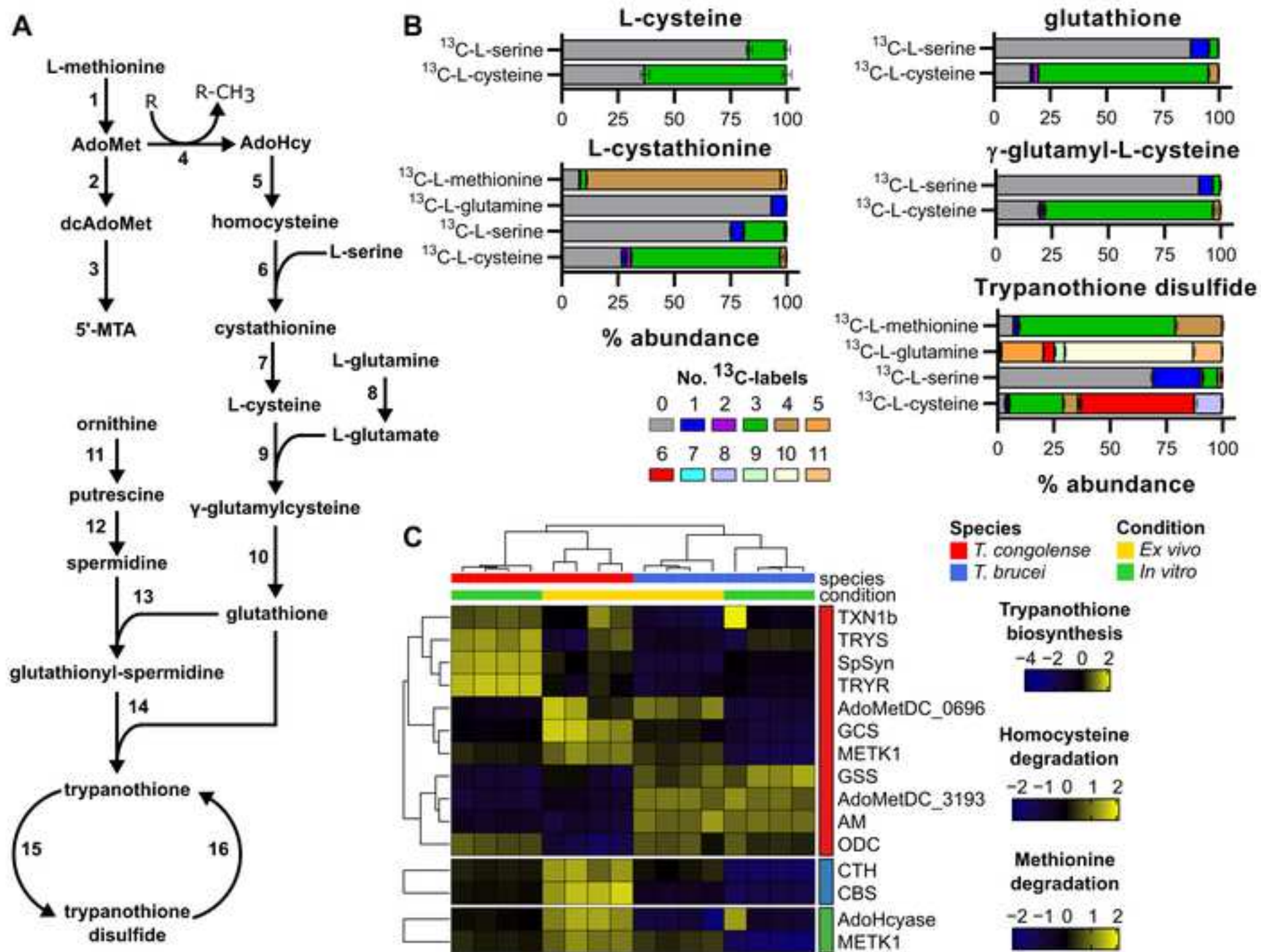


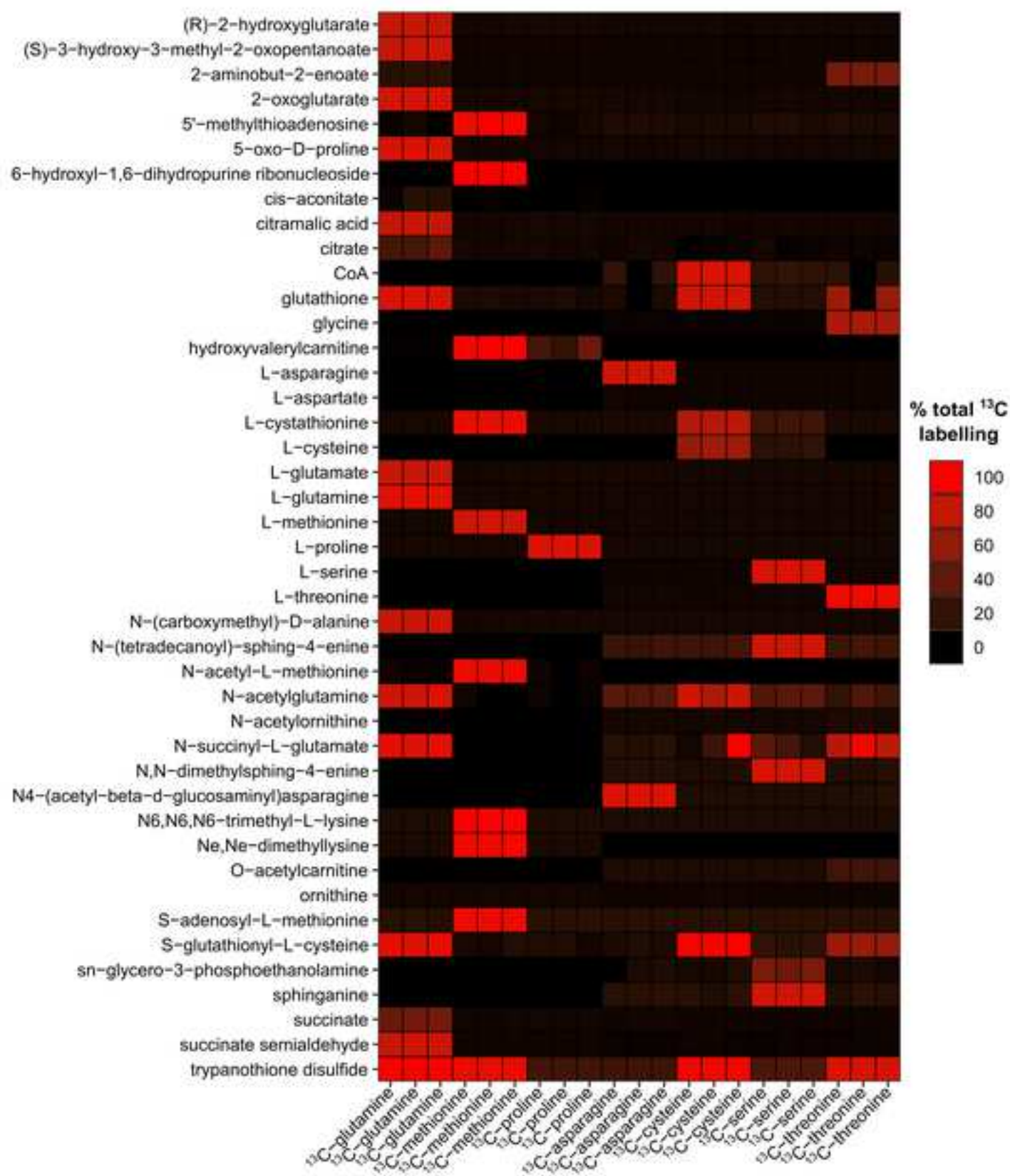


T. congolense growth ± L-cysteine







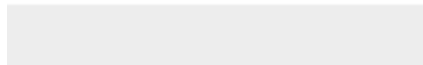




[Click here to access/download](#)

Supporting Information

[S1_Table_RNAseq_Tcongolense_vs_Tbrucei.xlsx](#)





Click here to access/download
Supporting Information
S2_Table_OrthoFinder_dataset.xlsx

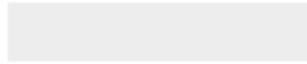


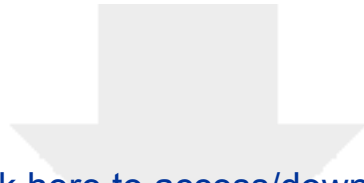


Click here to access/download

Supporting Information

S3_Table_RNAseq_Tcongolense_only.xlsx





Click here to access/download

Supporting Information

S4_Table_supernatant_metabolomics.xlsx

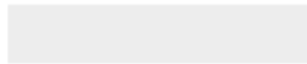




[Click here to access/download](#)

Supporting Information

[S5_Table_Trypanocyc_pathways_pseudo_genome.xlsx](#)

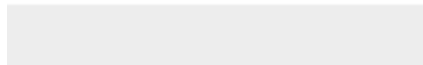




Click here to access/download

Supporting Information

S6_Table_SCM-6_SCM-7_formulations.xlsx





Click here to access/download
Supporting Information
S7_Table_primers.xlsx

